NOTICE

The quality of this microform is heavily dependent upon the quality of the original thesis submitted for microfilming. Every effort has been made to ensure the highest quality of reproduction possible.

If pages are missing, contact the university which granted the degree.

Some pages may have indistinct print especially if the original pages were typed with a poor typewriter ribbon or if the university sent us an inferior photocopy.

Previously copyrighted materials (journal articles, published tests, etc.) are not filmed.

Reproduction in full or in part of this microform is governed by the Canadian Copyright Act, R.S.C. 1970, c. C-30.

AVIS

La qualité de cette microforme dépend grandement de la qualité de la thèse soumise au microfilmage. Nous avons tout fait pour assurer une qualité supérieure de reproduction.

S'il manque des pages, veuillez communiquer avec l'université qui a conféré le grade.

La qualité d'impression de certaines pages peut laisser à désirer, surtout si les pages originales ont été dactylographiées à l'aide d'un ruban usé ou si l'université nous a fait parvenir une photocopie de qualité inférieure.

Les documents qui font déjà l'objet d'un droit d'auteur (articles de revue, tests, publiés, etc.) ne sont pas microfilmés.

La reproduction, même partielle, de cette microforme est soumise à la Loi canadienne sur le droit d'auteur, SRC 1970, c. C-30.

Canada

THE UNIVERSITY OF ALBERTA

A PALEO-GEOMAGNETIC STUDY OF PLEISTOCENE SEDIMENTS IN NORTHWESTERN CANADA

by

KEVIN PAUL GILLEN

A THESIS

SUBMITTED TO THE FACULTY OF GRADUATE STUDIES AND RESEARCH IN PARTIAL FULFILMENT OF THE REQUIREMENTS FOR THE DEGREE OF MASTER OF SCIENCE

IN

GEOPHYSICS

DEPARTMENT OF PHYSICS

EDMONTON, ALBERTA

FALL 1988

ISBN 0-315-45771-6

THE UNIVERSITY OF ALBERTA

RELEASE FORM

NAME OF AUTHOR KEVIN PAUL GILLEN

TITLE OF THESIS A PALEO-GEOMAGNETIC STUDY OF PLEISTOCENE SEDIMENTS IN NORTHWESTERN CANADA

DEGREE FOR WHICH THESIS WAS PRESENTED MASTER OF SCIENCE

YEAR THIS DEGREE GRANTED FALL 1988

Permission is hereby granted to THE UNIVERSITY OF ALBERTA LIBRARY to reproduce single copies of this thesis and to lend or sell such copies for private, scholarly or scientific research purposes only.

The author reserves other publication rights, and neither the thesis nor extensive extracts from it may be printed or otherwise reproduced without the author's written permission.

(SIGNED) .....

PERMANENT ADDRESS:

2841 DANDURAND BLVD.,
WINDSOR, ONTARIO
N9E 2E5

DATED Sept 30 1988

THE UNIVERSITY OF ALBERTA

FACULTY OF GRADUATE STUDIES AND RESEARCH

The undersigned certify that they have read, and recommend to the Faculty of Graduate Studies and Research, for acceptance, a thesis entitled A PALEO-GEOMAGNETIC STUDY OF PLEISTOCENE SEDIMENTS IN NORTHWESTERN CANADA submitted by KEVIN PAUL GILLEN in partial fulfilment of the requirements for the degree of MASTER OF SCIENCE in GEOPHYSICS.

Michael Evans

Supervisor

H. A. K. Charlesworth

J. C. Savigny

Douglas P. Hube

Date.....

Abstract

A total of 626 specimens was collected in two laterally equivalent vertical sections (each approximately 20m in height) from Pleistocene sediments exposed in river bank outcrops on the Old Crow River, Yukon Territory. Paleomagnetic examination revealed remanent magnetization records of both geological and geophysical interest. A sequence of three features appearing in both sections can be correlated with results obtained from previously sampled sections some 5 km upstream. This concordance between previous and present results suggests a geomagnetic perturbing source rather than a sedimentological one.

The remarkable correlation observed allows a date for these sediments to be established paleomagnetically. Previous results come from a site where the Old Crow Tephra is preserved. The unique paleomagnetic signal associated with this tephra is found in both sections of this present study (very good in one, but poorer in the second) and therefore fixes the age of the pertinent level in these sediments as equivalent to that of the tephra (149,000 ±13,000 years B.P.).

The remainders of both sections show features consistent with the idea of a stationary magnetic source in the outer core which has acted intermittently. These features involve perturbations of the remanent magnetization vector, along linear trajectories, in excess of 60° from the ambient position expected from a geocentric axial dipole

field. Elementary magnetostatic modelling shows that even the largest perturbation can be explained by an eccentric radial dipole at the Core-Mantle Boundary (CMB) with moment directed away from the geocentre and as small as about 8% of the moment of the main dipole. Such an outward moment vector would yield a patch of reverse flux at the CMB, very similar in many respects to patches of reverse flux currently existing in the southern hemisphere.

Acknowledgements

I wish to express my deepest appreciation to Dr. M.E. Evans for guidance and stimulating discussion during my work at the University of Alberta. Without his supervision, this thesis could not have been completed.

I am greatly indebted to both the Natural Sciences and Engineering Research Council and the Boreal Institute for Northern Studies for awarding me a [redacted]uate scholarship and partially funding my field wo[redacted]pectively. [redacted] wish to thank Dr. C.E. Schweger and Dr. J.V. Matthews their consultation in the field, my friend Philip Ingenkamp for his help in collecting the samples and Vaslov Fenoch for his help in processing them.

Finally I wish to thank my best friend Esther Methe for her encouragement and patience at all times.

Table of Contents

List of Tables

List of Figures

I. INTRODUCTION

The bulk of the magnetic field at the Earth's surface has its origin in the interior of the planet. Many of the methods used today to analyze the field, as well as the terms used to describe its character, have a considerable history. Thus a proper understanding of the present state of geomagnetism begins with a study of the past.

A. [illegible]agnetism

Some properties of magnetism are claimed by some historians to have been known in China as early as the second millenium B.C. and the Chinese are credited with the invention of the compass. After its introduction into Europe, it was noted that although the needle pointed roughly North (as defined by the pole star), it usually diverged by a small amount. This angular difference in one's local horizontal plane between true north and the compass went by various names but is today called *declination*. Sailors using the compass to navigate had to correct for this effect. When the needle was suspended through its centre of gravity and allowed to orientate itself in three dimensions, it was discovered that it also assumed an inclined position. This measure of the field is called *inclination* and is defined as the deviation of the field from the local horizontal plane. In the beginning, this property was probably a nuisance since the needle had to be weighted in order to force it to sit horizontally and give

the measure of declination which was desired for navigation. These measures of the field have remained with us to the present day, and along with a measure of the intensity, totally define the geomagnetic vector at a point of observation.

In the early stages of compass use, the origin of the force which caused the needle to orientate was unknown and surrounded by much folklore. In 1600, Sir William Gilbert, in his famous work "De Magnete", put forth the suggestion that the Earth is a great magnet, a conclusion which he had drawn from experimentation with a sphere cut from lodestone. This model was successful in predicting some of the observed characteristics of the geometry of the field, such as the increase of inclination with latitude which was subsequently confirmed by Hudson during his voyage in the Barents Sea in the early seventeenth century.

In 1634 Gellibrand discovered that the magnetic declination at London changed with time. This time-dependent behaviour of the field cast some doubt on the simple model of the Earth as a permanently magnetized body. It was later discovered that changes also occur in the inclination and intensity.

The suggestion of the dipolar nature of the Earth's field did, however, come to be verified. Gauss (1839), in his spherical harmonic expansion of the field in terms of the sum of multipoles, showed the dipole term to be dominant and in the process, verified that the field was of

predominantly internal origin. This initial work was done with the best data available at the time, which were sparse, but subsequent analyses with modern data have confirmed that the dipole term constitutes 95% of the total field as seen at the Earth's surface, while the remaining 5% represents the sum of the non-dipole terms. From this discovery naturally grew the custom of discussing the properties of the field in terms of its *dipole* and *non-dipole* parts, a practice which has continued to the present day.

The representation of the field as a sum of multipoles is simply a mathematical convenience, and warnings have been made of the potential dangers of thinking of these multipoles as having physical meaning. However, it was soon discovered that the changes which the Earth's field was undergoing manifested themselves differently in the dipole and non-dipole parts. For example, their time constants of change were found to be different. This led some authors (e.g. Barton, 1978) to suggest that there may actually be a physical basis which justifies the discussion of change in the total field in terms of its dipole and non-dipole components. As will be seen later, the most commonly invoked mechanism for change in the field is movement of field lines by circulation of fluid in the outer core, and since this process involves the main field, it is not at first glance apparent why the two parts should possess different modes of change and different time constants.

There have been several suggestions as to why these differences exist. For example, Le Mouel (1984) has calculated that the types of motions probably involved at the surface of the outer core give a time-dependent change to the non-dipole field, yet such motions are not involved in sustaining the axial dipolar part of the field and thus do not affect it significantly.

The changes in the field as recorded at magnetic observatories such as London and Paris (Figure 1-1) were observed to occur primarily as a result of changes in the non-dipole part. Such studies of the time-dependent behaviour of the field at several sites lead to the suggestion that the changes observed at these places were not only due to a time-dependent morphology change of the non-dipole field but also to a rotation of the field. This drifting phenomenon has been termed the "westward drift" because the movement is predominantly westwards. Bullard et al (1950) shifted several decades of non-dipole field data around the spin axis to the point of best match and thereby determined an average drift rate of 0.2 °/year to the west. It must, however, be emphasized that changing non-dipole features are regional, not global in their extent, and thus the above figure is an average. Not all of the field drifts in a westward sense (in fact, not only do some parts stand still, but at some locations eastward drift is observed). This behaviour has been likened to a drifting weather pattern which predominantly drifts westward but exhibits

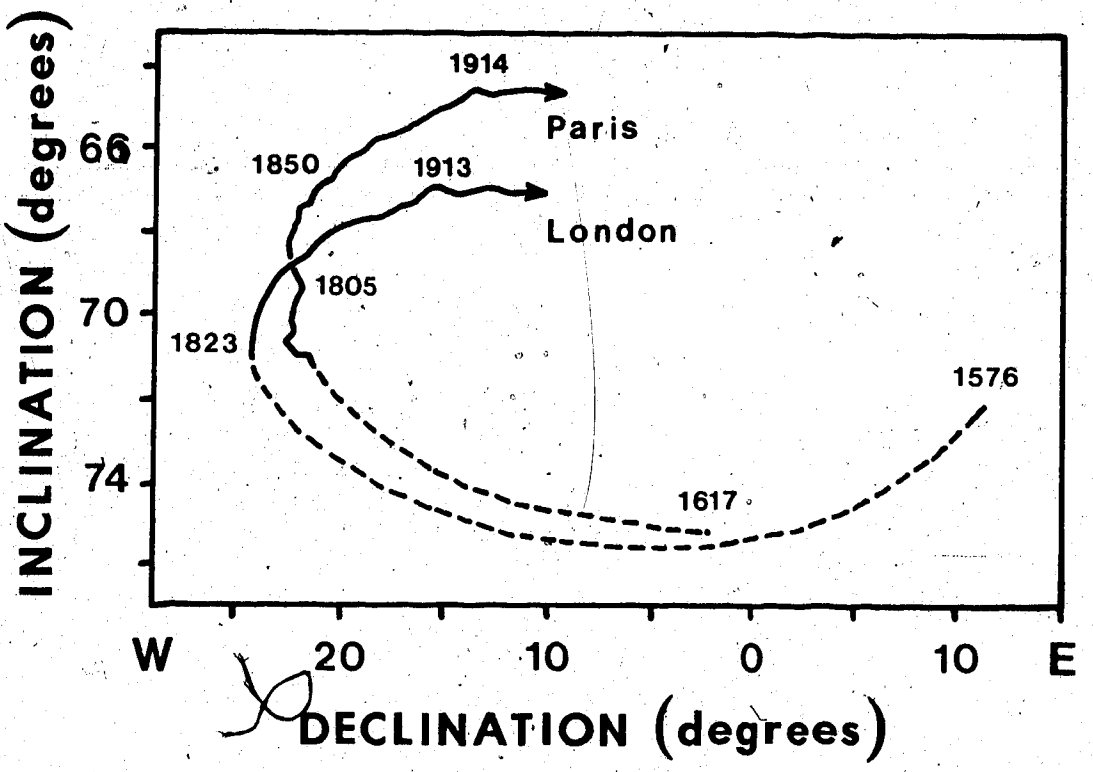

Figure 1-1: Inclination - declination variations at London and Paris (after Gaiber-Puertas, 1953).

regions in which some eastward movement occurs. A drifting feature in the non-dipole field is shown in Figure 1-2. Rates of change of the non-dipole field at the Earth's surface can be contoured as isoporic maps and reveal centres of high and low secular variation termed *isoporic foci*. Drift analysis, when applied to these foci gives a drift rate of 0.3°/year westward (Bullard et al., 1950). This higher rate results from the fact that stationary features in the non-dipole field are not present in an isoporic plot and thus do not contribute to bringing the average down. This is referred to as the *westward drift of the secular variation* whereas the former is known as the *westward drift of the non-dipole field*.

That part of the non-dipole field which does not appear to drift, exhibits regions which change their strength with time. The Mongolian positive anomaly, for instance, has strengthened with time at a linear rate of 53 nT/year over the past several hundred years while maintaining the same latitude and longitude throughout (Yukutake and Tachinaka, 1968) and is now at a level of 18,000 nT. The evolution of this anomaly with time is illustrated in Figure 1-2.

The main dipole (given by the first 3 terms in the spherical harmonic expansion) has also been observed to undergo some time-dependent behaviour. It has decreased in strength by 7% over the past 150 years (Bloxham & Gubbins, 1985). In fact, this appears to be part of a larger trend of main dipole decrease, as deduced from archeomagnetism.

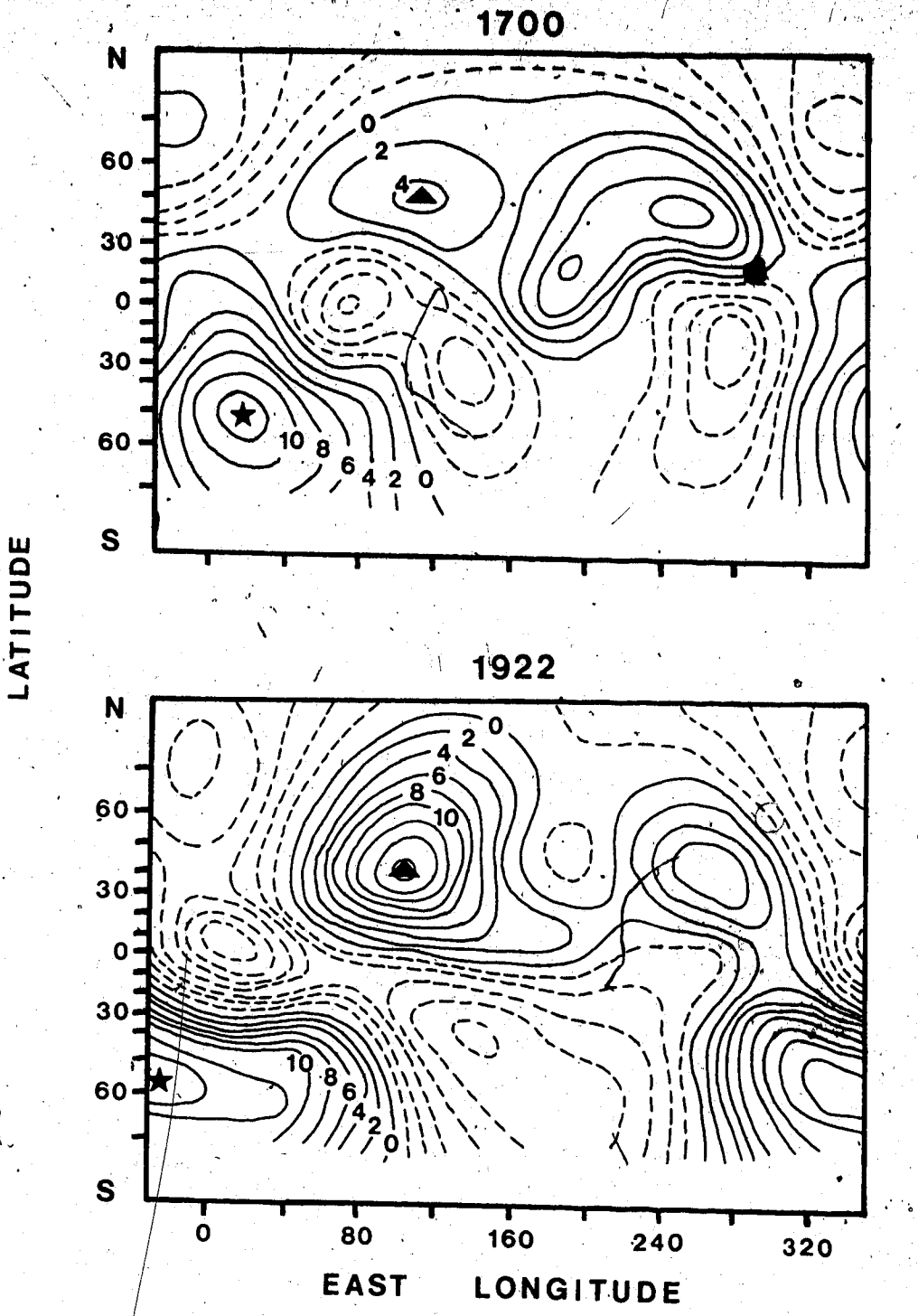

Figure 1-2: Anomalies in the vertical component of the non-dipole field at 1700 and 1922 A.D. Contour interval is 2000 nT, with solid line denoting +Z and dashed line representing -Z features. The triangle marks the position of a stationary feature which has strengthed over time (Mongolian anomaly). The star marks a westward drifting anomaly (after Yukutake and Tachinaka, 1968).

Archeological materials which are able to record the intensity of the field suggest that the main dipole moment has fluctuated in the past and has been as low as half and as high as twice its present value (Cox, 1968).

The orientation of the main dipole has not altered over the period of direct observation. At present, the axis is inclined at 11.5° to the axis of rotation and intersects the surface at 78.5° North, 70° West and 78.5° South, 110° East. This departure from the spin axis is attributed to *dipole wobble*. The nature and cause of dipole wobble is not understood but apparently involves a time scale of 10^3 years (too slow to be observed historically) with an average departure of about 10 degrees (McElhinny and Merrill, 1975).

In the modern field, we have not yet witnessed a complete cycle of change of any non-dipole or main dipole feature. For example, if the behaviour were periodic, the westward drifting features would take 1200 years (0.3°/year) to complete one revolution around the Earth and data on the modern field from direct observation go back no more than about 300 years. To extend the span of observation time, it is necessary to seek out geological material from which we might glean a chronicle of past geomagnetic field behaviour. Certain sediments may fulfil this requirement. The accumulation of detrital material, layer upon layer, yields a tape recording of the time variations of the field. Each sample collected from a section functions as a "fossil compass", providing a record of the direction of the

geomagnetic field at the time the magnetization was acquired. The record obtained is that of *paleosecular variation*. More will be said about the recording process in the next section.

Paleosecular variation records obtained from lake sediment have provided evidence of both standing sources which vary in intensity and sources which drift. Westward drift at various rates (e.g. 0.13°/year, Creer and Tucholka, 1982) has been observed, as well as some eastward drift (Denham, 1974). Features which appear to represent standing sources of varying intensity are also evident in some records (Evans, 1984; Hedlin and Evans, 1987; Latham et al., 1987). It must be emphasized, however, that the variations observed in sediments are most often of irregular period and amplitude (Creer et al., 1976; Mackereth, 1971). Typical amplitude variations for the vector at a site are usually less than 20 degrees from the position of the ambient vector.

In addition to the above, some paleosecular variation records show features which are not observed in the modern day field. The most important are polarity reversals. In such a case, the remanent magnetization vector in the material has an orientation roughly opposite to that expected from the present day dipole field. It usually remains to be established as to whether such a record represents global reversal (g$_1^0$ changes sign) or if it is a regional effect of some strong non-dipole disturbance. The

Second type of field behaviour seen is an anomalously large deviation from the direction expected at a given site (greater than average paleosecular variation amplitudes, but less than a full reversal). Such behaviour is usually called an *excursion*. An excursion is defined as a movement of the dipole axis away from the spin axis with amplitude greater than 40°, but not fully reversing. "Excursions" in sediment therefore indicate a location of a paleopole (ancient geomagnetic pole) which is greater than 40° from the spin axis, however it must be established that such a signal represents a global event before such a term can be applied. The nature and cause of excursions are not understood.

B. Fossil Magnetism

In a manner akin to the alignment of a compass needle, detrital magnetic grains within a matrix of sediment are brought into alignment with the geomagnetic field. Remanent magnetization acquired in this fashion is referred to as *detrital remanent magnetism* (DRM). If this process occurs at the time of deposition, it is called *depositional detrital remanent magnetism* (dDRM), whereas any realignment taking place after deposition is termed *postdepositional* DRM (pDRM) (Verosub, 1977). The realignment takes place because the water-filled pore spaces within the sediment skeleton free the smaller magnetic grains. De-watering of the sediment

usually brings a halt to further realignment. It must be noted that there are several other forces which compete with the magnetic field in the alignment of the particles (e.g. gravity, viscous forces from water flow, etc.).

Magnetic overprinting of the DRM component can take place without physical rotation of the remanence carriers. When exposed to a field different from that which gave the DRM, the sample will sometimes pick up a component in the direction of the new field. Resistance of the individual grain to such overprinting is a function of the strength of time exposed to the field and of the grain's *coercive force*. Since sediment is a collection of different magnetic grains with various coercive force values, the sample as a whole displays a *coercive force spectrum*. Such overprinting can usually be removed by alternating field (AF) demagnetization. The vector sum of all the magnetic components in a sample is referred to as the NRM (natural remanent magnetism).

The above discussion deals with the recording of direction only. The field, however, is a vector and also has a strength associated with it. How do sediments record the intensity of the geomagnetic field? The resultant magnetization results from the preferential alignment of moment vectors of individual grains. Theoretically, the stronger the field, the better the alignment and hence the higher the magnetic moment (up to a maximum attained when complete alignment is reached). This process is complicated

by variable composition. Variations in the amount of magnetic material will cause corresponding variation in intensity of magnetization. As a result, reliable paleofield intensities are rarely recovered from sediment.

C. Scope of thesis

The nature of paleosecular variation as recorded in sediment of Pleistocene age from the Old Crow Basin, Yukon Territory, Canada is examined. Two laterally equivalent vertical sections (approximately 20m and 21m in length) were sampled at stratigraphic intervals of roughly 10cm, yielding 626 samples for paleodirectional study. Fidelity of the material as a recorder of the Earth's field is established and the resultant remanent magnetization sequences are examined. Some perturbations present in this sequence of interest are modelled as sources located in the outer core, and these are compared with present day field characteristics.

II. SITE DESCRIPTION AND SAMPLING

The study area is located at latitude 67° 51' N and longitude 139° 48' W in the Old Crow Basin, Yukon Territory, Canada (Figure 2-1). The sampling sites (11 and 11N) are shown in Figure 2-2, which also shows the location of sites 15 and HH68-10 (sampled by Hedlin, 1986; Hedlin & Evans, 1987). The apparent lack of logic in the naming of these four sites is the result of the numerous investigations carried out by many different researchers over the past few decades.

The Basin itself is the product of deposition in glacial lakes formed as a result of ice damming during the Illinoian and Wisconsinan ice ages. Absence of these lakes during non-glacial periods allowed rivers to form fluvial deposits. The Old Crow and Porcupine Rivers, which presently transect the Basin, have cut down through this stratigraphy, thereby allowing it to be studied in riverbank sections. The limits of the last two ice advances (Figure 2-1) were such that the Basin was spared the effects of glaciation. Thus the NRM's recorded in the sediments potentially provide a relatively undisturbed and continuous record of the behaviour of the Earth's magnetic field during part of the Pleistocene.

A composite section of the relevant geology is given in Figure 2-3, in which Morlan and Matthews (1978) recognize nine units. This stratigraphy was compiled from several bluffs along the Old Crow valley and thus not all units are

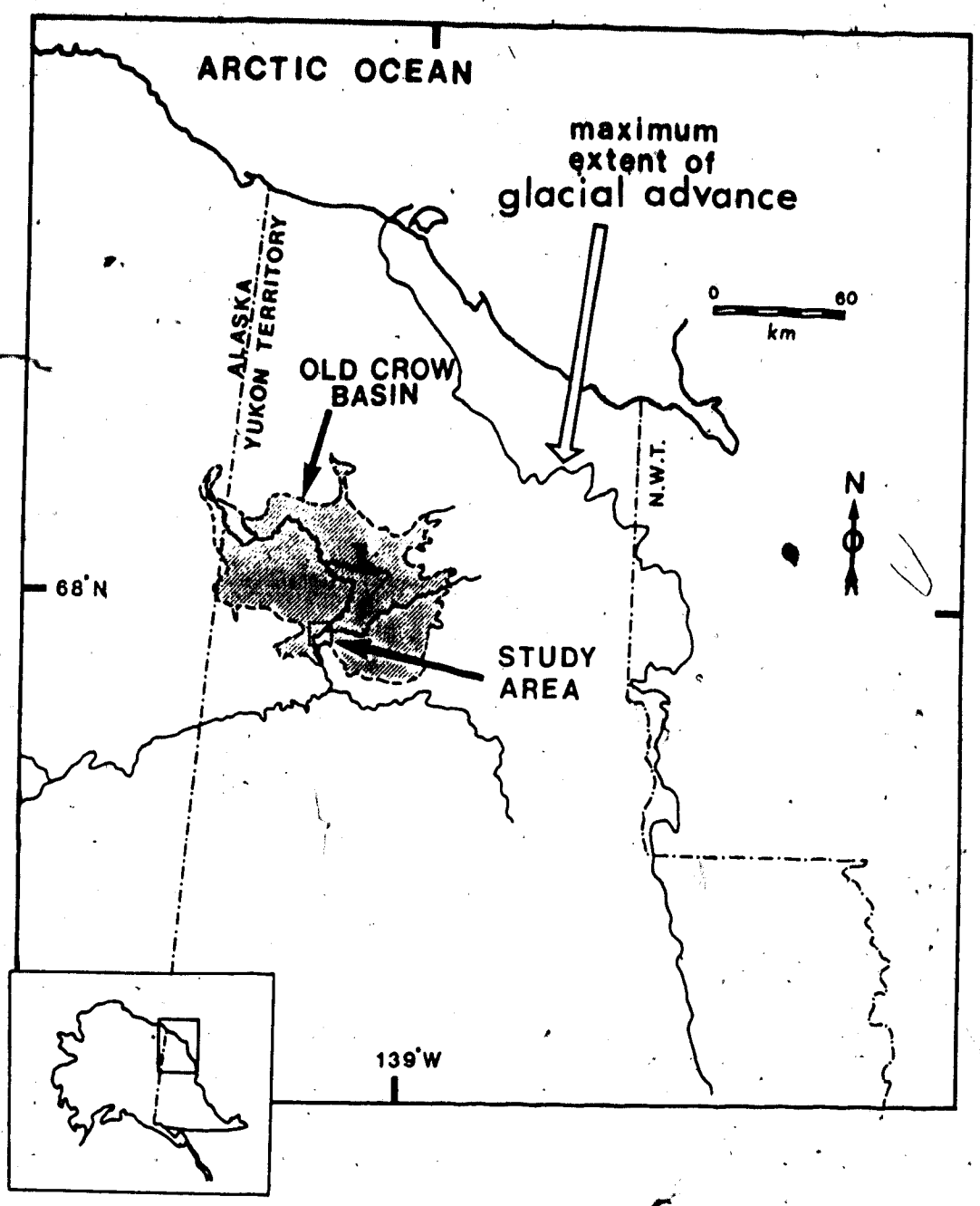

Figure 2-1: Location of the study area.

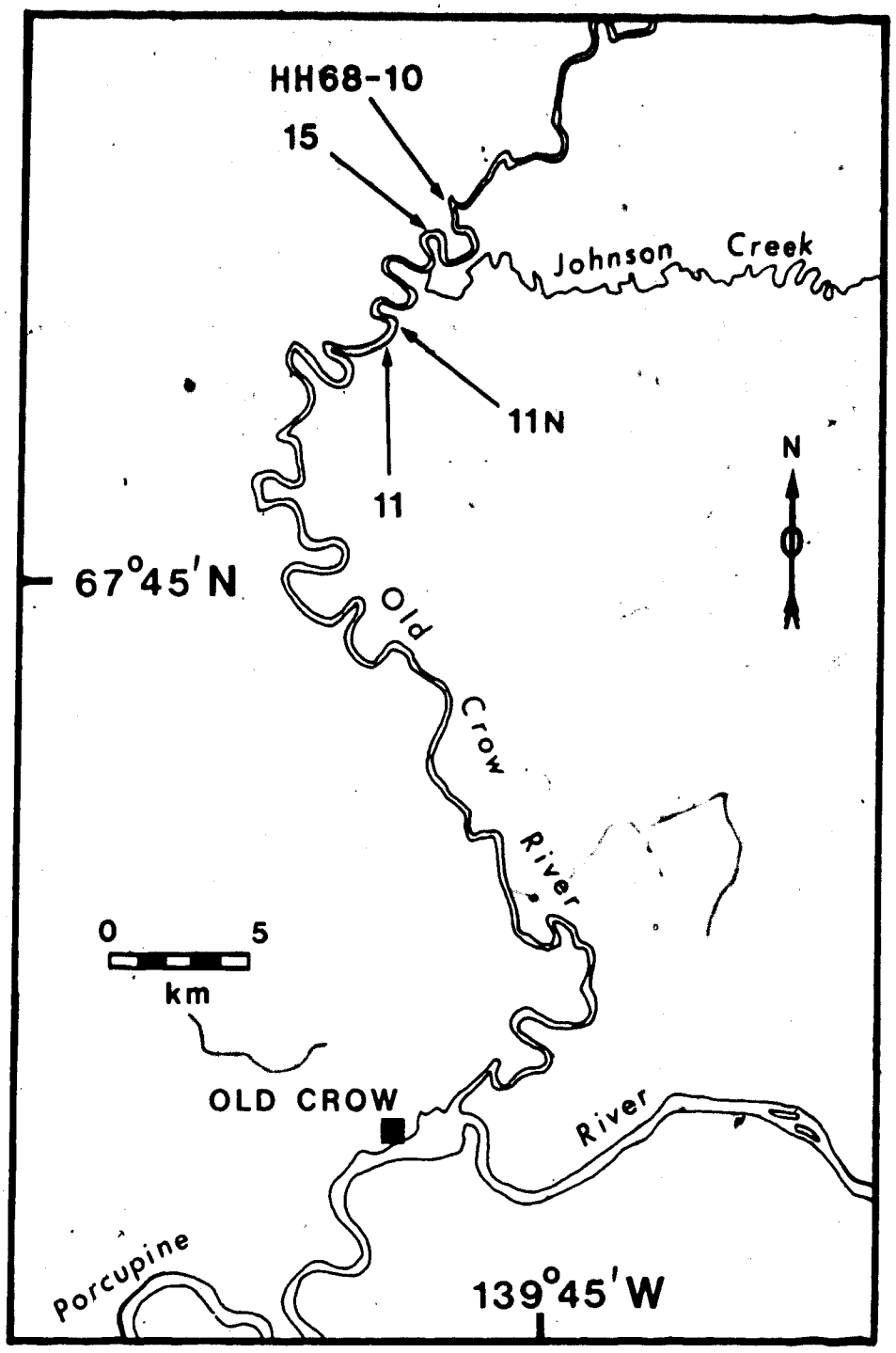

Figure 2-2: Location of sites 11 and 11N on the Old Crow River. Sites 15 and HH68-10 from Hedlin (1986) are also shown.

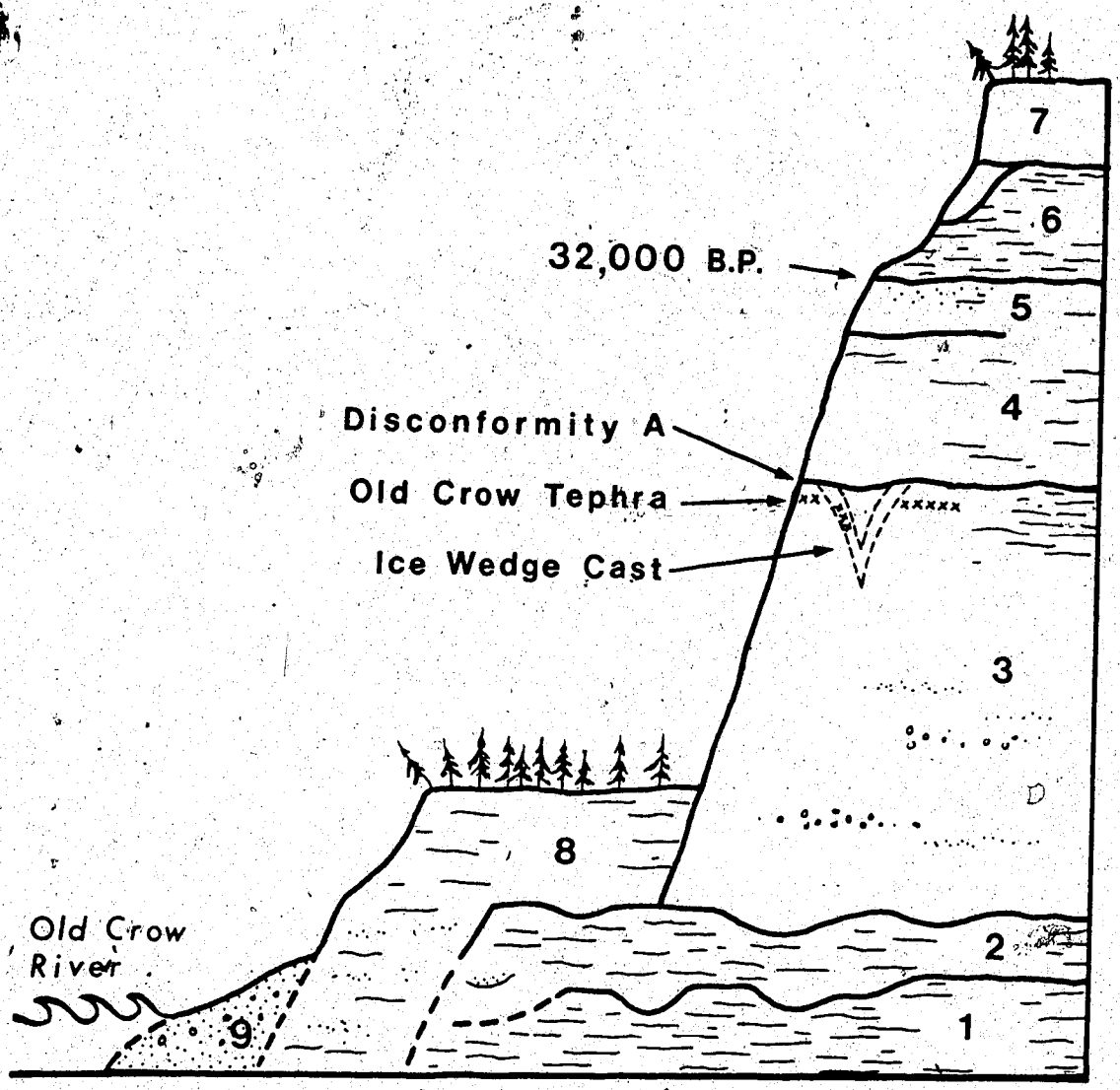

Figure 2-3: Composite stratigraphy of the Old Crow Basin. The numbers 1 through 9 denote the units as recognized by Morlan and Matthews (1978), the pertinent ones of which are described in the text.

necessarily represented at any individual site. Only four of the units (1,2,3 and 6) are present at sites 11 and 11N. The descriptions of these units by Morlan and Matthews are given below with additional detail from other pertinent studies where required.

Unit 1: Primary glacio-lacustrine clay, thought to be of Illinoian age.

Unit 2: Reworked glacio-lacustrine clay which may represent erosion and redeposition of unit 1.

Unit 3: Interbedded sands, silts and clays. In most outcrops, the upper bounding surface of this unit is disconformable and is referred to as disconformity A (Morlan, 1980). Below this level (generally a few tens of centimetres), an ash layer is sometimes found. This is the Old Crow Tephra which has a thermoluminescence age of 86,000 ± 8000 years B.P. (Westgate & Wintle, 1986). This age has inspired other researchers to look for evidence of the Blake Event (about 100,000 years B.P.) within unit 3 at various locations throughout the Basin (Hedlin & Evans, 1987; Westgate et al., 1985). The age of the Tephra is now under discussion, and is considered to be 149,000 ±13,000 years old (Westgate, 1988). The Old Crow Tephra is not present at sites 11 and 11N.

Cryoturbation features may be present near the top of this unit. At some other locations, volcanic ash is preserved in the slumped material present in ice wedge

casts.

Unit 6: Glacio-lacustrine clay, with age limit at base of 32,000 years B.P. (based on carbon 14).

Two vertical sections were sampled; one at site 11 (henceforth referred to as section KGA) and a second at 11N (section KGB). These sections are separated by a lateral distance of 500 m. Both sampled intervals start approximately 1 m below the contact between units 2 and 3 and continue upwards through the whole of unit 3. Section KGA spans a little more than 19 m of sediment and contains 318 samples for paleodirectional study and an additional 13 for susceptibility measurement and other purposes, while section KGB covers just less than 21 m, from which 308 paleodirectional samples were collected and an additional 2 for susceptibility. This makes a total of 641 samples of which 626 are for paleodirectional study.

Samples were collected using small plastic cubes (8 cc internal volume) which were inserted into the exposed sediments of the valley walls of the Old Crow River. Prior to cube insertion, slumped material was removed in order to obtain a fresh face. The bulk of the cubes were inserted by slowly pressing them into the sediment with the leverage obtained from a 2 m pole in order to minimize distortion of the samples, but in the more compacted material, the cubes were tapped in with a hammer (the direct blow of which was transmitted by a wooden block). Two samples were taken at each stratigraphic horizon, the horizontal distance between

them varying from 5 to 10 cm depending on brittleness of the sediments. Whenever possible, a 10 cm vertical spacing between sampled horizons was maintained.

Orientation was accomplished using a Brunton compass (used to measure strike) and a specially designed inclinometer, described by Hedlin (1986), which was used to measure dip and roll. Local magnetic declination was determined, from a total of 23 sun bearings, to be 033°26' azimuth with a standard error of the mean of 6'. After orientation, the cubes were removed from the face, and a lid was placed on each to minimize desiccation. Upon return to the laboratory, the samples were stored in a magnetically shielded room in which the ambient field is less than 50 nT (Reid, 1972).

III. NRM AND AF DEMAGNETIZATION RESULTS

NRM measurements were made on all samples from section KGA and KGB using a Schonstedt SSM spinner magnetometer. Magnetic moments were generally low (Figure 3-1), and consequently most samples were measured in either cart position 3 or 4 (position 4 being the closest to the sensor). The geometric mean of the NRM moments for sections KGA and KGB combined is 3.8×10^{-8} Am^2, which is low in comparison to that of most geological material measured in paleomagnetic studies (igneous rock and sedimentary rock averaging 2.8×10^{-5} Am^2 and 1.0×10^{-5} Am^2 respectively (Tarling, 1983)). The noise level quoted by the Schonstedt manufacturing company varies between 3×10^{-10} Am^2 and 1×10^{-10} Am^2 for the spin times used in this study. The quality of the NRM determinations was monitored throughout via the internal variance obtained from the spin sequence; each sample is spun around six axes, with two magnetic components measured each time, thus giving four estimates of each of the three orthogonal components (see Appendix A for details). Figures 3-2 and 3-3 show the NRM data for sections KGA and KGB respectively. In order to improve the reliability of these secular variation records, alternating field (AF) demagnetization was performed. The purpose of such treatment is to remove any secondary magnetic overprints which may be present. The presence of these overprints may be revealed by directional changes in the remanent magnetization (RM) vector during progressive

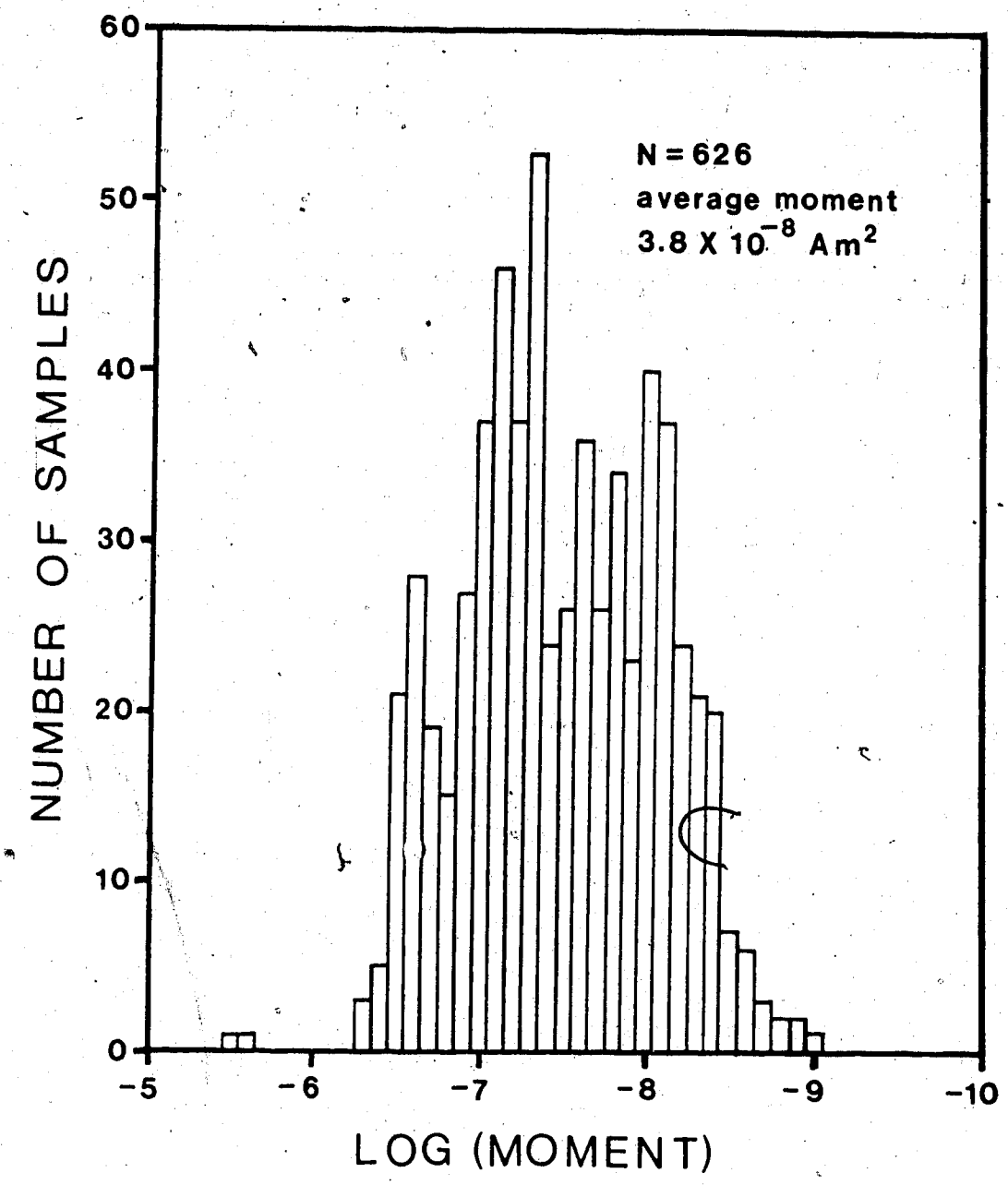

Figure 3-1: Histogram of NRM moments for sections KGA and KGB combined.

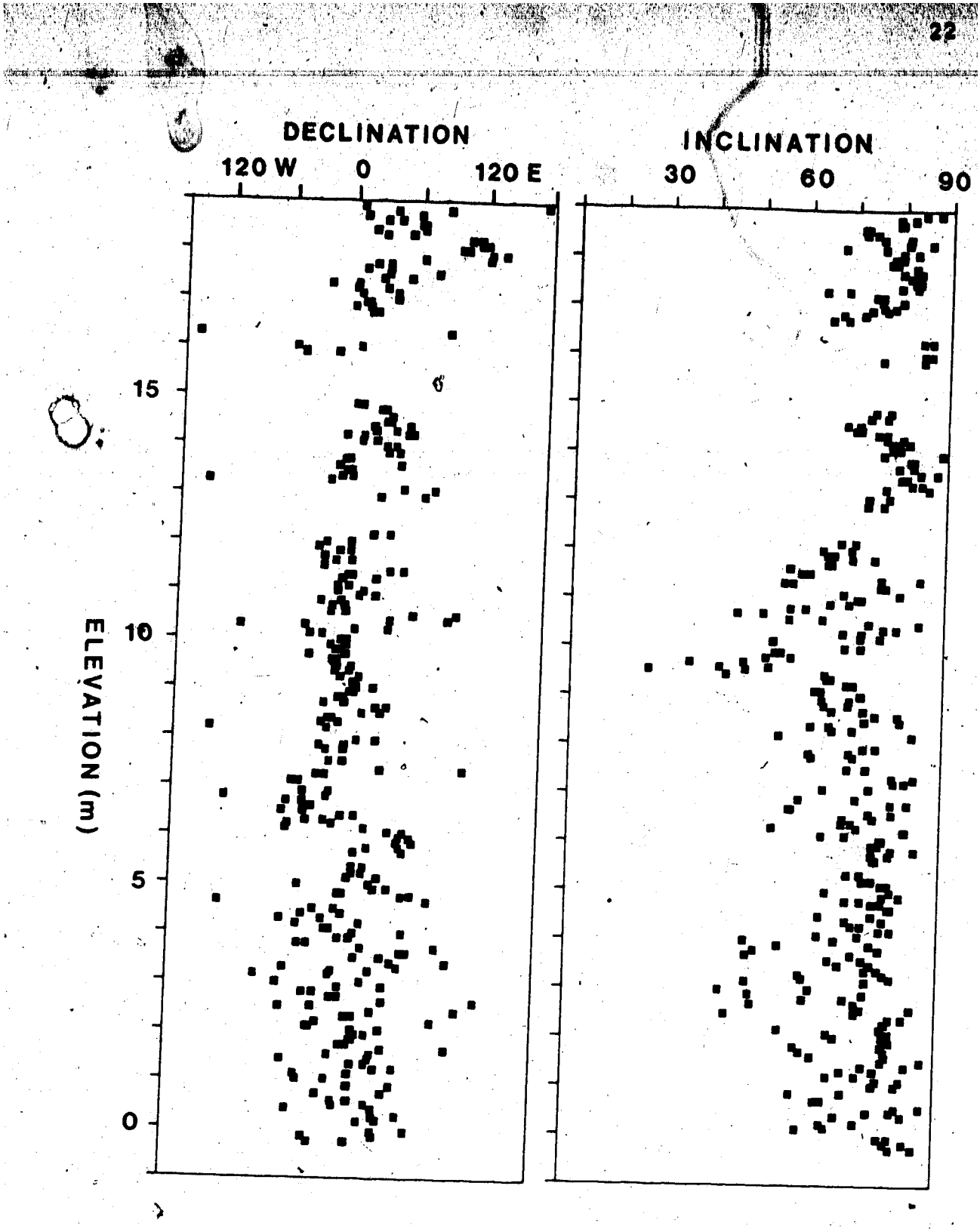

Figure 3-2: Magnetograms of NRM data for section KGA. Each square represents data from a single cube.

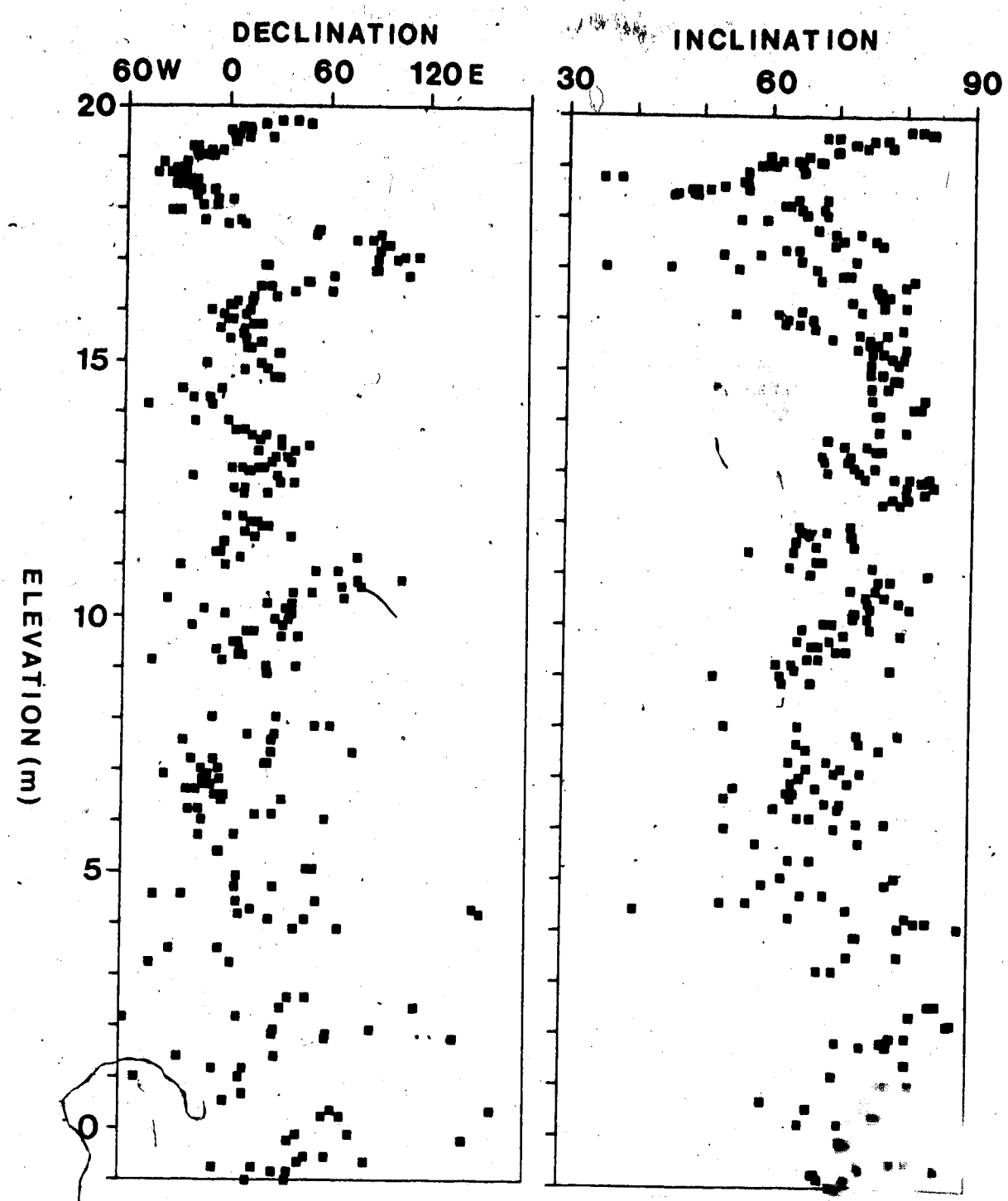

Figure 3-3: Magnetograms of NRM data for section KGB. [illegible] square represents data from a single cube.

demagnetization. In such cases, cleaning is deemed to be complete when the angular movement of the vector has stopped (McElhinny & Gough, 1963; As & Zijderveld, 1958). Twenty pilot samples were selected from sections KGA and KGB (10 from each) and subjected to detailed AF treatment with the goal of selecting the most effective peak field level for blanket treatment of the remaining samples. The equipment used was virtually identical to that described by Murthy (1969). Demagnetization steps were 0, 2.5, 5, 10, 15, 20, 30, 40, and 50 mT. A plot of normalized moment versus peak field is shown in Figure 3-4. The median destructive field (that field at which half of the original moment is destroyed) is 24 mT.

To assess changes in direction, the results from each sample were plotted on an equal area projection. This revealed that the bulk of the samples underwent little movement (only a few degrees) during the first few steps. After this level, some samples experienced large swings and became more difficult to measure, as their moments were quite low (less than 50% of their initial value) and the internal variance became large. This behaviour is demonstrated by sample KGA278 in Figure 3-5. The amount of movement seen between demagnetization steps depends on the size of the field increment. This can, to some extent, be compensated for by dividing the angular movement by the AF increment (Figure 3-6). This reveals a broad minimum between the 5 and 30 mT steps. Since the goal of demagnetization is

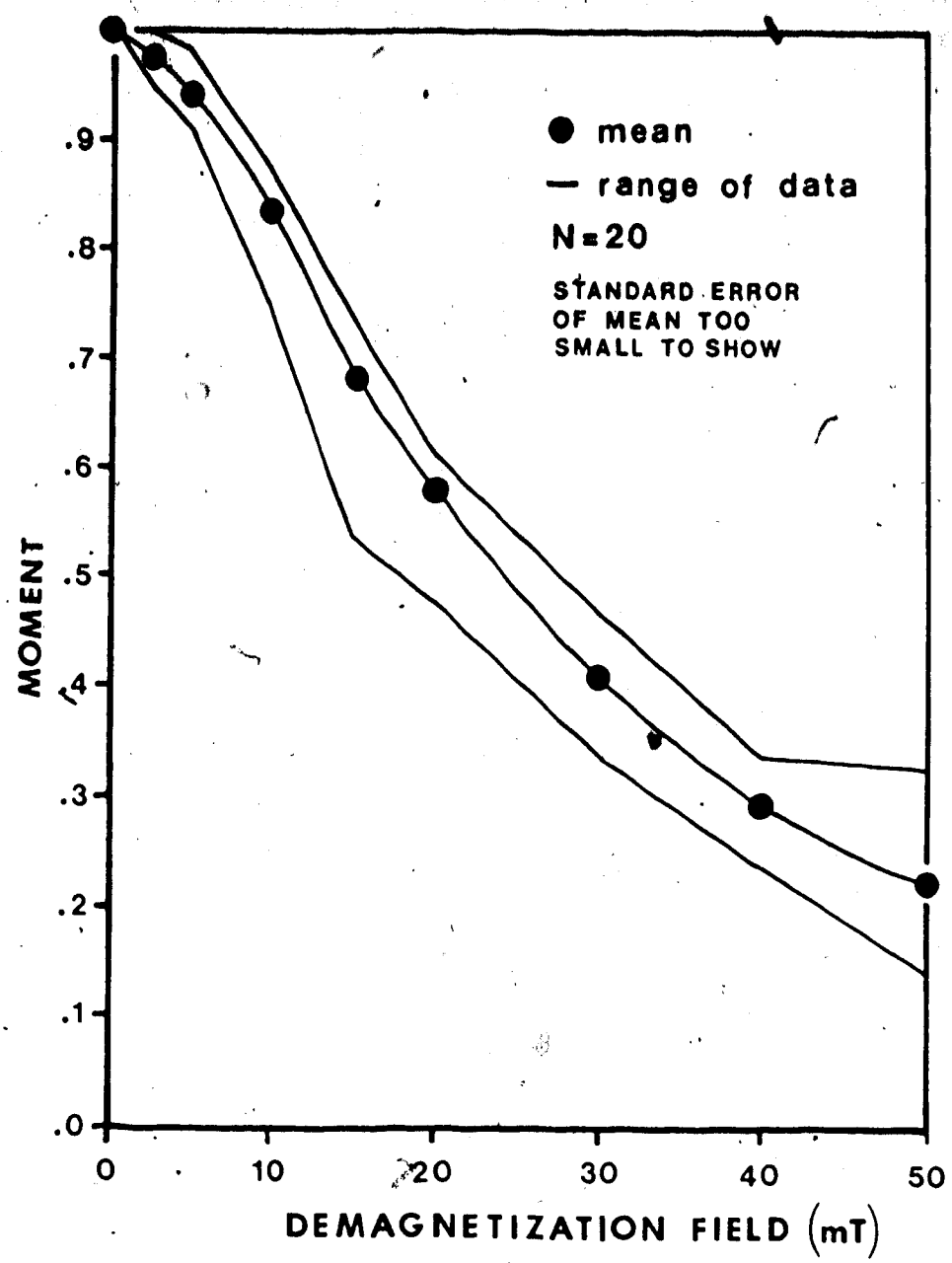

Figure 3-4: Normalized moment versus demagnetizing field (mT). Solid dots are average values of 20 data points. Solid bounding lines represent the overall range.

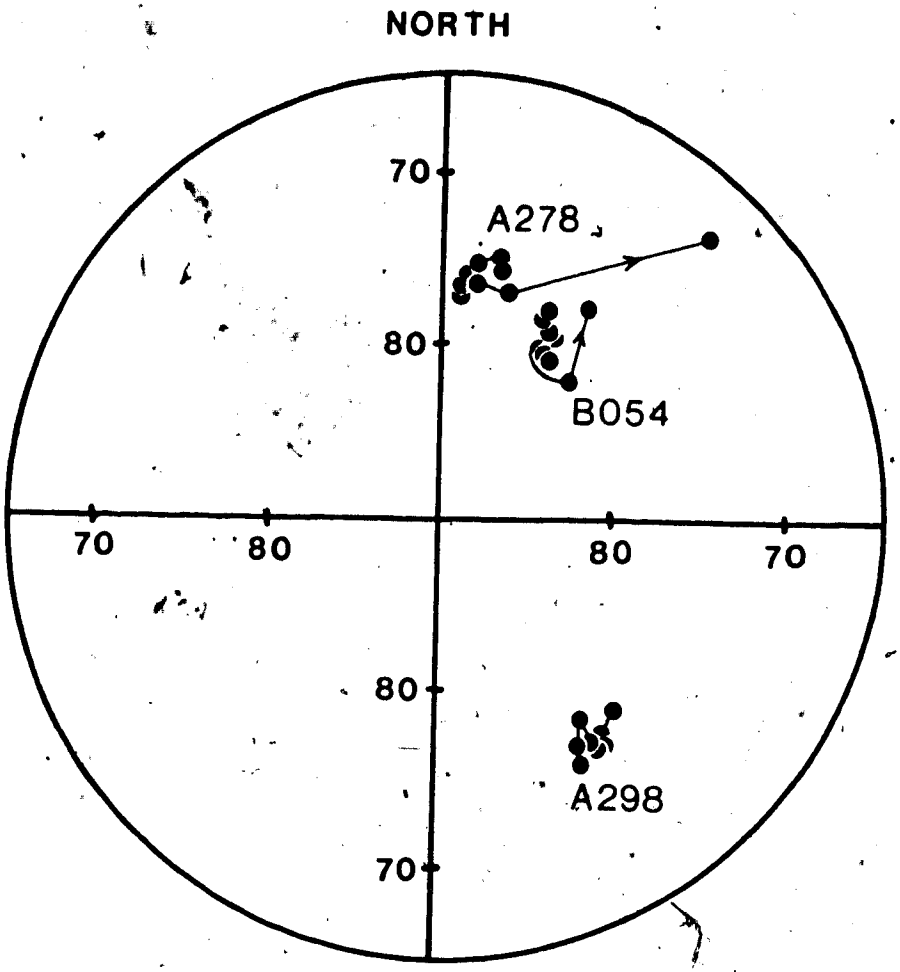

Figure 3-5: Typical pilot sample behaviour during demagnetization. (Equal area polar projection).

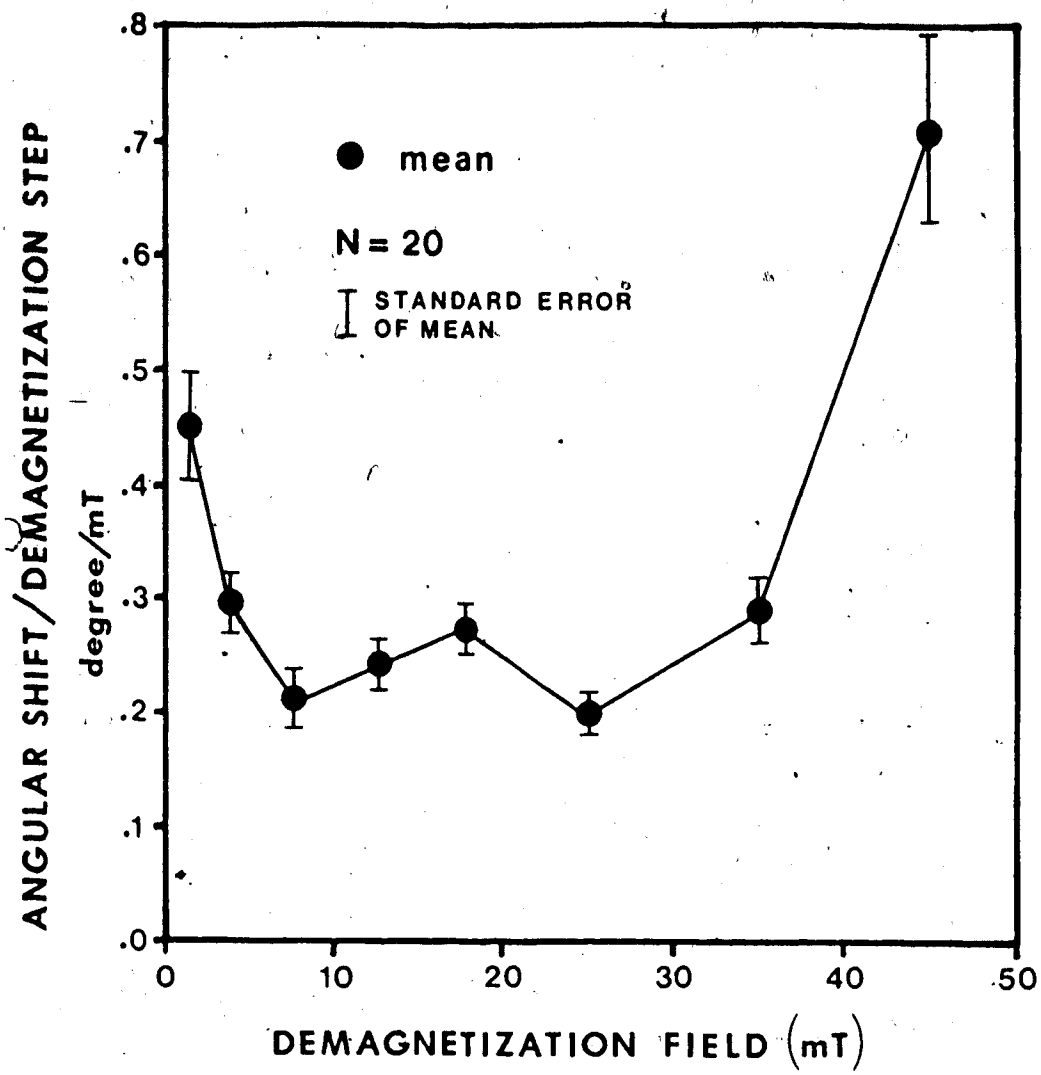

Figure 3-6: Angular shift between successive demagnetization steps normalized by increment of demagnetization field (degrees/mT). The solid dots are average values of 20 data points and are plotted at the midpoints between successive demagnetization steps.

to remove any secondary overprints with minimal degradation of the sample moment, it was decided to choose a peak value at the lower end of this broad minimum, and hence a peak field of 10 mT was selected for further blanket treatment.

During the initial stages of cleaning, it was noticed that the internal variance of most samples increased over their previous level for the NRM measurements. Large integration numbers (long spin times) were employed in an effort to bring down the internal variance of individual measurements and for some samples spin times of up to two hours were used. Even with this, many samples failed to improve, and some still got worse. It was therefore decided that some of the remaining samples were not of adequate quality to warrant this time-consuming treatment. The quality decreases towards the base of both sections, thus all samples in the zone 6 to 19 m from KGA, and those between 9 m and 21 m in KGB were demagnetized. Below these levels, only those pairs with promising initial internal variance were cleaned; this amounts to only 14 samples out of a total of 104 for KGA and 15 out of 106 for KGB.

Behaviour of the pilot samples predicted that any overprints would effectively be removed by the 10 mT alternating field and that the total movement during this treatment should be small (less than 10° as an arbitrary upper limit). The bulk of the samples behaved as expected, however the remanent magnetization (RM) vector of six specimens from KGA moved more than 10° during cleaning.

These samples were examined in detail by continuing the demagnetization process at 5 mT steps. Zijderveld plots shown in Figure 3-7 show movement towards the origin after 10 mT, suggesting that the characteristic RM has, in fact, been isolated by blanket cleaning.

The resulting declination and inclination profiles are illustrated in Figures 3-8 and 3-9. The strong similarity of these plots to their respective NRM counterparts confirms the previous assertion that the choice of 10 mT was not a critical one. Note that the data plotted are that which remained after an internal variance cutoff of 11° was applied (see Appendix A for details). Of the original 626 samples only 366 (59%) remain, 180 of the 260 rejected samples being lost at the base of both sections. This is a heavy price but worthwhile as the remaining secular variation sequences are of high quality.

The average vector removed during demagnetization may be found by examining the Fisher statistics of both the NRM and 10 mT data. In a Fisherian distribution, a group of directions is expressed as a vector mean direction with a confidence limit defined by a cone about this direction with semi-angle α. The most common level of confidence used in practice is the 95% level, hence this level is referred to as $\alpha 95$ (see Fisher, 1953; Watson, 1956).

The vector average for the 10 mT data of section KGA is declination (D) 350.5° and inclination (I) 72.3° with $\alpha 95$ of 2.1° (N=180), while the direction of the corresponding NRM

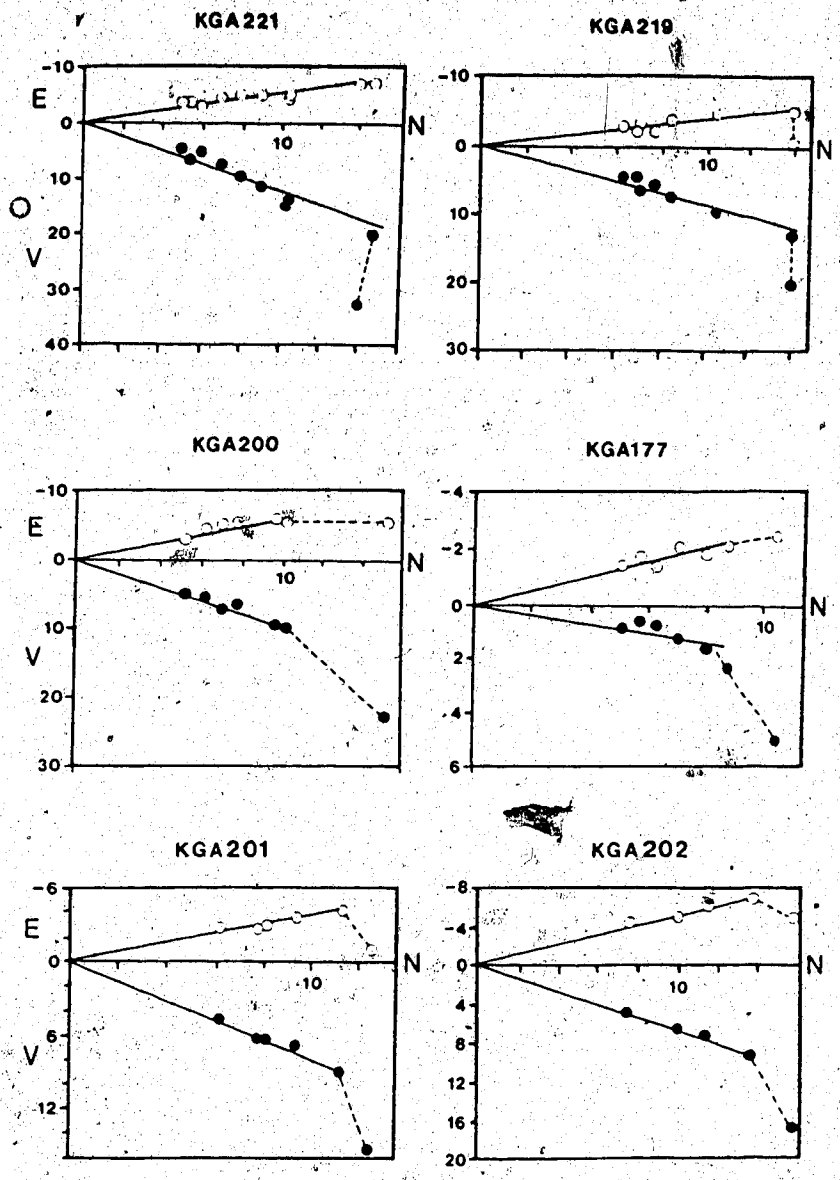

Figure 3-7: Zijderveld plots of further demagnetization performed on KGA samples the magnetizations of which moved by more than 10° during blanket cleaning of 10 mT. Points represent projections on orthogonal planes (labelled accordingly). The top box in each plot is the east-north (E-N) plane, while the bottom is the vertical-north (V-N).

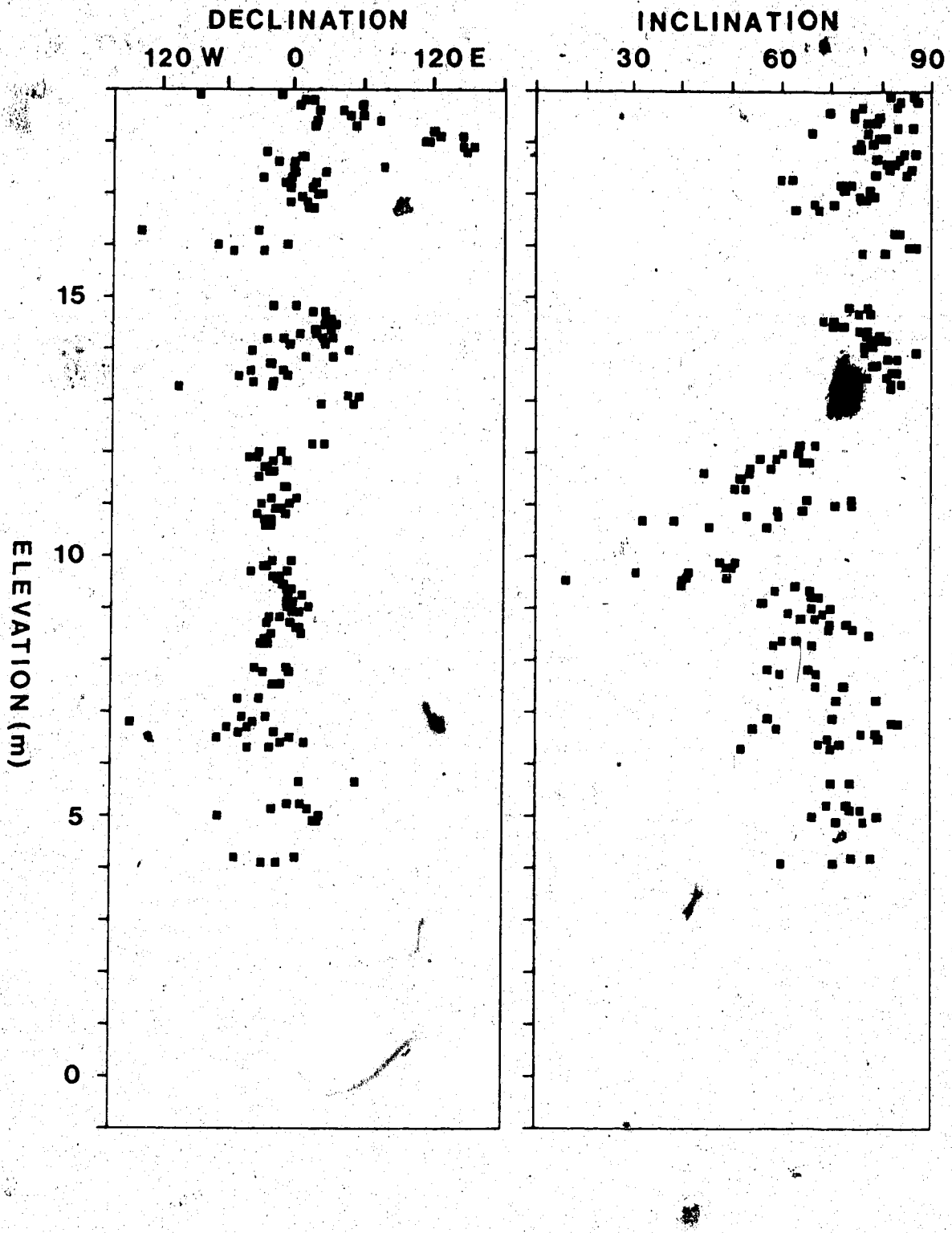

Figure 3-8: Magnetograms for 10 mT data from section KGA. Internal variance cut-off of 11.0° has been applied (see appendix A for details).

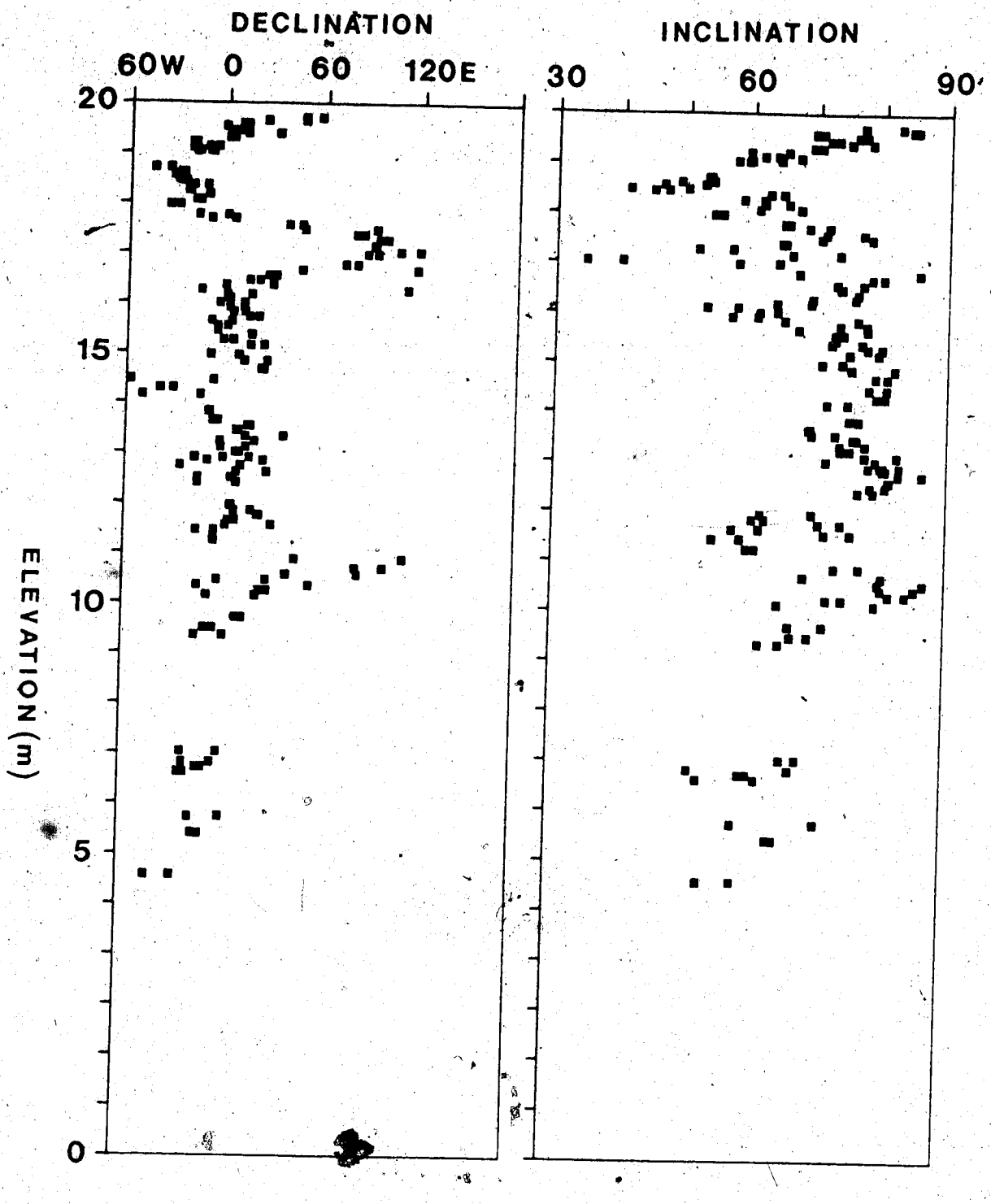

Figure 3-9: Magnetograms for 10 mT data from section KGB. Internal variance cut-off of 11.0° has been applied (see appendix A for details).

points is D=000.8° I=74.3° with $\alpha 95$ = 1.8° (N=180). This represents a general movement away from the present Earth's field (82° at 033°) of only 3.6°. This movement away from the present field suggests that this low coercivity component is a viscous overprint from the present day field at this site (Figure 3-10).

The vector average for the 10 mT data of section KGB is D=002.7° I=72.7° with $\alpha 95$ of 2.0 (N=186), whereas the corresponding NRM points give an average of D=009.5° I=73.2° ($\alpha 95$=1.9). As in the case of KGA, the movement is small (2.1°) and is generally away from the present field. Table 3-1 summarizes the statistics for KGA, KGB and both sections combined.

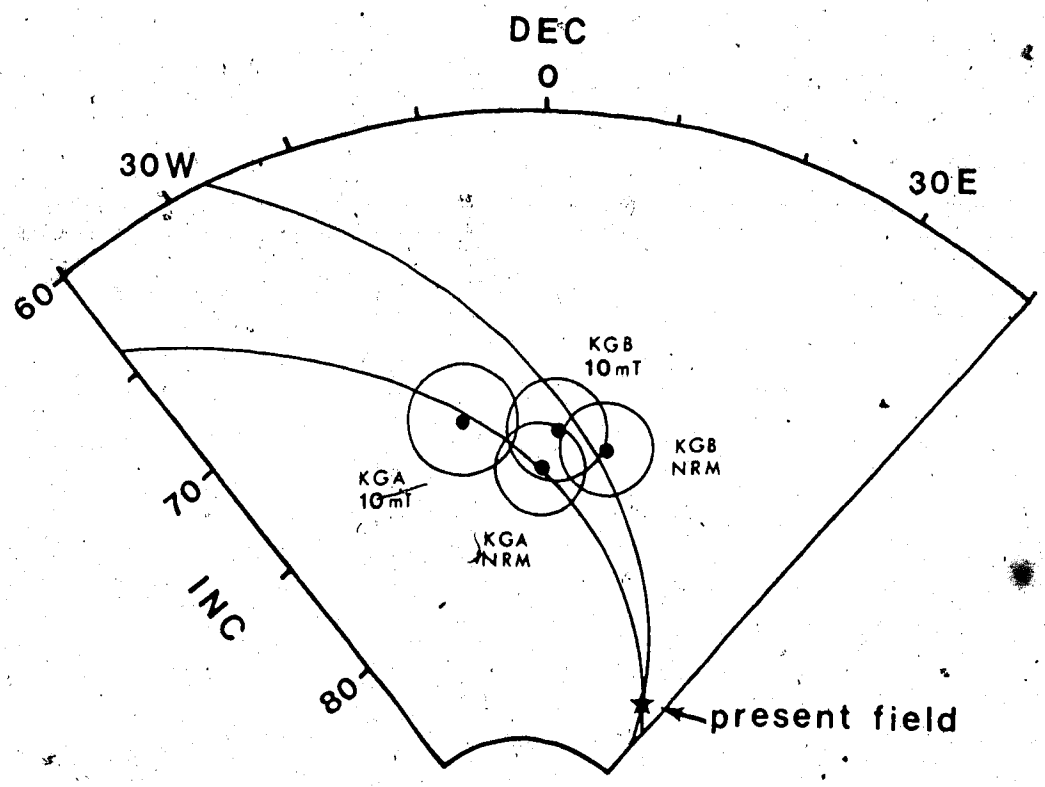

Figure 3-10: Vector averages for NRM and 10 mT data of KGA and KGB. The circles about the points are the associated $\alpha 95$, and the curves are great circles.

	DEC	INC	α95	N	MOVEMENT
KGA NRM	000.8	74.3	1.8	180	3.6
KGA 10 mT	350.5	72.3	2.1	180	
KGB NRM	009.5	73.5	1.9	186	2.1
KGB 10 mT	002.7	72.7	2.0	186	
KGA and KGB NRM	005.3	73.9	1.3	366	2.8
KGA and KGB 10 mT	356.6	72.6	1.4	366	

Table 3-1: Table of vector statistics for NRM and 10 mT data of KGA and KGB.

IV. DECLINATION AND INCLINATION OSCILLATIONS

A. Section KGA

The sampled sequence is a function of elevation, and although it is desirable to express the results as a function of time, this is not easily done. The age of the sediment is beyond the range of carbon dating and thus the organic fragments occasionally observed in the section cannot be dated by this means. Although a general rule of thumb is that clays take longer to be deposited than coarser material such as silt and sand, a reliable estimate of the exact time represented by a given thickness of sediment is virtually impossible . There is, however, one modification which can be made to the section to bring it closer to a true time series. Sand is generally deposited so rapidly when compared to silt and clay that it can be approximated as representing zero time, and therefore removed. Between 11 and 17 m there are, in fact, four sand layers, totalling 3.0 m as indicated in Figure 4-1. Also note that between the 10.3 m and 10.7 m marks there is a sequence of finely interbedded silt and sand layers (accented with a large hollow arrow). The sand layers here represent 40% of the thickness, and this interval was therefore compressed accordingly. The effects of these modifications on the magnetograms are shown in Figure 4-2. The features of interest are labelled A1, A2, A3, A4 and A5 (in order of increasing time), the divisions being more or less

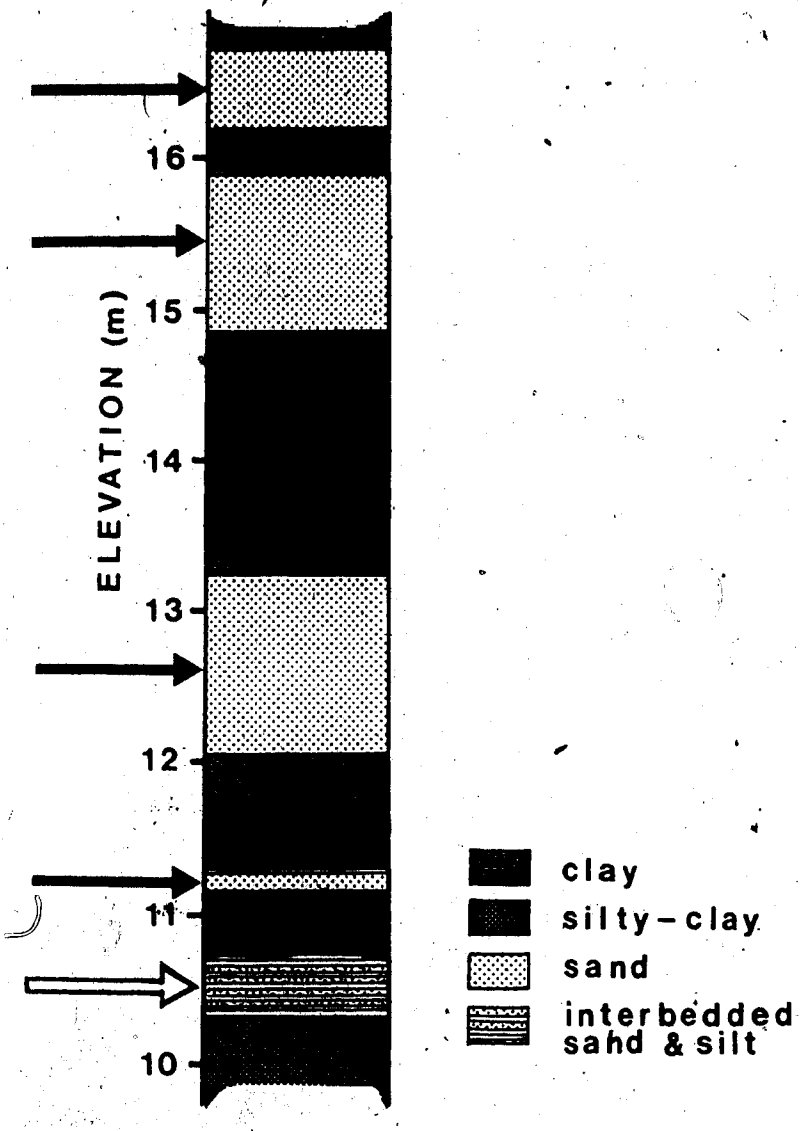

Figure 4-1: Lithology between 10 m and 17 m of section KGA. The solid arrows mark the sands to be removed. The hollow arrow highlights the zone of 40% sand.

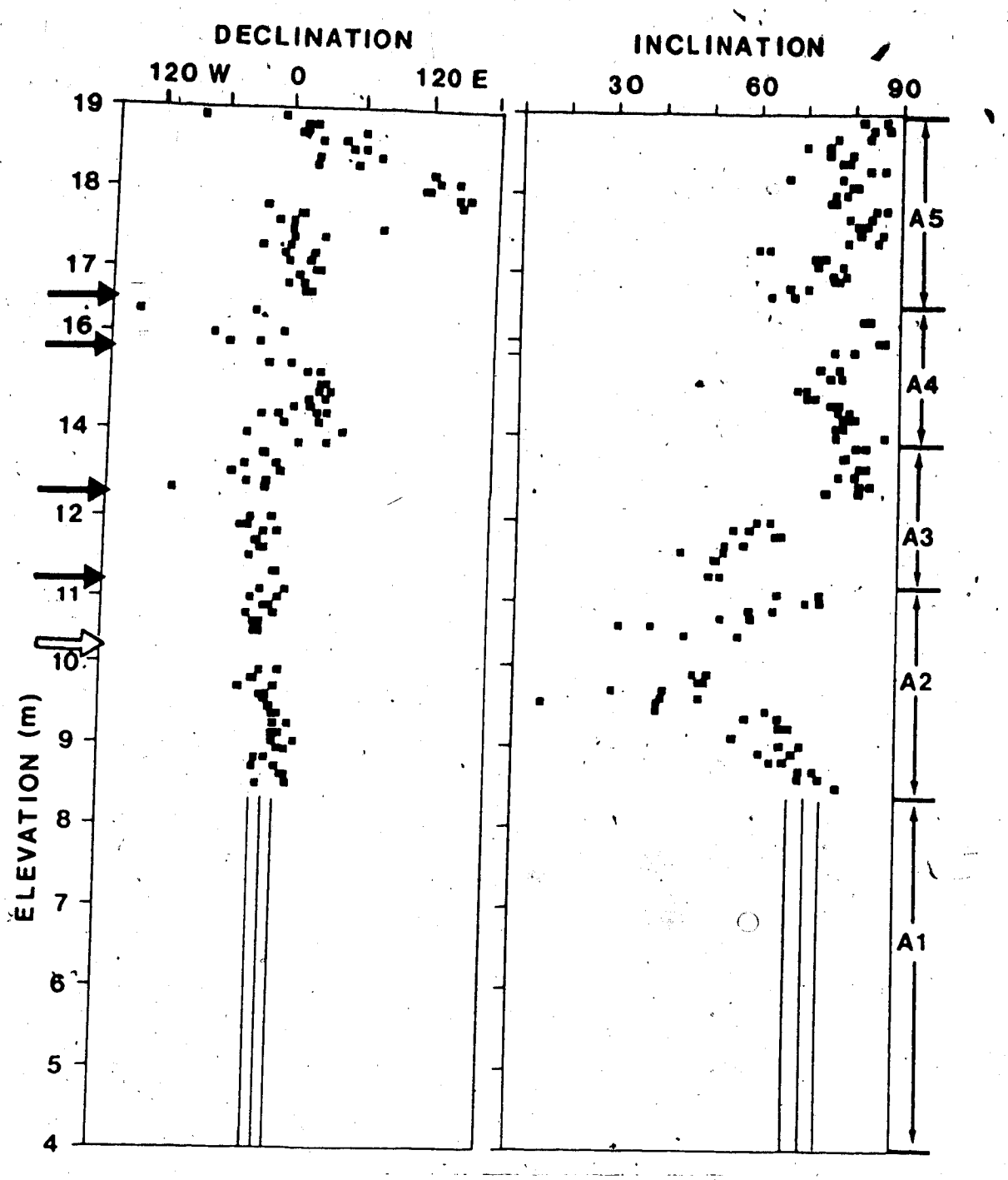

Figure 4-2: Expanded version of Figure 3-8 after removal of sand layers. The arrows of Figure 4-1 are indicated. Features of interest are labelled on the right.

arbitrary. Starting at the 4.0 m mark, we progress upwards through A1, the top of which is arbitrarily defined as the 8.4 m mark. The internal variance cutoff of 11° resulted in the rejection of 34 of the original 76 samples in this interval, leaving only 21 pairs over 4.4 m. Consequently, the resulting density of sampling is too low for investigation of secular variation and the data over this interval have simply been averaged as indicated (refer to Figure 3.8 for original data).

Feature A2 begins at the 8.4m mark and runs to 11.3m, a distance of 2.7m on this modified elevation scale. Magnetograms such as those in Figure 4-2 facilitate the recognition of individual features within the RM record, but in order to visualize the movement of the vector in three dimensions, equal area plots are more effective (Figure 4-3). Note that only those pairs in which the angular difference between individual pair members was less than 10° are plotted in Figure 4-3. The reasoning behind this need not concern us at this time and will be discussed later in this section. Suffice it to say for the present that, under enforcement of this criterion, only the highest quality data are preserved.

The character of the perturbation path for A2 (lefthand side of diagram) is a linear one, there being changes in inclination with relatively little change in declination. The shallowest direction attained is 35.3° at 22.8° west of north. This feature represents a large perturbation

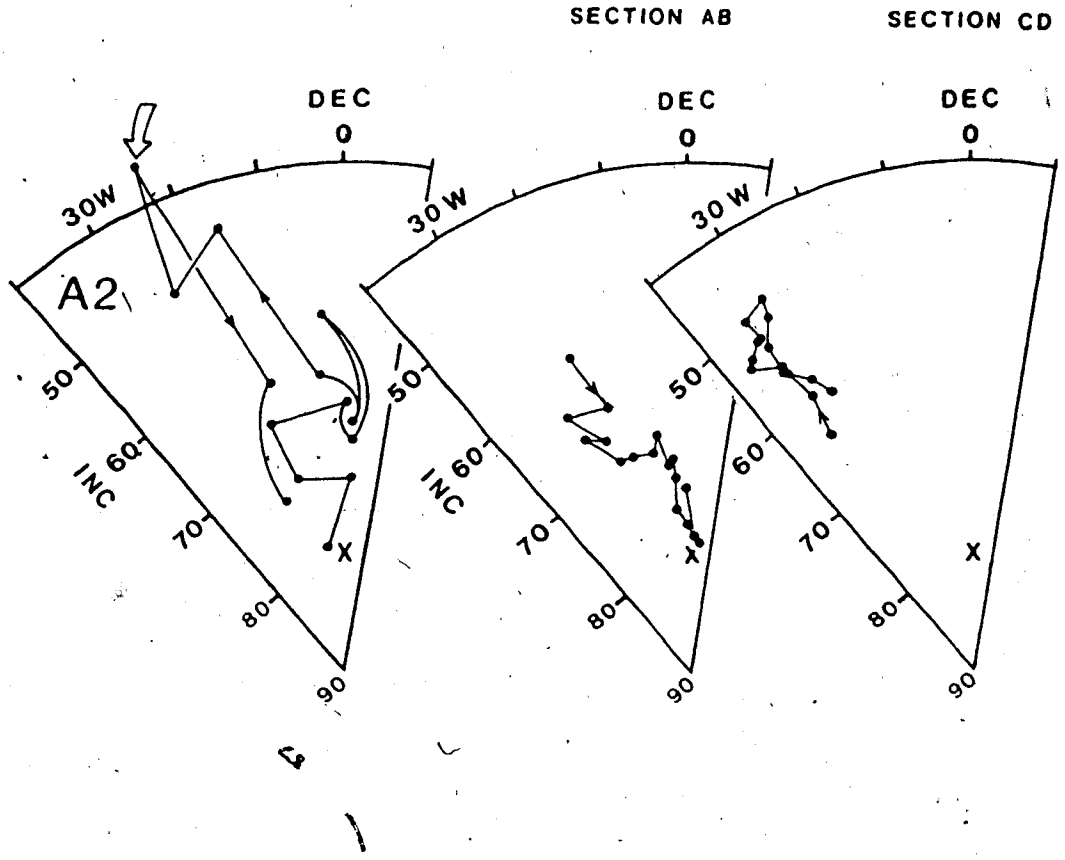

Figure 4-3: Declination-inclination equal area plots of feature A2 (unsmoothed). Internal variance of 11.0° (see Appendix A) and within-pair dispersion cut-off of 10° have been applied. The "X" marks the position of the field vector due to an axial geocentric dipole. Each point represents the average of a pair of samples. Corresponding features from previous work (Evans et al., 1988; Hedlin and Evans, 1987; Hedlin, 1986) (5 point running mean) are included. The curved hollow arrow represents the perturbation point used in modelling.

(approximately 40°) of the local field away from the direction predicted by an axial dipole field (shown by the "X"). The reality of this feature is confirmed by the presence of corresponding features (shown on right hand side of Figure) in two outcrops over 5 km away (sites 15 (AB) and HH68-10 (CD) from Evans et al (1988), sampled by Hedlin (see Figure 1-3)). As stated by Turner (1983), the supreme test of the reality of a feature in an RM sequence is reproducibility in outcrops separated by large distances. This test is rarely successful in practice and it is commonly observed that for every signal found in a single outcrop there are many outcrops in the surrounding area in which it cannot be found. For instance, Palmer et al (1979) had trouble correlating fine features in their lake sediment RM records even over 1 km. A successful correlation of the feature A2 with signals over 5 km away confirms the idea that the perturbing source is a true geomagnetic field variation and not simply a local sedimentological effect.

Next we encounter A3, which represents a return to steep inclinations from shallow values of roughly 50° (shallowest value is 49.0° at 19.2° west of north). The outward trajectory is not represented, its absence being attributed to a break between A2 and A3. There is a sudden jump in inclination of about 20° which suggests that some time is not represented here. The end of this feature is defined as the point at which the field has returned to steep inclinations and is arbitrarily taken as 14.0m. The

equal area plot of Figure 4-4 reveals that the perturbation path for A3 is also linear, and again we are able to find correlatable features at sites 15 and HH68-10.

Between 14.0 and 16.5 we find A4. This feature (Figure 4-5) can be convincingly correlated with an easterly shallowing of the geomagnetic field which occurs between -11.0 cm to +50.0 cm in section AB of Hedlin and Evans (1987). On this modified elevation scale, feature A4 spans a thickness of 1.8m which is approximately 3 times that of the corresponding feature in section AB, reflecting a difference in sedimentation rate. The Old Crow Tephra, which is present in section AB, occurs by chance at the point of maximum perturbation. Thus the point of shallowest inclination in A4 (14.6m) is taken to represent the time of deposition of tephra in the Basin as a whole, although it does not appear to have been preserved in section KGA. Susceptibility measurements were made on Hedlin's samples from sites 15 and HH68-10 and revealed that the Old Crow Tephra is present not only visually at these sites, but also as a susceptibility maximum (Evans et al., 1988). If the Tephra is present in a cryptic form it may manifest itself as a susceptibility increase. In order to test this, low-field susceptibility measurements were made of all samples from KGA using a Conservation Instruments Susceptibility meter type M.S.1 with sensor type M.S.1.B. Calibration with eight paramagnetic salts showed that the instrument behaved linearly over the range of interest (Figure 4-6). Figure 4-7

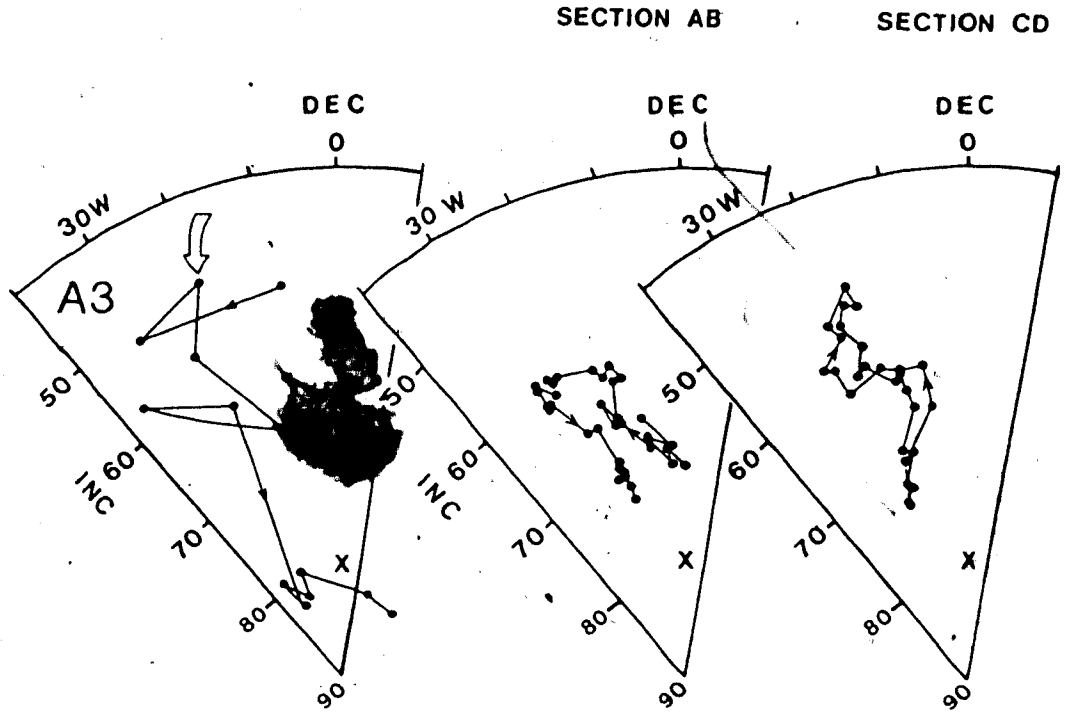

Figure 4-4: Declination - inclination equal area plot of feature A3 with corresponding features from previous work (see Figure 4-3 for full explanation).

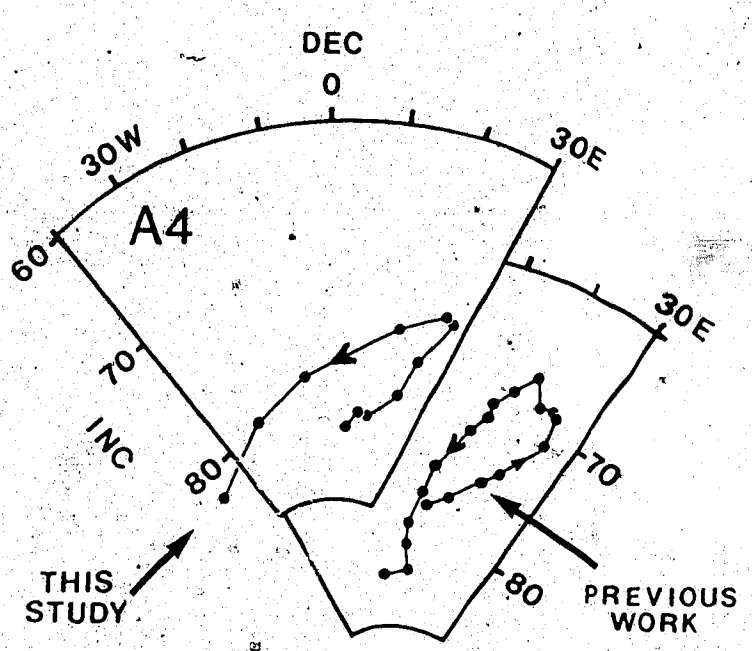

Figure 4-5: Declination-inclination equal area plots for A4 (3 point running mean) and corresponding feature from -11.0 cm to +50.0 cm mark of previous work (Evans et al., 1988; Hedlin and Evans, 1987; Hedlin, 1986) (5 point running mean).

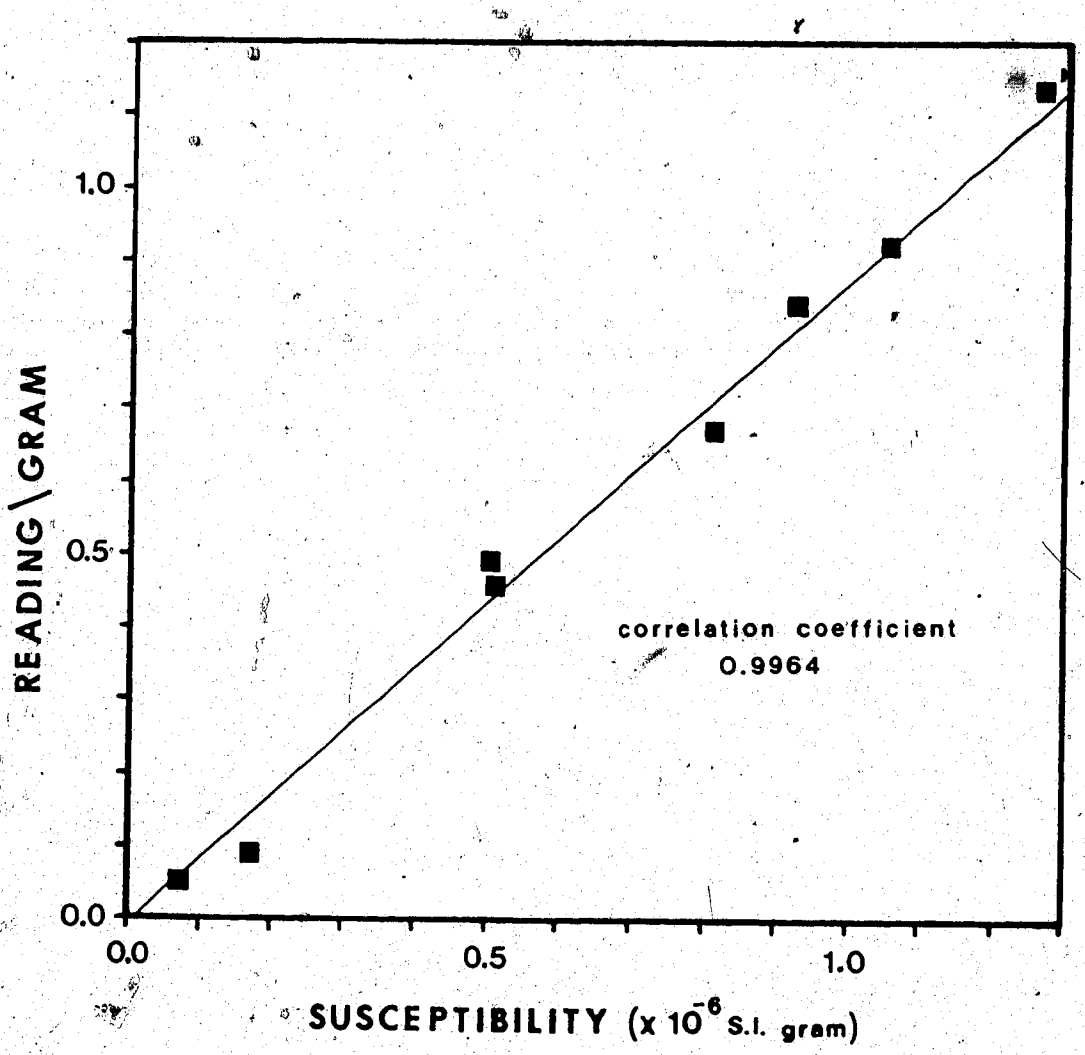

Figure 4-6: Calibration curve for Conservation Instruments M.S.1 susceptibility meter.

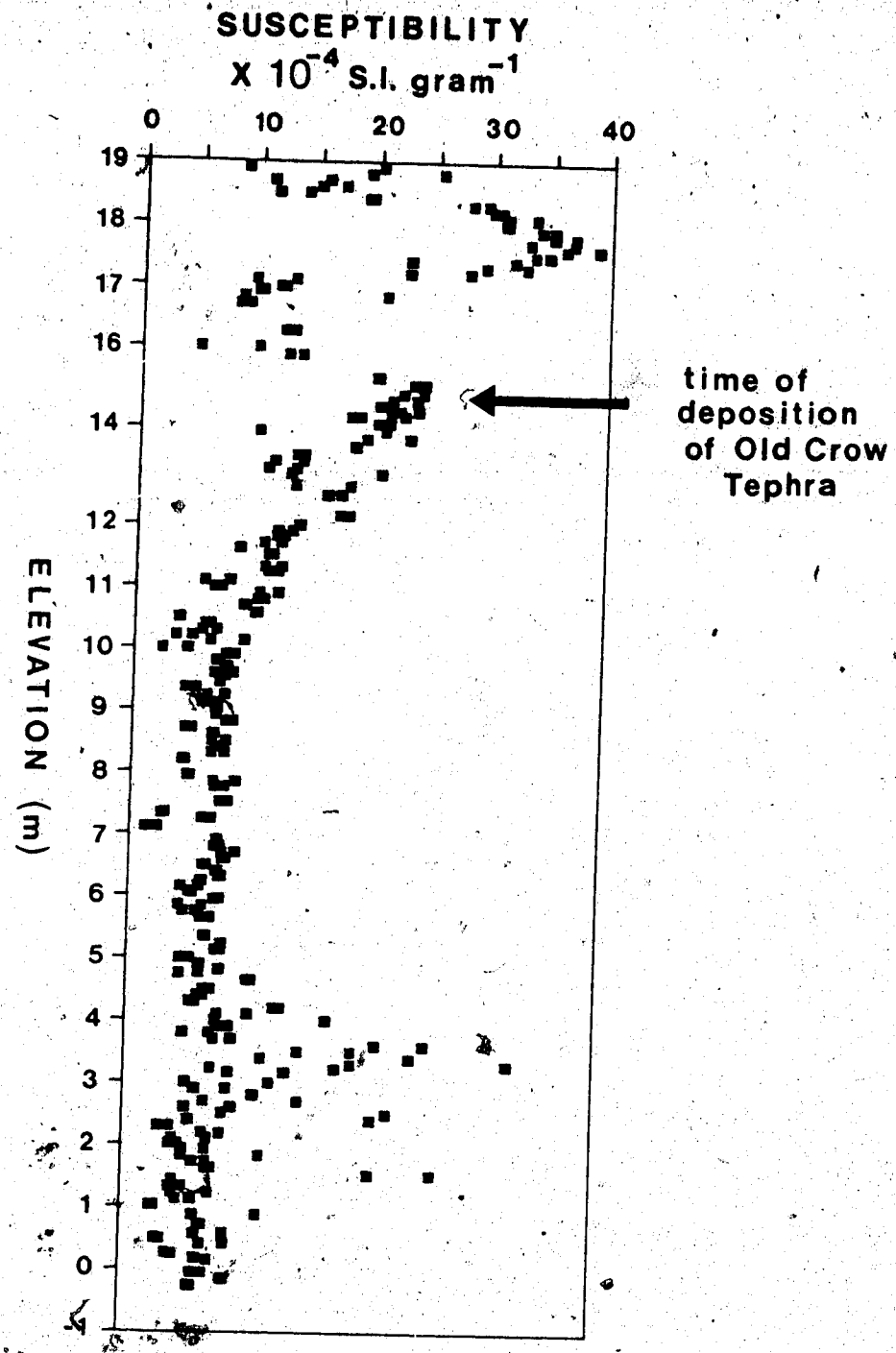

Figure 4-7: Susceptibility versus elevation for section KGA. The elevation thought to represent the time of deposition of the Old Crow Tephra in the Basin is indicated.

shows the results plotted against elevation, with the presumed time of deposition of the Old Crow Tephra indicated. There is indeed a significant increase in the susceptibility around this point, but further work involving a search for chemical evidence would be required to verify its existence.

The reality of A2, A3 and A4 is confirmed by the fact that corresponding features exist in the records recovered from sites [illegible]68-10 by Evans et al (1988), and also by the fact that all correlatable features occur in the same order in each record. Furthermore, these cannot be perturbations introduced by the method of sampling. Sampling of soft sediment with plastic cubes using the method described in chapter II has been shown to produce a "push error" in some cases, i.e., a magnetic component seems to be added in the direction of cube insertion (Lovlie, pers. comm., 1988). Such a mechanism could not have produced the shallowing seen here since the declination of these features in roughly north, while the direction of push is predominantly east. In addition, the corresponding features in section AB were recovered from cubes which were pushed to the west, the opposite direction of that involved in collecting section KGA, yet the declination of all features is virtually identical. These facts attest to the fidelity of the sediments in this region as good recorders of geomagnetic field variations.

Feature A5, which overlies A4, is a perturbation of the RM vector to the east of south. The most extreme value attained is 149.2° declination and 75.4° inclination. This feature is illustrated in the equal area plot of Figure 4-8. Unfortunately, a great deal of faith cannot be placed in the orientation of this feature in space since these beds may have been distorted. The sediments containing this feature are divided from the horizontal beds below it by a sharp high angle plane of discontinuity. Although the beds containing A5 are massive clay and contain no indications of horizontal, the beds immediately above this zone are deformed and tilted to the south-east in what appears to be an ancient slump. This massive clay may have been involved in the deformation and thus may be responsible for the south-east orientation of A5.

At this point we return to the reasoning behind the plotting of only those pairs in which the angular difference between the two RM vectors of individual members of sample pairs was less than 10°. If members of a pair represent the same point in time, their directions of magnetization should agree. This is referred to as the within-pair dispersion, and was applied by rejecting any pairs for which the angular separation in space between members exceeded 10°. Hedlin and Evans (1987) arbitrarily used a value of 10°, noting that this is a very strict criterion (the angle between a pair of vectors must exceed 26° before they can statistically be considered at the 95% level to be from a random population).

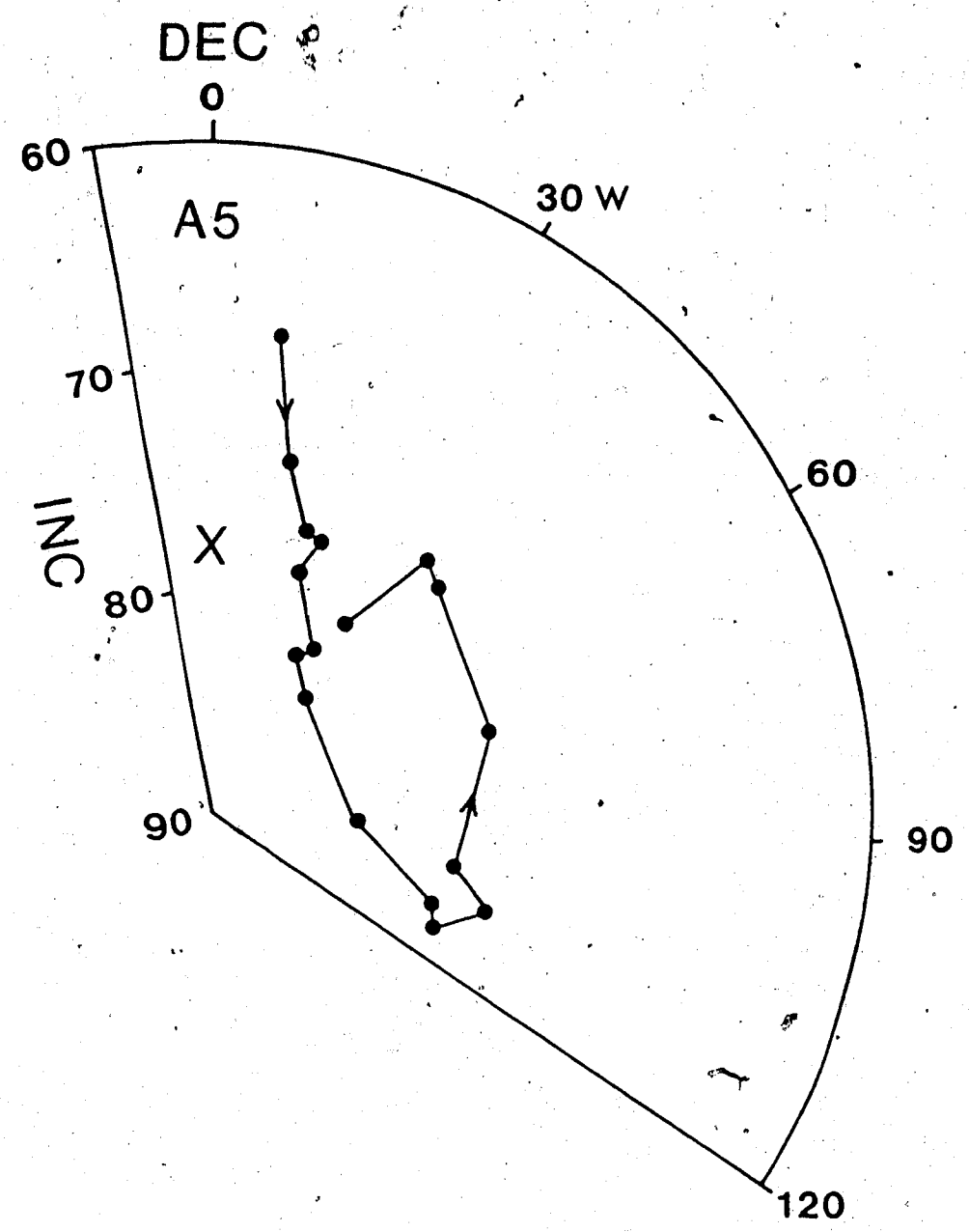

Figure 4-8: Declination - inclination equal area plot of feature A5 (3-point running mean). The "X" marks the position of the field vector due to an axial geocentric dipole.

Application of this filter to A3 resulted in rejection of only a single pair (for which the angular separation was 16.5°), thus in this case, we need not consider further the ramifications of this quality criterion on the character of that feature. Similarly, A4 loses only 2 of its original 13 pairs (within-pair separations of 13.5° and 16.5°) and A5 loses 4 of 23 of which no pair rejected showed a within-pair separation exceeding 11.6°.

By contrast, A2 lost 7 of its original 21 pairs. Consequently, we examine in greater detail the effect of the within-pair dispersion cut-off of 10° on this feature. The pairs rejected have angular separations varying from 10.7° to 27.1°. If the basic assumption that the members of a sample pair represent the same point in time is violated, this criterion is no longer applicable. In such a case, angular discrepancies may very well be due to secular variation processes, not error in recorded field direction. Slight misalignments in elevation are possible, since the measured elevation is only accurate to ± 0.5 cm at best. High temporal 1st derivatives of the geomagnetic field direction and/or slow deposition rates will yield zones of high spatial 1st derivative in the remanence signal. In such intervals, it may be necessary to relax the within-pair dispersion criterion. The question of how much to relax is a difficult one. It is best approached by totally lifting the filter and observing the consequences. Figure 4-9 shows the outcome. The important point is that the essential

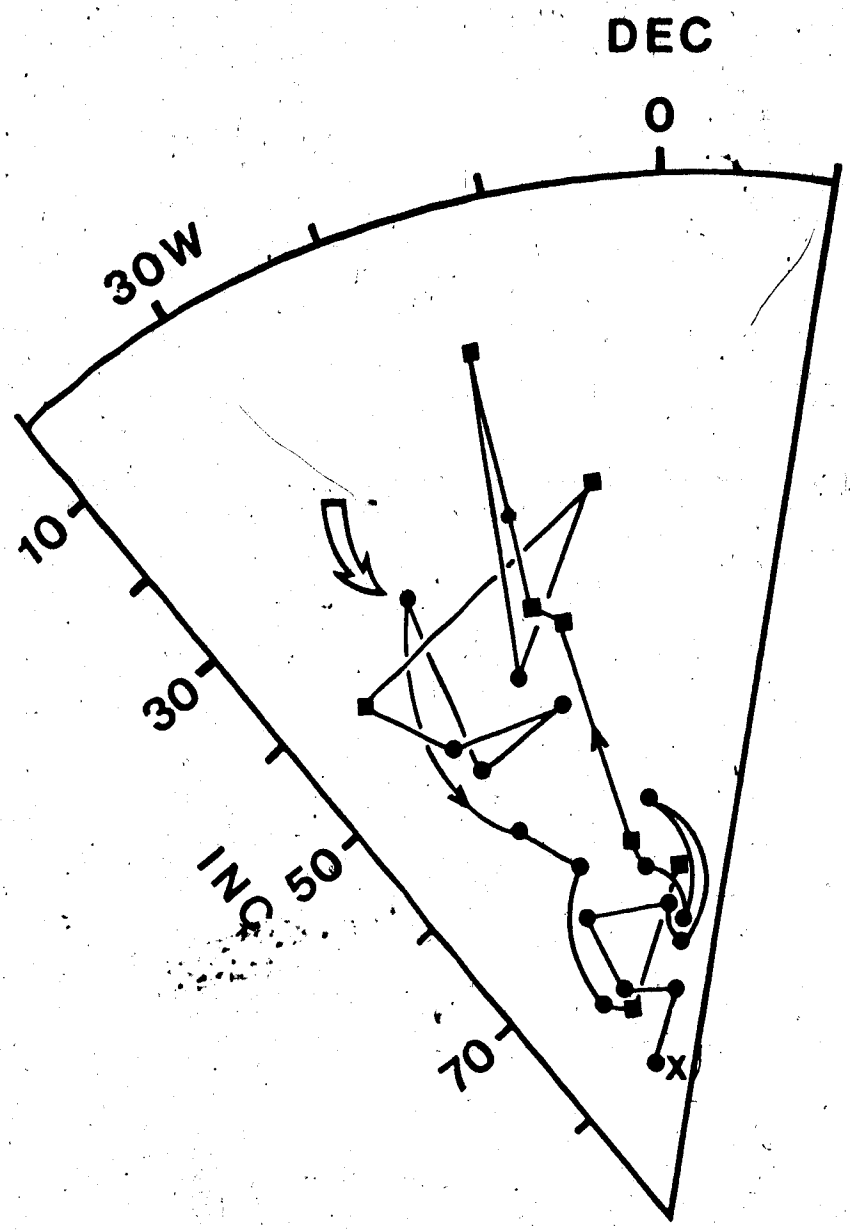

Figure 4-9: Declination-inclination equal area plot for A2 with in-pair dispersion criterion removed. Individual members of pairs with angular separations of greater than 20° are plotted as squares. The new points with angular separations of greater than 10° but less than 20° are averaged and plotted as circles for the sake of clarity. The squares are joined with the lines which represent the minimum path length. The curved arrow marks the position of the previous minimum in inclination from figure 4-3.

characteristics with respect to the pattern of movement of the geomagnetic vector remains unaltered, but the feature is reinforced by the added points. The only change which results is the extension of the signal to shallower inclinations (16.5° at 12.5° west of north). For comparison the position of the previous extreme is indicated.

Feature A1 also suffers under the within-pair cutoff of 10°, losing 12 of its original 21 pairs. The average of all vectors is declination 340.1° and inclination 71.1° with $\alpha 95$ = 3.3°. Removal of all pairs which do not meet the within-pair cutoff yields an average of declination 346.5° and inclination 71.5° with $\alpha 95$ of 3.6° which is not statistically different from the average of all samples in A1 at the 95% level. Thus the final result remains the same.

B. Section KGB

Adjustments to elevation for two sand layers between the 8 and 10 m marks (total thickness 1.3 m) were made as was done for section KGA. The resulting sequence is shown in Figure 4-10, with the arrows on the left marking the positions of the removed sands and the features of interest indicated to the right. In section KGA features A2, A3 and A4 could be confidently correlated with signals reported by Evans et al., (1988). A similar sequence of three features can be identified in section KGB. B1 (from 4.0 m to 11.0 m, a thickness of 5.7 m on this modified elevation scale), B2

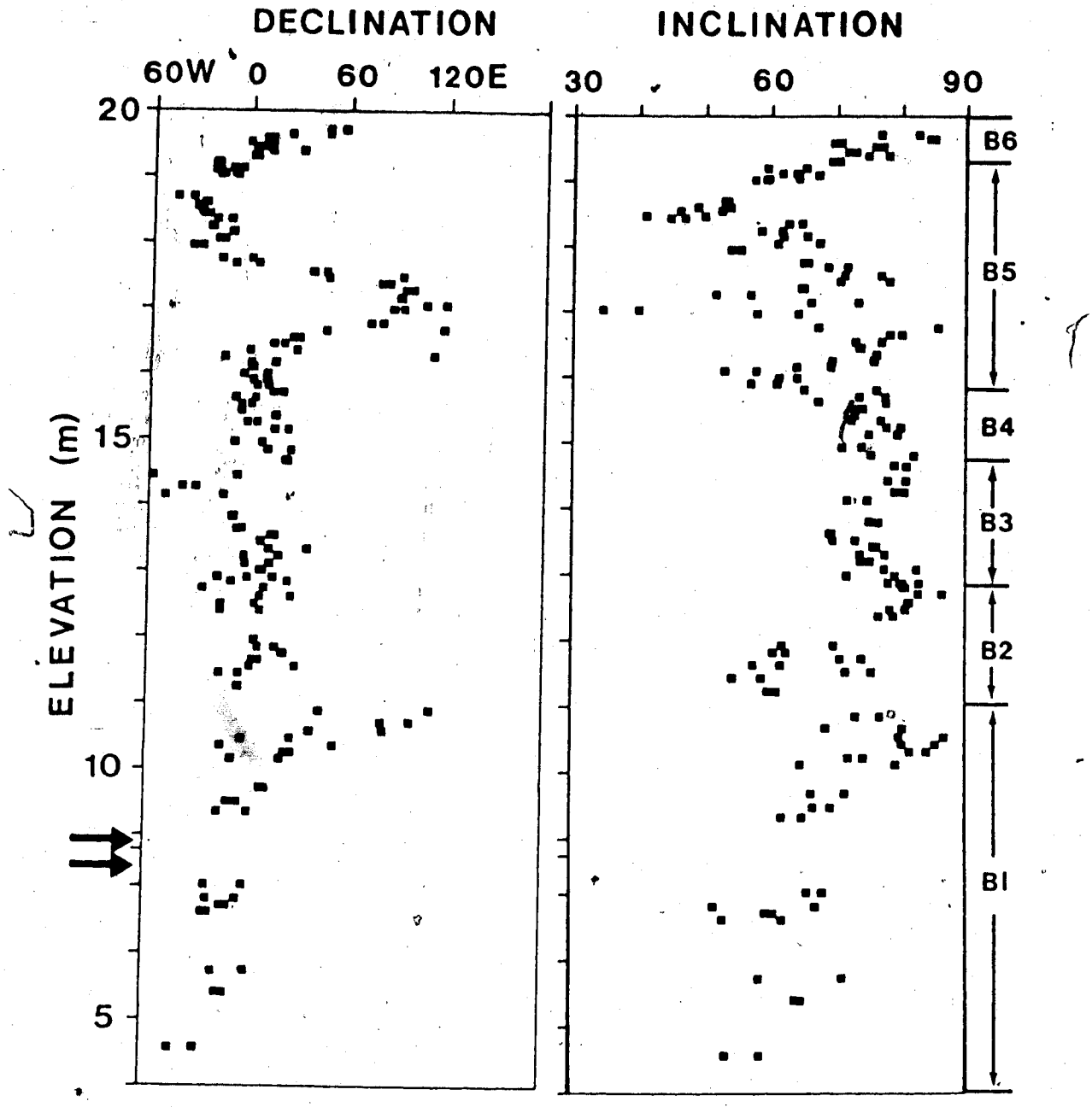

Figure 4-10: Expanded version of Figure 3-9 after removal of two sand layers (indicated by the horizontal arrows). Features of interest are labelled to the right.

(11.0 m to 12.87 m) and B3 (12.87 m to 14.5 m) are replotted on the equal area plots of Figure 4-11, with the corresponding signals from the sequence reported by Evans et al. Note that the increased noise level requires that some smoothing be done; the 3 horizon (6 samples) running mean is plotted here. Admittedly, at first glance the correlation is not as strong as it is for A2 to A4. The similarity of any individual signal with its counterpart is not as good here, as for example the case of B2 where the shallowing of the vector trends northward rather than west of north. In addition, only the return trajectories from positions of shallow to steeper inclinations are represented here by B1 and B2. However, the fact that three similar features in KGB appear in the same order and at approximately the same elevations as those in KGA makes the correlation more convincing. Section KGB thus provides useful supporting evidence for the reality of the geomagnetic features evident in KGA and in the work of Hedlin (1986).

Features B1, B2 and B3 are taken from a zone of horizontal bedding. Above B3 we encounter two intervals of tilted strata. The first of these is labelled B4 and runs from 14.5 m to 15.8 m. The dip of the strata is 29° west with a strike of 162° azimuth. Figure 4-12 shows the pattern of movement on an equal area plot with no tilt correction applied. There is no interesting pattern of movement to this signal and as a consequence, it is not discussed further.

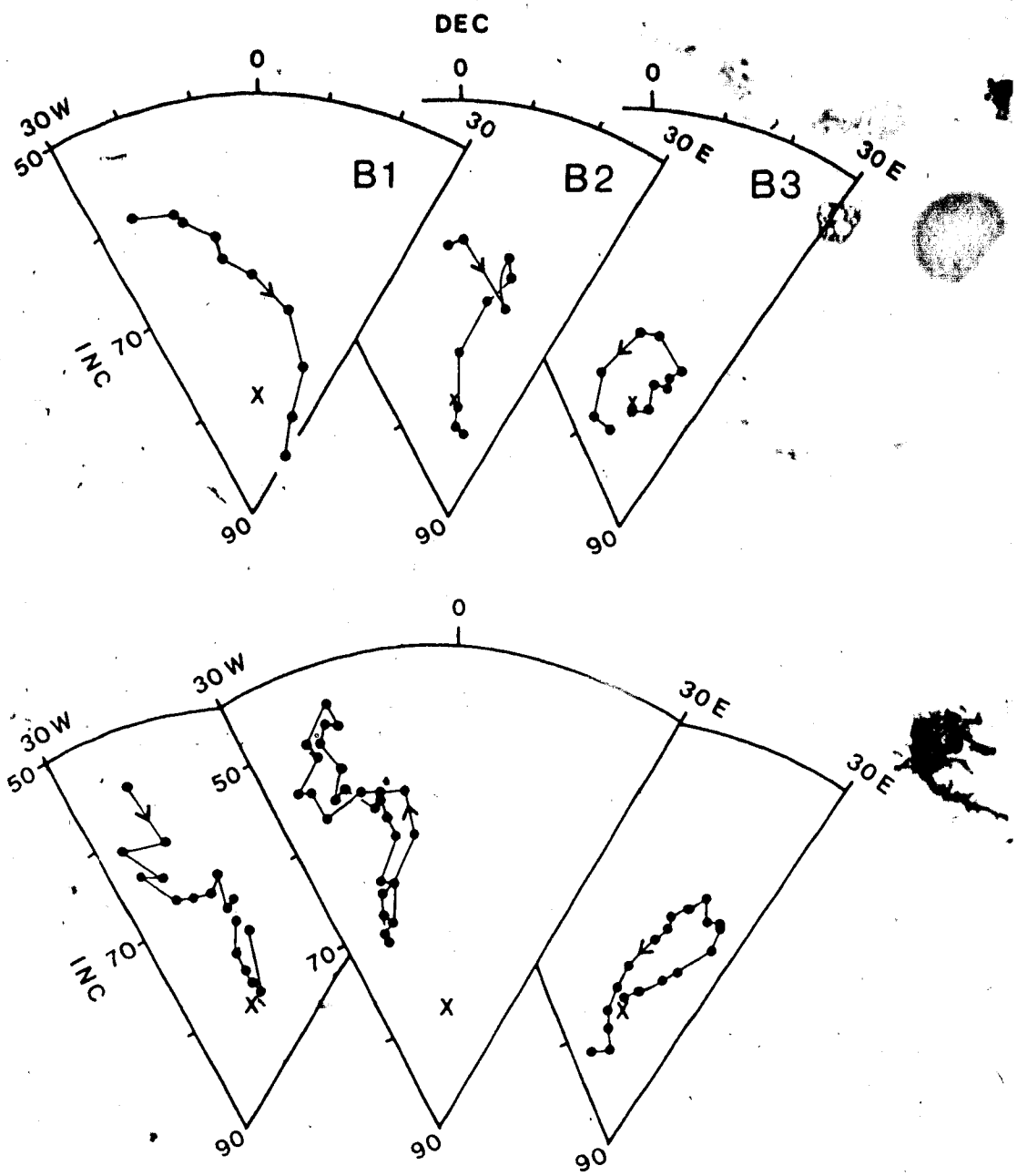

Figure 4-11: Declination-Inclination equal area plots for features (a) B1, B2 and B3 (three horizon (i.e., 6 sample) running mean). Internal variance of 11.0° (see Appendix A) and within-pair dispersion cut-off of 10° have been applied. The "X" marks the position of the field vector due to an axial geocentric dipole. Similar features from previous work (Evans et al., 1988; Hedlin and Evans, 1987; Hedlin, 1986) (5 horizon running mean) are included.

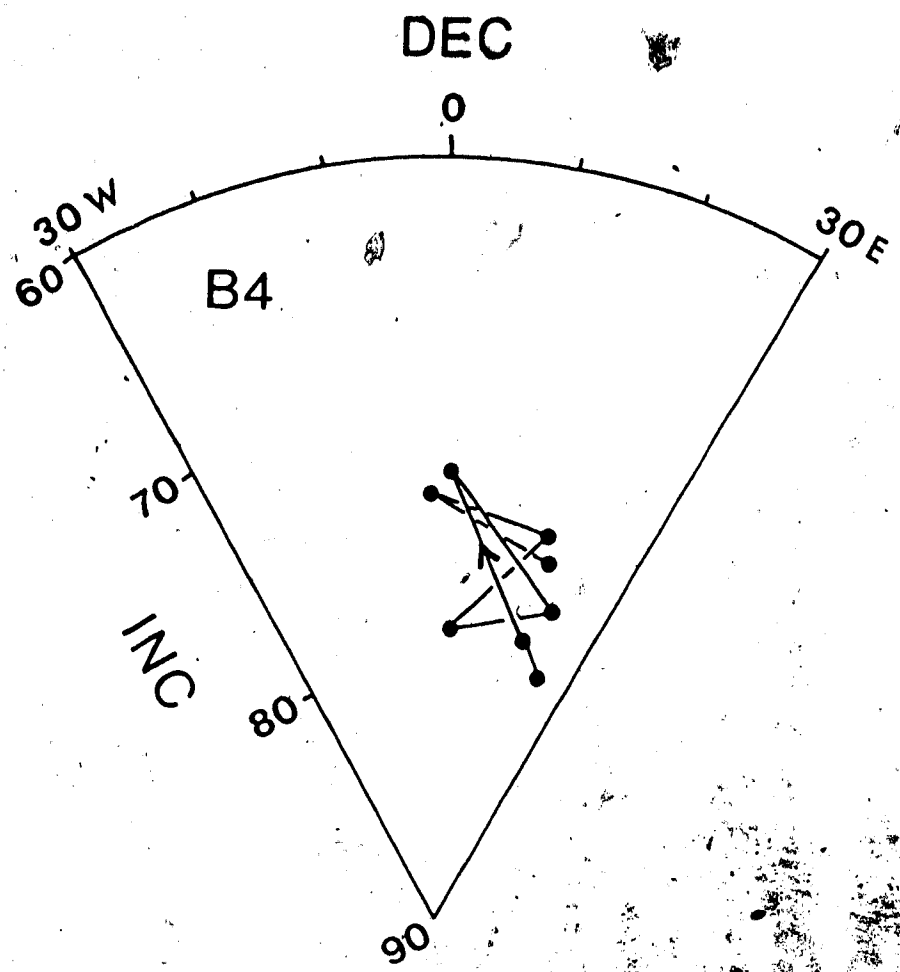

Figure 4-12: Feature B4 with no tilt correction.

Above B4 the bedding tilts in the opposite direction, dipping between 20° East and 26.5° East with strike varying from 010.0° to 017.0° azimuth. The end of the feature in this interval (B5) is designated as the 19.4m mark, as the bedding suddenly returns to horizontal at this point. An equal area plot of the data before and after correction to the tilted zone is presented in Figure 4-13 (the signal B6 from the horizontal beds above this zone contains only 6 pairs of which the pattern on an equal angle plot is not interesting enough to warrant further discussion, but is included in the Figure for completeness). The zone containing B5 is separated from the sediments below it by a steep plane of discontinuity, above which the package of sediments is undeformed internally and is tilted as a block, the general character being reminicent of an ancient slump feature. If the sediment layers were originally deposited horizontally then the correction made to rotate tilted beds back to the horizontal assumes that the rotation has taken place about the existing line of strike. If this is not the case, declination will be in error, thus one must view the resulting declinations with caution, but the inclination will be correct. With or without rotation, two remarkable characteristics of this feature remain clear; it is linear and large. The RM vector moves in a definite linear fashion for an angular distance of 70.5°. This angle is based on the points indicated in Figure 4-13. All solid triangles and circles have had an arbitrary within-pair cut-off of 10°

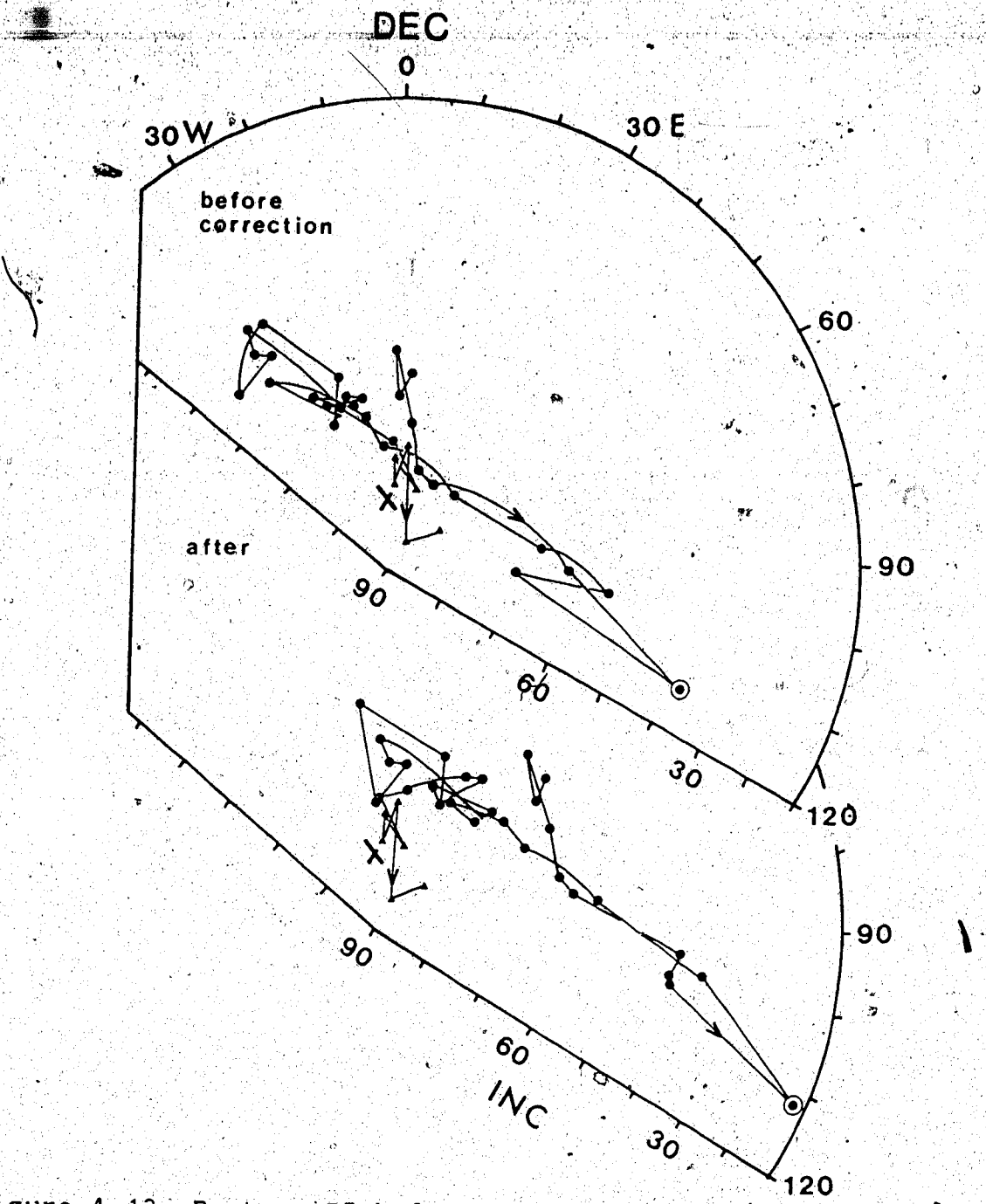

Figure 4-13: Feature B5 before and after tilt correction. The solid triangles are feature B6 (horizontally bedded sediment) and have had internal variance cut-off of 11° and within-pair dipersion cut-off of 10° applied. The solid circles are feature B5 (strata tilted to the east), with the same cut-off criteria as above. The solid circle with the ring around it represents the new minimum in inclination when the within-pair cut-off is removed. Before correction plot shows B5 with no tilt adjustment, while the lower plot shows B5 after correction for tilt. The "X" marks the position of the field due to an axial geocentric dipole.

applied. Under this cut-off B5 lost only 7 out of 42 pairs, of which all but one fall inside the linear track defined by the remaining points. The single pair which falls outside this range is plotted in the figure as a circled dot (see figure caption) and has a within-pair separation of only 11.1°. Using this point in the previous calculation gives a total angular movement of 90.8°. Therefore, although the true orientation of this feature is not known, it nevertheless presents evidence of a third linear perturbation in these sediments.

V. ANALYSIS OF GEOMAGNETIC SECULAR VARIATION

When plotted on an equal area plot, the track of typical paleosecular variation records generally resembles a "plate of spaghetti" (Constable and McElhinny, 1985, p. 117). Features A2 (=B1) and A3 (=B2), however, display perturbations of the geomagnetic field with remarkably linear trajectories and hence are of great geophysical interest. These signals are the type to be expected from stationary sources of secular variation (Evans, 1984) as opposed to the commonly observed westerly drifting sources described in Chapter I. They have therefore been selected for a more detailed analysis with a view to determining their likely origin.

A. Modelling of features A2 and A3

In this section the goal is to develop the simplest physical model capable of explaining the observations. We therefore start by calculating the minimum perturbing field necessary at the site to generate the observed features. The minimum perturbing vector (Pmin) is perpendicular to the resultant vector (R) (Figure 5-1). In vectorial terms this is equivalent to the subtraction of the background field vector (F - due to a geocentric axial dipole) from its projection on the perturbed one.

The directions and magnitudes of Pmin for the shallowest inclinations in A2 and A3 are listed in Table 5-1. Since the magnitudes of F and R are unknown, Pmin is

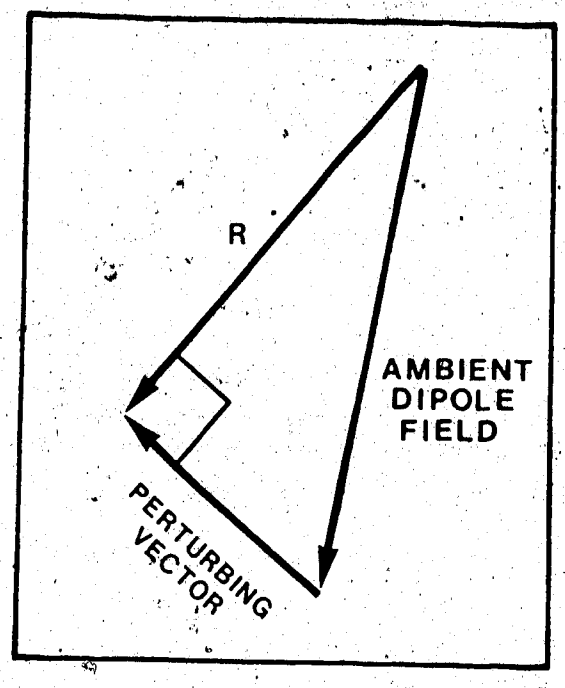

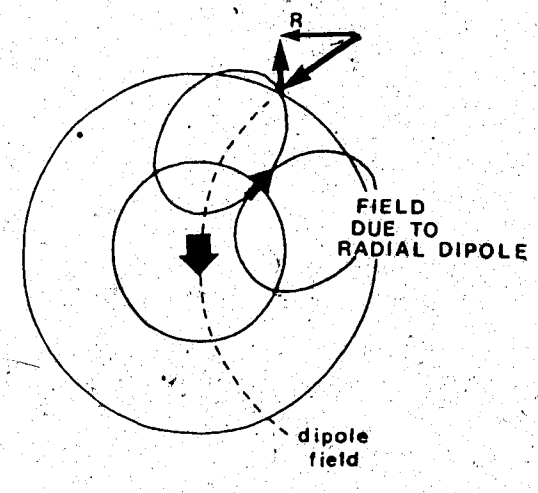

Figure 5-1: The top box illustrates the relationship between the minimum perturbing vector and the ambient and resultant fields. The bottom cartoon demonstrates how this vector relationship applies to the model used herein.

feature	perturbation		elevation (m)	P_{min}				radial dipole solution							
								outward				inward			
	dec	inc		dec	inc	mag*	angle+	M_{rd} M%	lat	long E	M_{rd} M%	lat	long E
A2 within-pair cut	337.2	35.3	11.3–14.0	326.3	-54.2	69.9	44.3	7.4	64.7	230.1	69.8	66.0	87.3
A2 no within-pair cut	347.5	16.5	11.3–14.0	337.8	-73.3	88.8	62.4	8.4	66.2	224.3	131.4	56.0	62.0
A3	340.9	49.0	8.4–11.3	331.1	-40.6	50.7	30.4	6.1	62.3	230.6	35.4	73.0	91.5

* magnitude as a % of background field

+ angle between background and perturbing field

Table 5-1: Modelling data and results for A2 and A3.

expressed as a percentage of F. The smallest perturbing field necessary to explain A3 (the smaller perturbation of the two) is 51% of the ambient field (geocentric axial dipole). This amounts to a field at the Earth's surface of 29,600 nT (for a main dipole moment of 8×10^{22} Am^2, the present-day value) directed at 29° west of north and 41° upwards. Not only is this anomalous field intense, but it points in the wrong direction to that expected in the northern hemisphere (the Z component of which is expected to point towards the geocentre). In the case of the greatest shallowing of the field (A2) the perturbing field is 89% of the intensity of the main field and corresponds to 52,000 nT directed 22° west and 74° upwards. This is a very intense anomalous field directed almost radially away from the geocentre.

The source of the perturbing field can be modelled as a radial dipole (r.d.) at the Core-Mantle Boundary (CMB). Representation as a dipole source is only a convenience. It has long been argued that the sources of secular variation are, in fact, electric currents flowing in the outer skin (approximately 40 km) of the liquid outer core (Lowes and Runcorn, 1951), while the contribution of deeper current systems to rapidly varying B is suppressed by electromagnetic shielding. This skin depth is a rough calculation based on a plane wave and solid conductor possessing typical values of pertinent core parameters. A more recent detailed calculation by Le Mouel and Courtillot

(1982) using a different technique gives estimates of 100 to 200 km for the thickness of the outer portion of the outer core that gives rise to secular variation (SV). The horizontal dimensions of typical SV foci are on the order of 1000 km. Since the moment perpendicular to a given cross-section is proportional to the current density times the area of that cross-section, the section with the greatest area will contribute most to the total moment (assuming constant current density). Since the SV foci have approximately a 10:1 ratio of horizontal to vertical dimensions, the product of current density and horizontal area will dominate. The equivalent dipole moment vector for such a situation will have a radial orientation. This is a physical justification for the use of a radial dipole suggested previously. Indeed, radial dipoles have provided good fits to both the present day non-dipole and SV fields (Alldredge and Hurwitz, 1964; Lowes and Runcorn, 1951; Alldredge and Stearns, 1969).

The perturbed and unperturbed directions at the site can be used to provide the locations of possible r.d.'s which are able to explain the observations. R and F define a plane in which such a source must lie. The assumption that the source must lie on the CMB further constrains it to a locus of points, and the final position of the minimum r.d. can be found by iteration as was done by Hedlin and Evans (1987) for their Bond Crow results. This process can be repeated with a series of possible perturbing vectors (ot

than the minimum) to produce the graph shown in Figure 5-2. Point 5 represents the position of closest approach to the site and it is from this point that the angular distances in Figure 5-2b are measured. Points 2 and 6 represent the minima for the inwardly and outwardly directed moment r.d. solutions respectively. The gap between the two curves results from the fact that the geometry does not allow any r.d. solution in this interval.

Inspection of Table 5-1 reveals that for all three inclination minima modelled, the minimum perturbing vector is directed away from the geocentre (negative inclination). This can result either from an r.d. close to the site with an outwardly directed moment, or from an r.d. located somewhat further away with an inwardly directed dipole moment. Obviously the latter will have greater moment than the former due to its greater distance from the site. The minimum r.d.'s required to produce the observed perturbations are given in Table 5-1 and vary from 5% to 9% of the strength of the main dipole. The corresponding inwardly directed r.d.'s for the same perturbations are much higher (35% to 131%) leaving outward moment r.d.'s as a much more attractive model. The fact that moments of only a few percent are required in order to explain these results underscores the robustness of this model (i.e. stationary eccentric radial dipoles which pulse in strength). Malin and Bullard (1981) were able to explain the looping behaviour of the field at London over the past several hundred years by

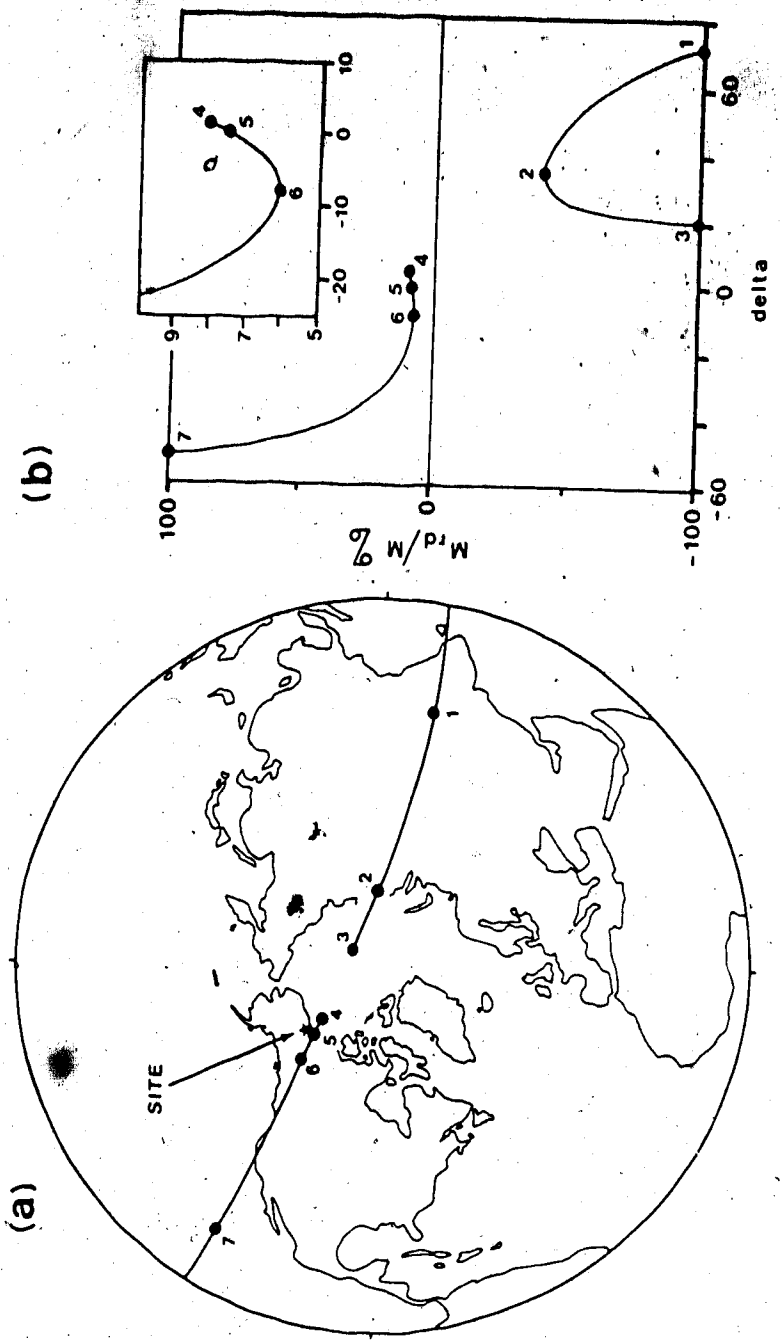

Figure 5-2: The possible locations on the CMB (a) and magnitude (b) of radial dipoles capable of explaining the shallowest inclination for feature A3. Magnitude is expressed as a percentage of the main dipole. Delta refers to the angle from the position of closest approach to the site (point 5). Points 2 and 6 represent the two minima. Points 1,3 and 7 denote the locations where the ratio is 100%.

drifting an r.d. of 3% past that site in a westward direction. The fact that other secular variation features of the geomagnetic field, such as the ones being examined in this study, are likewise explainable by r.d.'s of only a few percent makes the outwardly directed moment solutions very credible.

These results represent the lowest possible value that the r.d. can assume since they are placed at the CMB. There are, however, physical reasons why they should be placed deeper. The equivalent dipole for a spherical cap of current would be at some distance below the CMB, but the appropriate depth is not known. Lowes and Runcorn (1951) fitted dipoles to the SV field and found the majority of them to be radial and at a distance from the geocentre of from 0.35 (1,200 km below CMB) to 0.55 Re (roughly on the CMB). Much greater depth, corresponding to a distance from the geocentre of 0.28 Re (1780 km below the CMB), was determined by Alldredge and Hurwitz (1964) using best fit r.d.'s to represent the present global non-dipole field. In order to assess the effects of depth variation on the results for A2 and A3, the change in the minimum moment of the inwardly directed r.d. with increasing depth below the CMB is illustrated in Figure 5-3. As an upper limit we may examine the effect of placing the r.d. used to explain the most extreme value of A3 (declination 347.5, inclination 16.5) at a depth of 1780 km (the maximum depth given by Alldredge and Hurwitz). The Figure shows that an outward moment r.d. of 35% will explain

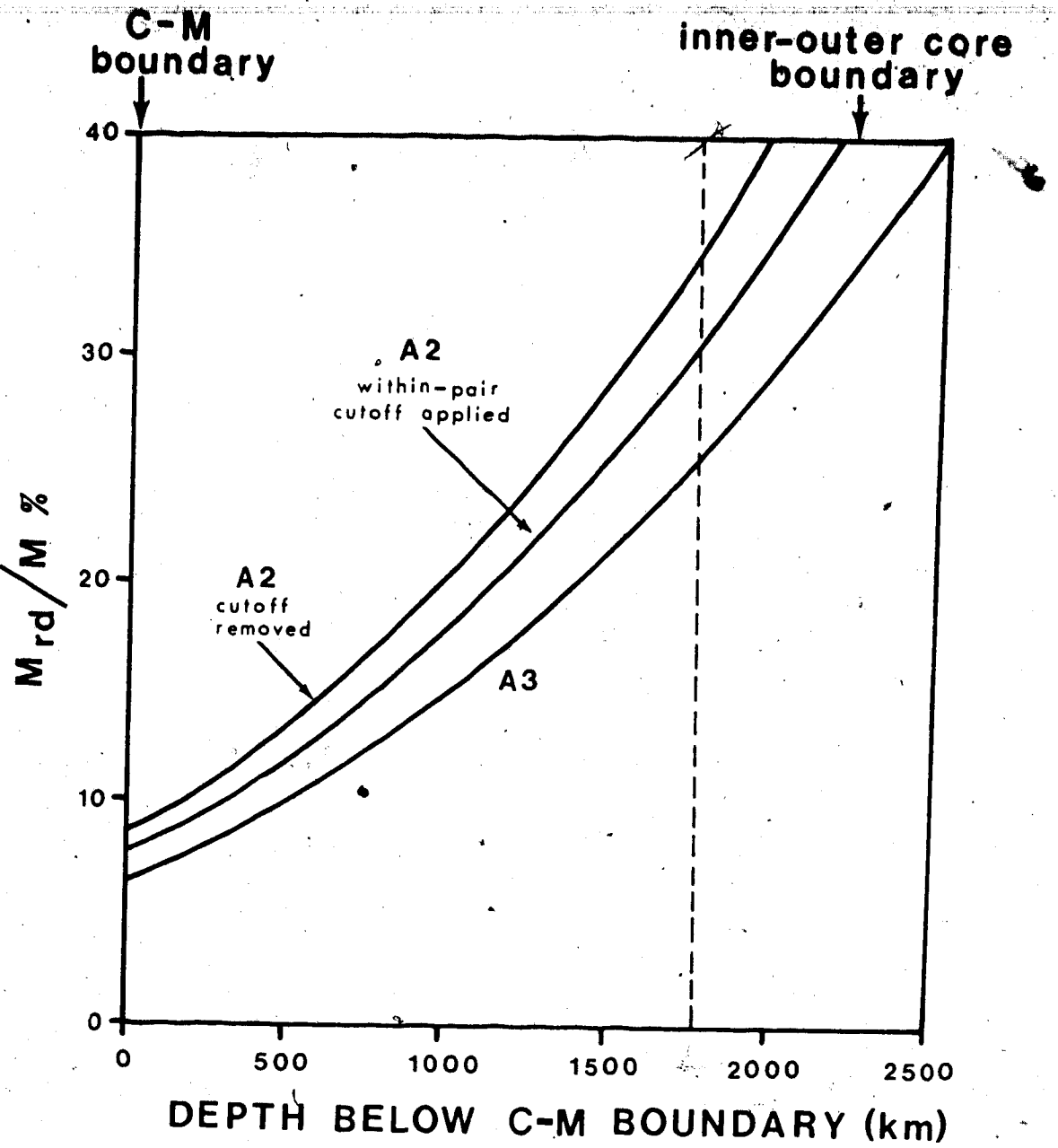

Figure 5-3: Variation of the moment of the radial dipole used to explain features A2 and A3 with depth below the Core-Mantle interface. Magnitude is expressed as a percentage of the main dipole. The vertical broken line refers to the maximum depth used by Alldredge and Hurwitz (1964) and is discussed in the text.

this feature and lesser values are obviously required to explain the other shallow inclinations listed in Table 5-1. It is not known how strong such r.d.'s may get, however it is probably reasonable to be suspicious of solutions which require moments in excess of that of the main dipole. This result emphasizes the fact that we need not invoke moments of much greater than one third the main dipole moment even in this extreme case. In contrast to this, the inward moment r.d. solution for even the smallest perturbation value of the three listed in Table 5-1 (declination 340.9, inclination 49.0) must exceed the main dipole (108%) when placed at these depths, once again showing the outward solution to be the more attractive solution.

B. Comparison with the modern field

The next question to be addressed is that of the existence of similar sources in the present field. As pointed out previously, modern field observations extend back only a fraction of the postulated period of change for non-dipole features. In addition, the Earth's field has had a long history of change of which we presently see only one of many possible configurations. Hence it should not greatly disturb us if a perfect analogy to the modelled perturbing source cannot be found in the present field.

As distance from the sources increases, the characteristics of an individual anomaly may be obscured by its neighbours. It is therefore more desirable to have an

expression for the geomagnetic field at the CMB rather than at the surface if one is to hypothesize about possible sources for paleofield results by studying modern day analogues. Downwardly continued maps of the field have been produced by Bloxam and Gubbins (1985) from various data of the Earth's field spanning several decades.

The modelling of features A2 and A3 revealed that an r.d. with moment vector directed away from the geocentre is the most plausible perturbing source. Such an r.d. would produce a patch of concentrated reversely directed flux vertically above itself, i.e., contoured values of the Z component of the field would reveal a circular patch of flux directed away from the geocentre in the northern hemisphere where flux is normally directed inwards. Such patches do in fact, exist today, the most prominent being in the southern hemisphere (Figure 5-4a). The reversely directed flux (inward for the southern hemisphere) of these features is claimed by Gubbins (1987) to be responsible for the 7% drop in the main dipole over the last 150 years. Over this period, both anomalies have intensified. This rapid intensification makes them attractive analogues to the r.d. model used to explain A2 and A3. As Gubbins points out, we have not yet seen a complete cycle of growth and decay of these features, so we have no idea of the time scale and hence our understanding of these features is incomplete. Over the period of observation, these anomalies have exhibited some westward drift and consequently do not

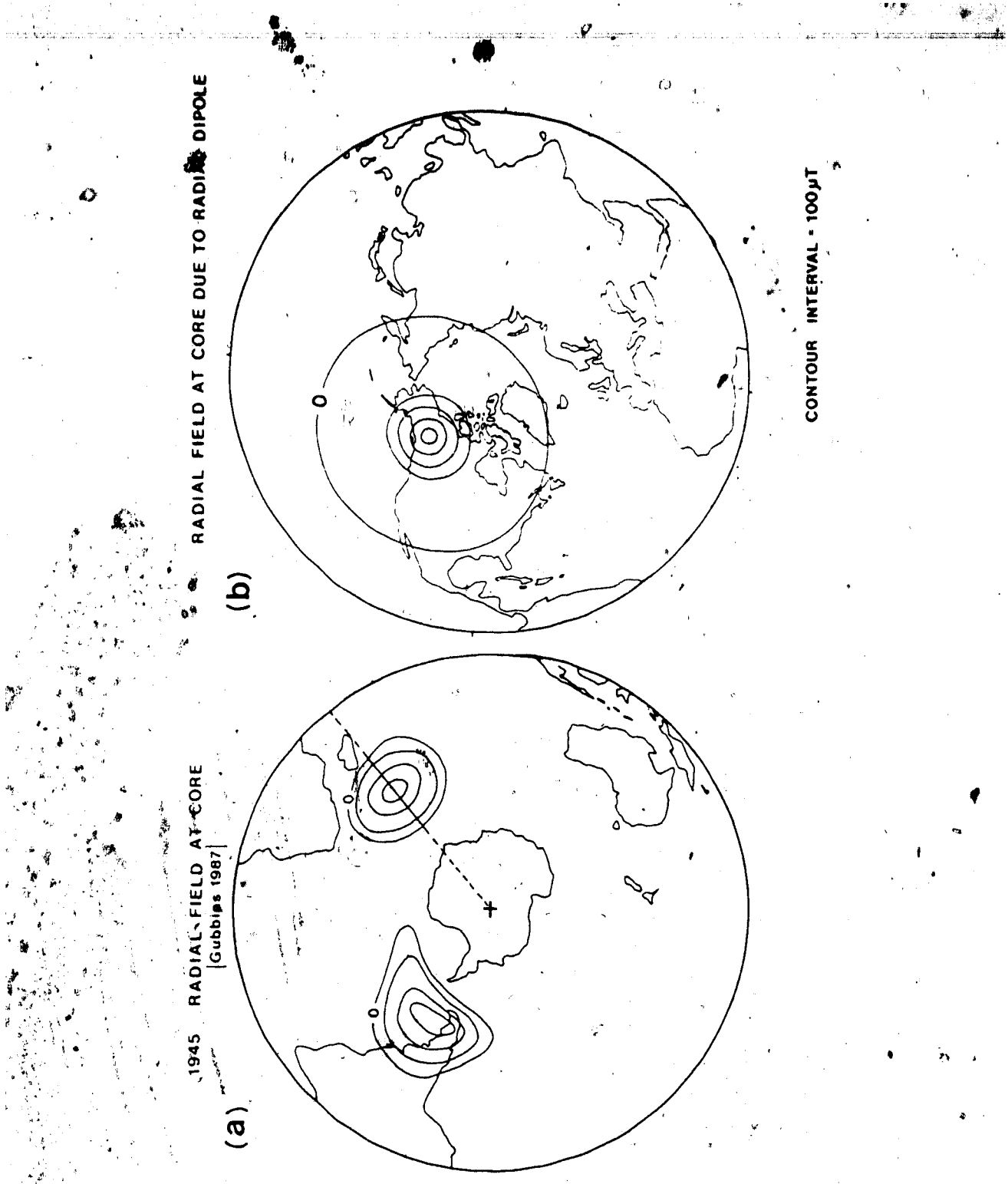

Figure 5-4: (a) Reverse flux patches at the Core-Mantle interface in the 1945 radial field component. Contour interval is in 100 microtesla. (adapted from Gubbins, 1987). Profile line used in Figure 5-6 is indicated. (b) Radial field at the CMB due to a radial dipole of moment 1% placed at 700km below interface with outwardly directed moment.

strictly comply with the requirement that the source be stationary. However, the movement has slowed somewhat in more recent times. Despite this movement, the characteristics of reverse flux and rapid intensification make further analysis worthwhile.

The anomalies in Figure 5-4a are roughly circular in plan and suggest sources which can be modelled as radial dipoles. We can therefore obtain minimum estimates for the moments of the paleosources in the following manner. On the original plots (Gubbins, 1987) there are no values of $Z\cos(\theta)$ greater than 300 microTesla. For the colatitude at which these anomalies occur (θ approximately 50° S) this corresponds to approximately 460 microTesla as a maximum that the radial field (Z) may attain. Since we seek a minimum for the ratio of the moment of the paleosources to the moment of the present-day sources (Mrd/Mpd), we must find the largest value of Mpd and the smallest value of Mrd. As we have just seen, the present-day source may have a maximum of 460 microTesla at the CMB, which for a given depth fixes the upper limit of Mpd. The lower limit for Mrd is obtained by using the minimum outward solution (Table 5-1). To be conservative, we approach the problem by using the linear feature with the smallest perturbation (i.e. A3). Calculating Mpd values for various depths below the CMB using the 460 microTesla limit on Z, and dividing these by the Mrd of A3 obtained from Figure 5-3 for corresponding depths gives the curve of Figure 5-5, which represents the

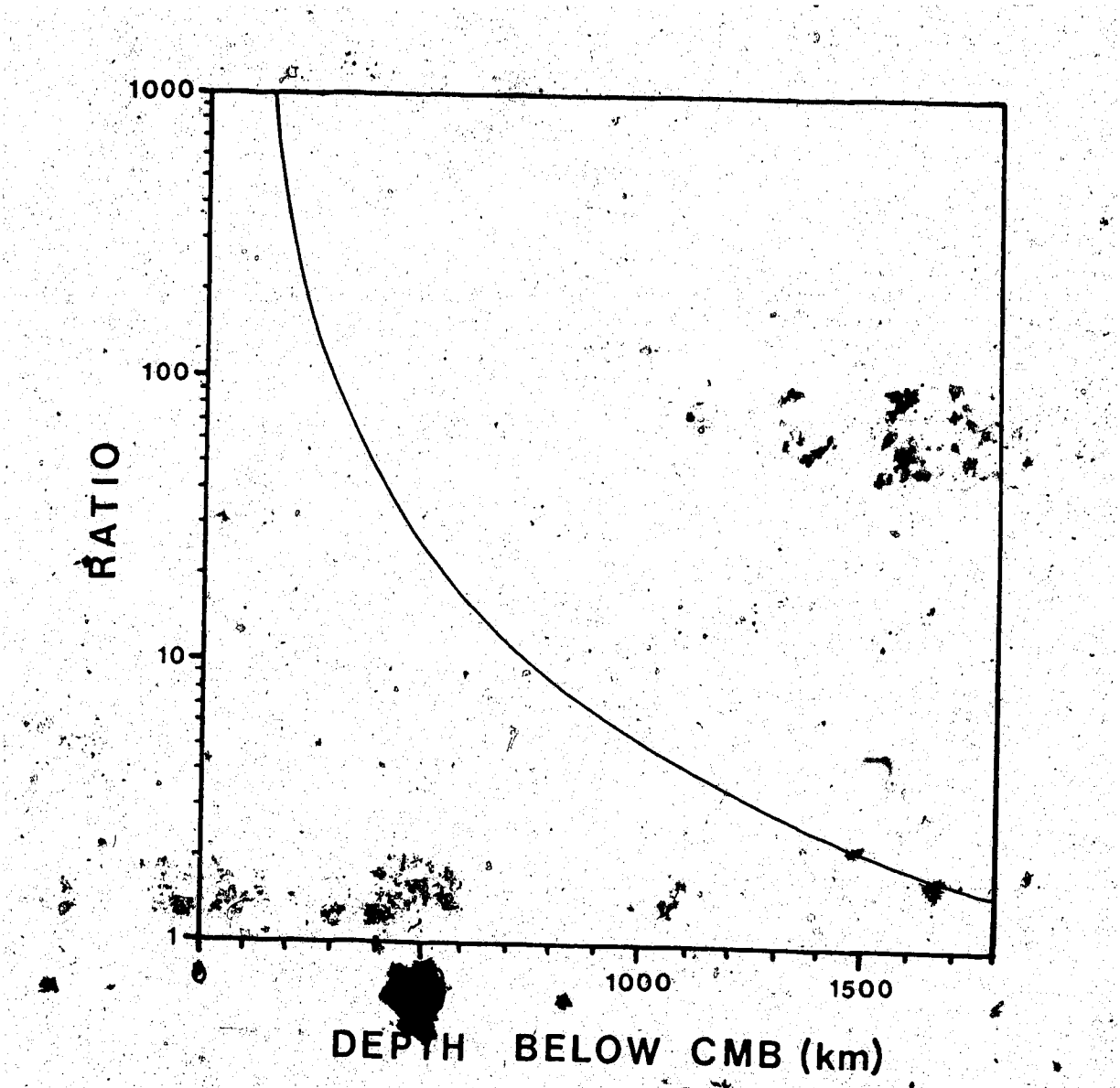

Figure 5-5: Minimum values of ratio of moments of paleosources to present-day sources with depth below the CMB.

minimum values of Mrd/Mpd. This value decreases monotonically with increasing depth and therefore we must identify the maximum depth at which we may place the r.d. in order to find the minimum ratio. This is determined by taking a profile across the feature of interest in Figure 5-4a, placing r.d.'s of various strengths at different depths below the anomaly centre and examining the fit. Since the starting point in this procedure was a small published diagram, a rigorous fitting procedure is not justified, and given that we seek only an order of magnitude comparison, a fit by eye is adequate. Figures 5-6a through 5-6c show the procedure for r.d.'s of moments 1% (Figure 5-6b), 5% (5 times greater - Figure 5-6c) and 0.2% (5 times less - Figure 5-6a). The best-fitting curve of Figure 5-6a (depth = 410km) underestimates most of the values on the flanks. A better fit is provided by the 1% r.d. at 700 km (Figure 5-6b) which also has the advantage, that it slightly overestimates the values of Z and hence gives a maximum depth. Figure 5-6c shows that once a value of 5% is reached, a good fit cannot be found. We select the 700km 1% solution, and reference to Figure 5-5 then gives a ratio of at least 12 to 1. The same procedure using perturbation A2 without the within-pair cutoff gives a ratio of 16 to 1. Therefore it appears that the paleosources required to explain the observed perturbations are at least an order of magnitude higher than present-day reverse flux features.

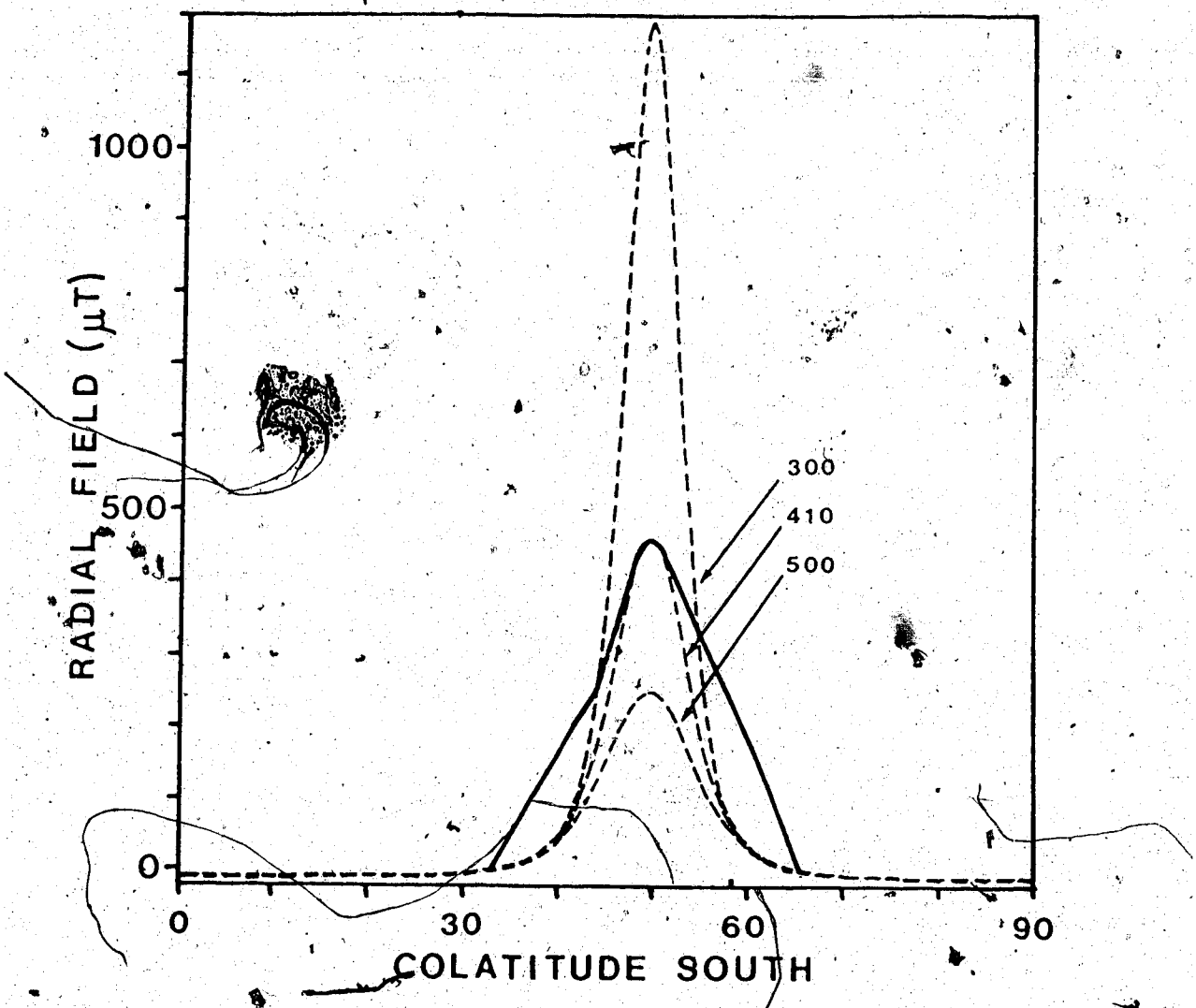

Figure 5-6: Comparison of profile of Z field feature of Figure 5-4 with Z profiles (broken curves) generated by radial dipoles of arbitraty strengths (a) 0.2%, (b) 1%, and (c) 5%, placed at indicated depths below the CMB.

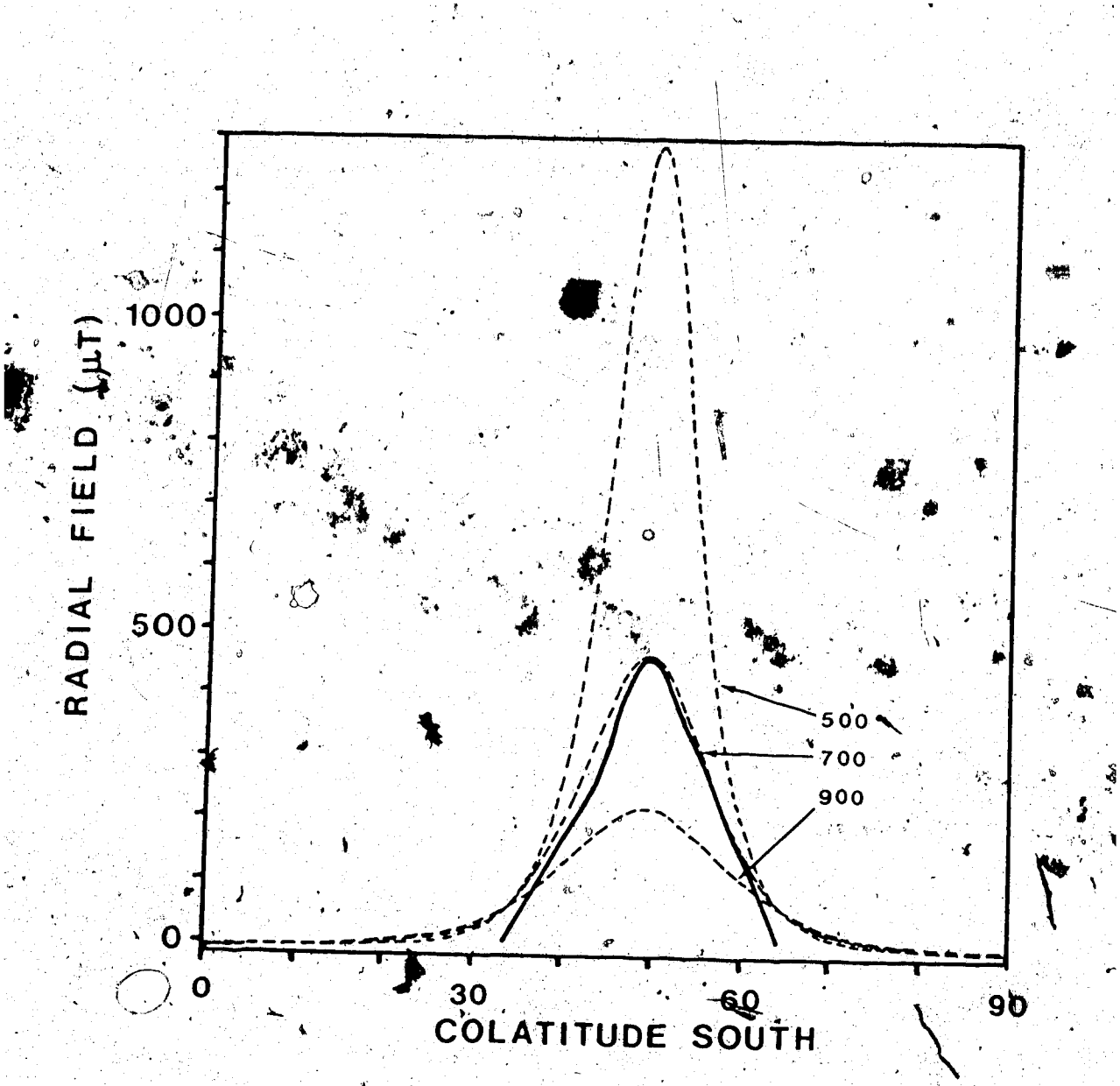
RADIAL FIELD (μT)
1000
500
0
0
30
60
90
COLATITUDE SOUTH
500
700
900

Figure 5.6(b)

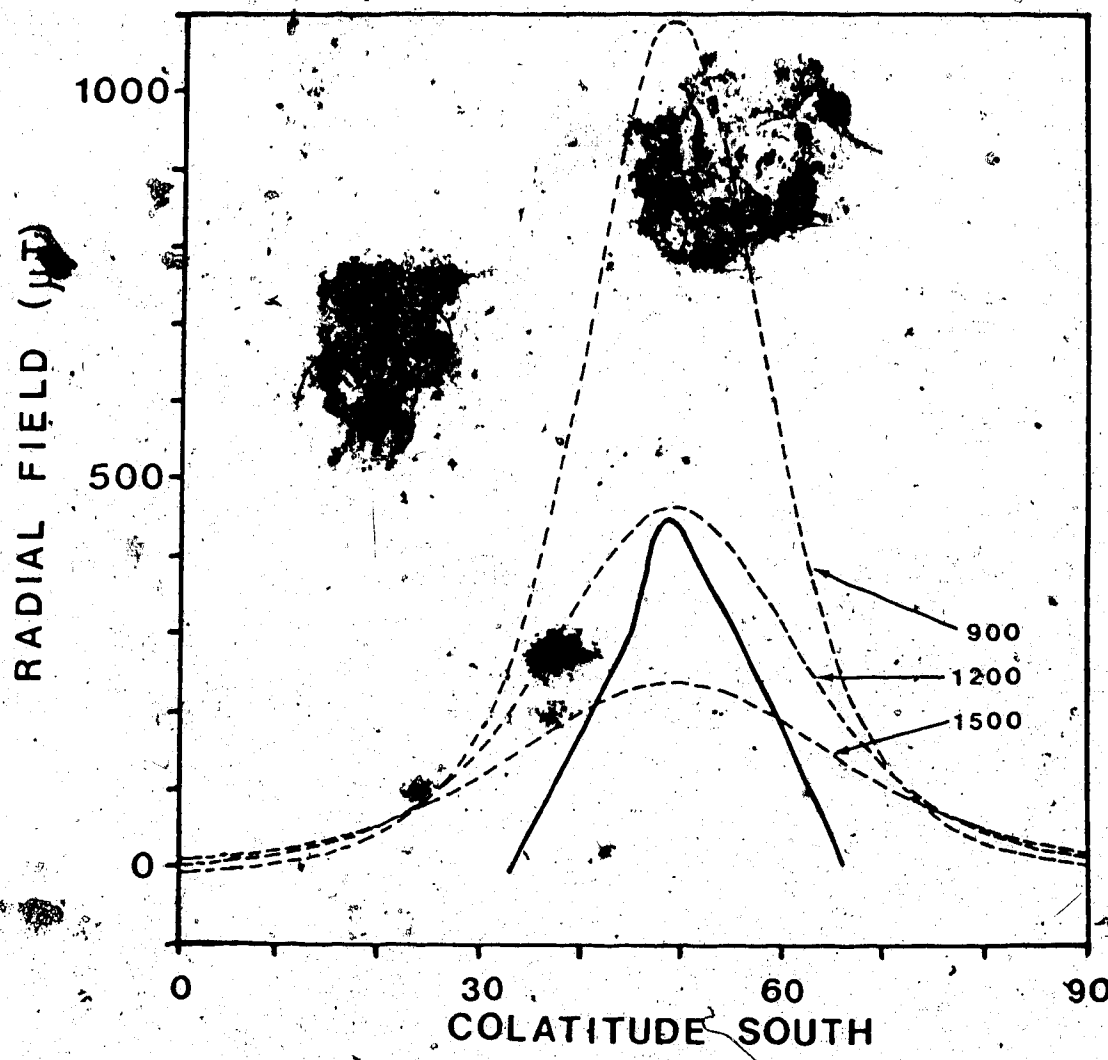
1000
500
0
RADIAL FIELD (μT)
900
1200
1500
0
30
60
90
COLATITUDE SOUTH

Figure 5-6(

VI. SUMMARY AND CONCLUSIONS

The remanent magnetization records recovered from two sections of Pleistocene sediments (each approximately 20 m in vertical extent) exposed in the valley walls of the Old Crow River display features of both geological and geophysical interest. The fact that a sequence of three features (A2, A3 and A4) can be correlated with previous findings from other sections upstream supports their reality, and the fact that these and the previously sampled sections are separated by over 5 km favours a geomagnetic perturbing mechanism over a sedimentological one. This remarkable correlation of three features allows a date to be established for these sediments by paleomagnetic means. A volcanic ash (the Old Crow Tephra) present at the outcrop at which Hedlin and Evans (1987) recovered their records showed a distinctive paleomagnetic signature. The age of this tephra is currently believed to be 149,000 ±13,000 years (Westgate, 1988) and thus sediments at the 14.6m level in KGA which display this characteristic paleomagnetic signal are believed to represent this age, i.e. the time of deposition of the Old Crow Tephra in the Basin. The same RM signal is suggested at the 13.3m mark in section KGB, although the quality is not as good.

The paleosecular variation sequences recovered also display behaviour consistent with the existence of several cycles of growth and decay of stationary sources at the CMB. These involve perturbations of the RM vector in linear

trajectories up to 62.4° from the ambient position dictated by an axial geocentric dipole field. Such features can be easily modelled by elementary magnetostatic theory by placing an eccentric radial dipole at the CMB. The strength for an r.d., the moment vector of which is directed outwards (away from the geocentre) need only be a few percent of the dipole, even in the most extremely perturbed case (declination 347.5, inclination 16.5). The results for the corresponding inwardly directed moment r.d.'s are always much higher and in the case of the above perturbation, exceed the strength of the main dipole itself. This leaves the outward solution as a much more attractive explanation. Such r.d's would produce patches of concentrated reversely directed flux at the CMB (i.e., outwards in the northern hemisphere where flux should be inwards). No perfect analogue can be found in the modern field, but patches of rapidly intensifying reversely directed flux do exist. Simple magnetostatic modelling of such a patch currently existing in the southern hemisphere demonstrates that a radial dipole with moment approximately 1% of that of the main dipole produces an excellent fit when placed under these anomalies at a depth of 700 km below the CMB. At this same depth, r.d.'s ranging from 12% to 16% are required to explain the features A2 and A3, thus suggesting an order of magnitude difference.

As Bloxham and Gubbins (1985) mention, the pattern of fluid flow in the outer core is unlikely to remain

stationary with respect to the mantle, so the existence of static features implies that this flow must be coupled to the lower mantle in some regions. The coupling mechanism could be thermal, electromagnetic, topographical or some combination of these. Topographic coupling seems plausible insofar as recent seismic tomography results suggest that topography exists today at the CMB and thus there is no reason to believe that it would not have existed in the past. Hide and Malin (1971) demonstrated that even small scale vertical relief (small on the planetary scale) of only a few kilometres at the CMB could cause fluid flow perturbations which could penetrate to great depths within the core. The general idea is that fluid flow encountering local topography on the CMB is induced to flow in what is loosely termed an "eddy", and whatever the exact motion is, it is sufficient to generate magnetic flux by virtue of the velocity and magnetic field interaction. Certainly the regular appearance of several linear perturbation features in these paleosecular variation records (and the lack of such features in most other RM records from around the world) suggests that there was some property of the CMB which was in the past inducing these sources to form and/or causing them to be localized in the general vicinity of this site.

REFERENCES

Alldredge, L.D. and Stearns, C.O., 1969, Dipole model as the sources of the earth's main magnetic field, *J. Geophys. Res.*, 74, 6583-6593.

Alldredge,L.D. and Hurwitz,L., 1964, Radial dipoles as sources of the Earth's main magnetic field, *J. Geophys. Res.*, 69, 2631-2640.

As, J.A., and Zijderveld, J.D.A., 1958, Magnetic cleaning of rocks in paleomagnetic research, *Geophys. J.*, 1, 308-319

Barton, C.E., 1978, *Magnetic studies of some Australian lake sediments*, Unpub. Ph.D. thesis, Australian National Univ.

Bloxham,J. and Gubbins,D., 1985, The secular variation of the Earth's magnetic field, *Nature*, 317, 777-781.

Bullard,E.C., Freedman,C., Gellman,H., Nixon,J., 1950, The westward drift of the Earth's magnetic field, *Phil. Trans. Roy. Soc. London*, A243, 67-92.

Constable, C.G. and McElhinny, M.W., 1985, Holocene geomagnetic secular variation records from north-eastern Australian lake sediments, *Geophys. J. R. astr. Soc.*, 81, 103-120.

Cox, A.V., 1968, Lengths of Geomagnetic Polarity Intervals, *J. Geophys.*, 73, 3247-3260.

Creer, K.M., and Tucholka, P., 1982, Secular variation as recorded in lake sediments: a discussion of North American and European results, *Phil. Trans. R. Soc., Lond.*, A306, 87-102.

Creer, K.M., D.L. Grosss and J.A. Lineback, 1976, Origin of regional geomagnetic variations recorded by Wisconsinan and Holocene sediments from Lake Michigan, USA, and Lake Windermere England, *Geol Soc. Amer. Bull*, 87, 531-540.

Denham, C.R., 1974, Counter-clockwise motion of paleomagnetic directions 2400 years ago at Mono Lake, California, *J. Geomag. Geoelect.*, *26*, 487-498.

Evans, M.E., Gillen, K.P., and Hedlin, M.A.H., (in press), Further paleomagnetic results from northern Canada.

Evans, M.E., 1984, Paleomagnetic evidence for stationary sources of geomagnetic secular variation, *Phys. Earth Planet. Interiors*, *35*, 223-226.

Fisher, R.A., 1953, Dispersion on a sphere, *Proc. Roy. Soc.*, *A217*, 295-305.

Gaiber-Puertas, C., 1953, *Variacion [illegible]ar del campo geomagnetico*, Obser. del Elso, Memo no 11 (4).

Gubbins, D., 1987, Mechanism for Geomagnetic polarity reversals, *Nature*, 326, 167-169.

Hedlin, M.A.H., 1986, *A Pleistocene high-latitude geomagnetic study*, Unpub. M.Sc. thesis, Univ. of Alberta.

Hedlin, M.A.H., and Evans, M.E., 1987, A paleomagnetic study of some Pleistocene sediments in northern Canada and its bearing on the secular variation of the geomagnetic field, *Geophys. J. R. astr. Soc.*, *90*, 693-703.

Hide, R. and Malin, S.R.C., 1971, *Bumps on the Core Mantle Boundary*, Comments on Earth Sciences: Geophysics 1-13.

Le Mouel, J.L., 1984, Outer-core geostrophic flow and secular variation of Earth's geomagnetic field, *Nature*, *311*, 734-735.

Le Mouel, J.L., and V. Courtillot, 1982, On the outer l[redacted]s of the core and geomagnetic secular variation, *J. Geophys. Res.*, *87*, 4103-4108.

Lowes, F.J. and Runcorn, S.K., 1951, The analysis of the geomagnetic secular variation, *Phil. Trans. R. Soc., Lond., A243*, 525-546.

Mackereth, F.J.H., 1971, On the variation in direction of the horizontal component of remanent magnetization in lake sediments, *Earth Plan. Sci. Let.*, 12, 332-338.

Malin,S.R.C. and Bullard,E.C., 1981, The direction of the Earth's magnetic field at London, 1570-1975, *Philos. Trans. R. Soc. London, Ser A, 299* 357-423.

McElhinny, M.W., and Gough, D.I., 1963, The paleomagnetism of the Great Dyke of Southern Rhodesia, *Geophys. J.*, *7*, 287-303.

Merrill, R.T. and McElhinny, M.W., 1983, *The Earth's Magnetic Field*, 401 p., Academic Press, International Geophysics Series, 32.

Molyneux,L., 1971, A complete result magnetometer for measuring the remanent magnetization of rocks, *Geophys. J. Roy. Astr. Soc.*, *24*, 429-433.

Morlan,R.E., 1980, *Taphonomy and Archaeology in the Upper Pleistocene of northern Yukon Territory: A glimpse of the peopling of the New World*; National Museum of Man (Mercury Series), Archaeological Survey of Canada, Paper 94.

Morlan, R.E., and Matthews, [redacted] 1978, New dates for early Man, *GEOS*, Winter, 2-5.

Murthy,G.S., 1969, *Paleomagnetic Studies in the Canadian Shield*, Unpub. Ph.D. thesis, Univ. of Alberta.

Palmer, D.F., Henyey, T.L., and Dodson, R.E., 197[illegible] Paleomagnetic and sedimentological studies at L[illegible] Tahoe, California Nevada, *Earth Planet Sci. Lett.*, 46, 125-137.

Reid, A.B., 1972, A paleomagnetic study at 1800 m[illegible] years in Canada, Unpub. M.Sc. thesis, Univ. of A[illegible]

Tarling, D.H., 1983, *Paleomagnetism: principles and applications in geology, geophysics and archaeology*, 379 pp., Chapman and Hill Ltd., London.

Turner, G.M., 1983, Comment on "A paleomagnetic record from Tangle lakes, Alaska: large amplitude secular variation at high latitudes" by K.L. Verosub, *Geophys. Res. Lett.*, 10, 185.

Verosub, K.L., 1977, Depositional and postdepositional processes in the magnetization of sediments., *Revs Geophys. Space Phys.*, *15*, 129-143.

Watson, G.S., 1956, Analysis of dispersion on a sphere, *Mon. Not. Roy. Ast. Soc., Geophys Supp.*, *7*, 153-159.

Westgate, J., 1988, Isothermal plateau fission-track age of the late Pleistocene Old Crow Tephra, Alaska, *Geophys. Res. Lett.*, 15, 376-379.

Westgate, J., and Wintle, 1986, Thermoluminescence age of Old Crow tephra in Alaska, preprint.

Westgate, J., R.C. Walter, G.W. Pearce, and M.P. Gorton, 1985, Distribution, stratigraphy, petrochemistry, and paleomagnetism of the late Pleistocene Old Crow tephra in Alaska and the Yukon, *C.J. Earth Sci.*, 22, 893-906.

Yukutake,T. and Tachinaka,H., 1968, The non-dipole part of the Earth's magnetic field, *Bull. Earthq. Res. Inst., Tokyo*, *46*, 1027-1074.

APPENDIX A - Theta

The purpose of the work herein is to establish a relationship between "theta" values obtained from the Schonstedt SSM-2 and Molspin (Molyneux, 1971) magnetometers. Theta is a measure of the internal variance of a measurement and is defined as:

$$\text{theta} = \sin^{-1}\left(\frac{\sqrt{(\text{disX}^2 + \text{disY}^2 + \text{disZ}^2)}}{\text{moment}}\right)$$

where $\text{disX} = \frac{1}{4}\sqrt{\Sigma(\bar{X}-X)^2}$

and similarly for disY and disZ.

The value obtained from a sample is a function of (a) magnetometer noise and (b) inhomogeneity of magnetization.

(a) In order to assess the effects of noise only, we require a perfectly homogeneous specimen. For most cities, air will suffice for this purpose, and thus the magnetometers were operated with the sample holders empty. Theoretically, noise will be reduced by the act of stacking together repeated measurements on a single sample. This process is refered to as "integration" and the number of determinations stacked in called the integration number. The noise level at different integration numbers for both the Schonstedt and Molspin are shown in Figure A-1.

The Molspin has a tendency to drift and consequently at long integration numbers (long spin times) it is unable to attain the low noise levels possible in the Schonstedt. The lowest levels attainable for the Molspin and Schonstedt are of the order of 1×10^{-9} and 1×10^{-10} respectively. Note that although the Schonstedt approaches 1×10^{-11} for

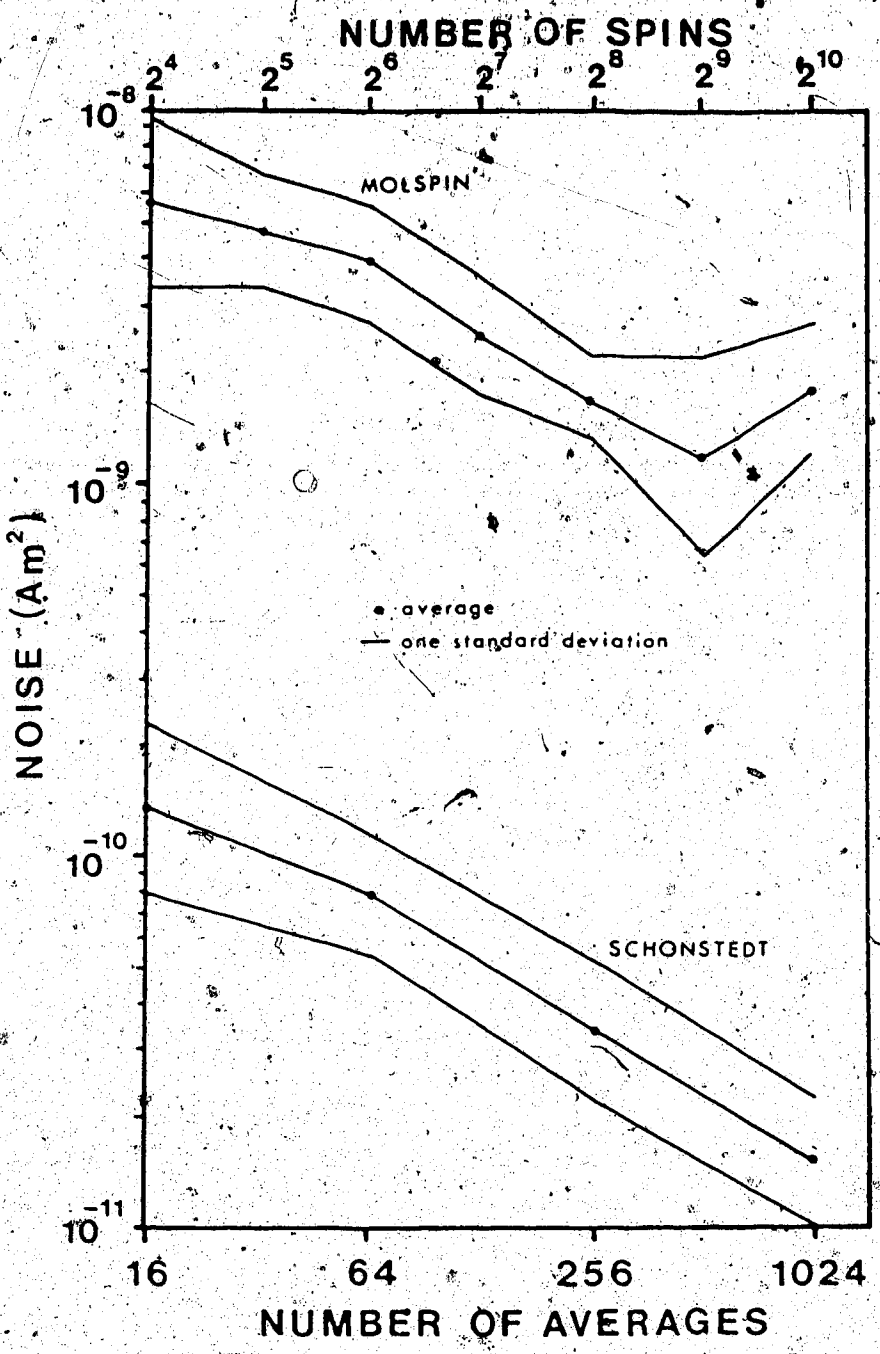

Figure A-1 Comparison of noise for Molspin and Schonstedt system designs.

averages 2^{9} and 2^{10}, these excessively long spin times were only used in cases where inhomogeneous samples were measured in cart position 3, and in this position, the sample moment as seen by the sensor is reduced by a factor of ten, thus effectively increasing system noise by a factor of ten. Therefore the figure of 1×10^{-10} is still applicable. This allows us to calculate the lowest moment level for a homogeneous sample at which it will exceed a theta of 5°.

$5° = \arcsin(1 \times 10^{-9}/Mmol)$

$5° = \arcsin(1 \times 10^{-10}/Msch)$

therefore,

$Mmol = 1 \times 10^{-8}$

$Msch = 1 \times 10^{-9}$

This explains why Hedlin could not measure his weakest samples (less than 1×10^{-8} Am^2) with enough precision (theta less than 5°). For moments less than 1×10^{-8} Am^2, even a perfectly homogeneous sample will give theta greater than 5° on the Molspin.

(b) Determination of the effect of sample inhomogeneity requires samples with sufficiently high moments to render noise insignificant. In addition, the specimen cannot have low theta, since it is not inhomogeneous in this case. Unfortunately, most samples with high moments also had low theta and consequently only 5 specimens were judged suitable. These were measured on both magnetometers. For the Schonstedt, the position of the sample from the sensor is adjustable (4 possible "cart positions", 1 being furthest

and 4 being closest) with the effect that increasing distance reduces the apparent degree of inhomogeneity. Since all measurements were made using cart position 3 or 4, the comparison between device designs was made using cart position 3 (the further). Table A-1 summarizes the results.

A plot of theta from columns 2 and 3 is shown in Figure A-2. The slope of the best fit line through the origin is 2.4, thus showing that a theta of 5° on the Morspin (used by Hedlin) corresponds to 12° on the Schonstedt (used in the present study). To be conservative, the actual value selected was 11°, but the actual value chosen is not critical to the form of the magnetograms for both sections. Plots made with theta cut-offs of 10°, 11°, 12°, and 13° simply affects the number of points in the plots, but the geophysical interpretation is unaffected.

	Theta		
sample	Molspin	Schonstedt	Ratio(Sch/Mol)
KGA067	3.1	6.1	2.0
KGA073	4.7	11.9	2.5
KGA050	4.5	13.2	2.9
KGA053	3.9	8.9	2.3
KGA059	3.4	8.5	2.5

Table A-1: Table of theta values used to construct Figure A-2.

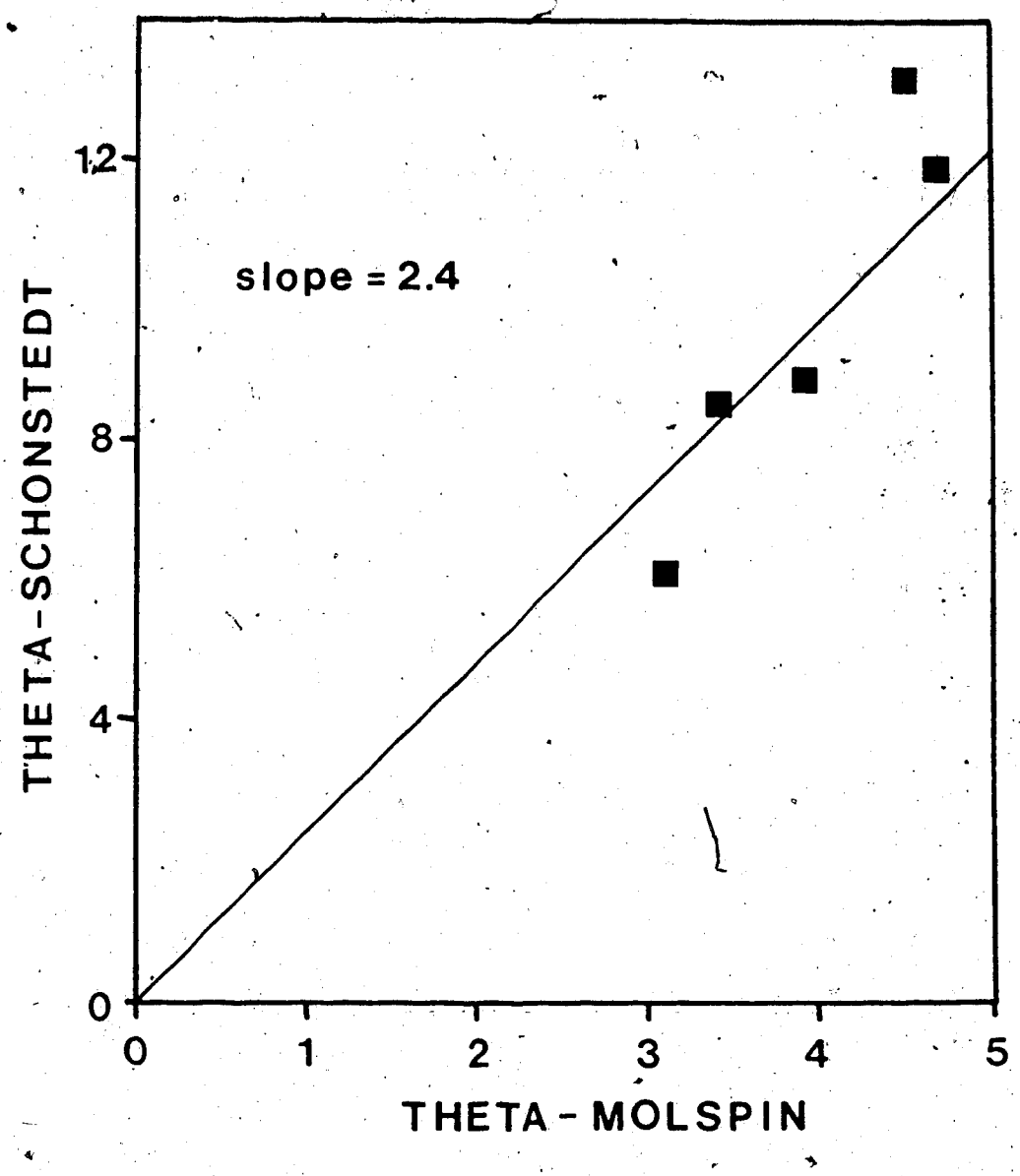

Figure A-2: Comparison of theta for Molspin and Schonstedt system designs using the best measurements obtained from selected specimens.

APPENDIX B - Data

The data used to produce this thesis are contained herein.

THIS FILE CONTAINS ALL DATA USED IN THE PRODUCTION OF KEVIN GILLEN'S M.Sc. THESIS

COLUMN 1 ..... SAMPLE NUMBER
COLUMN 2 ..... ELEVATION
COLUMN 3 ..... DECLINATION
COLUMN 4 ..... INCLINATION
COLUMN 5 ..... DEC (CORRECTED FOR BEDDING)
COLUMN 6 ..... INC (CORRECTED FOR BEDDING)
COLUMN 7 ..... INTERNAL VARIANCE
COLUMN 8 ..... MOMENT (CGS)
COLUMN 9 ..... PERCENT ERROR IN MOMENT
COLUMN 10 ..... A.F. TREATMENT

A	1	-0.260	11.50	80.80	0.0	0.0	4.70	0.331E-02	8.3	0
A	2	-0.260	336.70	85.70	0.0	0.0	4.10	0.313E-02	7.2	0
A	3	-0.150	331.30	83.80	0.0	0.0	8.20	0.319E-03	14.3	0
A	4	-0.150	37.30	79.60	0.0	0.0	3.40	0.191E-02	5.9	0
A	5	-0.050	66.70	78.30	0.0	0.0	3.90	0.613E-04	6.8	0
A	6	-0.050	35.90	80.40	0.0	0.0	3.90	0.184E-03	6.8	0
A	7	0.150	22.20	60.90	0.0	0.0	18.00	0.411E-04	30.8	0
A	8	0.180	40.10	67.10	0.0	0.0	8.90	0.370E-04	15.5	0
A	9	0.250	36.70	66.10	0.0	0.0	33.20	0.661E-04	54.7	0
A	10	0.260	58.20	73.30	0.0	0.0	13.60	0.277E-04	23.6	0
A	11	0.410	35.90	83.30	0.0	0.0	12.30	0.630E-04	21.3	0
A	12	0.410	314.80	69.10	0.0	0.0	24.80	0.102E-03	42.0	0
A	13	0.500	28.80	80.60	0.0	0.0	13.20	0.270E-04	22.8	0
A	14	0.490	359.60	76.00	0.0	0.0	11.70	0.330E-04	20.3	0
A	15	0.580	358.10	87.10	0.0	0.0	10.70	0.799E-04	18.6	0
A	16	0.570	12.70	81.90	0.0	0.0	12.30	0.349E-04	21.4	0
A	17	0.730	44.10	66.20	0.0	0.0	10.80	0.586E-04	18.7	0
A	18	0.720	342.90	64.70	0.0	0.0	21.20	0.630E-04	36.2	0
A	19	0.880	12.40	70.40	0.0	0.0	18.90	0.142E-03	32.4	0
A	20	0.870	51.30	59.40	0.0	0.0	19.40	0.909E-04	33.3	0
A	21	1.030	324.10	81.70	0.0	0.0	9.90	0.348E-04	17.2	0
A	22	1.030	350.80	77.00	0.0	0.0	8.60	0.383E-04	14.9	0
A	23	1.130	12.30	82.70	0.0	0.0	12.20	0.723E-04	21.1	0
A	24	1.130	322.00	77.70	0.0	0.0	17.20	0.690E-04	29.6	0
A	25	1.230	36.50	67.30	0.0	0.0	9.20	0.227E-04	16.0	0
A	26	1.230	53.60	73.40	0.0	0.0	9.20	0.863E-04	16.1	0
A	27	1.330	27.40	70.20	0.0	0.0	15.00	0.307E-04	25.9	0
A	28	1.330	14.40	77.10	0.0	0.0	9.50	0.517E-04	16.4	0
A	29	1.430	308.50	83.80	0.0	0.0	12.70	0.455E-04	22.0	0
A	30	1.430	30.90	74.70	0.0	0.0	16.90	0.452E-04	29.1	0
A	31	1.530	353.10	78.70	0.0	0.0	10.70	0.333E-03	18.5	0
A	32	1.530	32.80	87.10	0.0	0.0	7.90	0.391E-03	13.8	0
A	33	1.630	42.30	79.50	0.0	0.0	4.80	0.567E-04	8.3	0
A	34	1.630	102.00	63.70	0.0	0.0	29.40	0.691E-04	49.1	0
A	35	1.730	9.80	79.30	0.0	0.0	10.00	0.352E-04	17.4	0
A	36	1.730	3.90	61.30	0.0	0.0	15.00	0.516E-04	25.9	0
A	37	1.830	15.00	78.60	0.0	0.0	9.00	0.377E-04	15.7	0
A	38	1.830	13.00	60.00	0.0	0.0	13.70	0.148E-03	23.7	0
A	39	1.930	17.90	79.90	0.0	0.0	9.30	0.116E-03	16.2	0
A	40	1.930	26.70	80.30	0.0	0.0	9.30	0.598E-04	16.2	0
A	41	2.020	14.10	68.60	0.0	0.0	8.60	0.416E-04	15.0	0
A	42	2.020	40.00	78.80	0.0	0.0	6.30	0.509E-04	10.9	0
A	43	2.100	334.40	67.10	0.0	0.0	19.60	0.627E-04	33.5	0
A	44	2.100	332.20	80.10	0.0	0.0	6.50	0.349E-04	11.4	0
A	45	2.180	87.70	56.50	0.0	0.0	25.80	0.443E-04	43.5	0
A	46	2.190	340.40	78.30	0.0	0.0	8.60	0.509E-04	15.0	0
A	47	2.300	7.60	79.00	0.0	0.0	5.90	0.281E-04	10.4	0
A	48	2.300	13.80	79.30	0.0	0.0	9.50	0.260E-04	16.5	0
A	49	2.400	31.60	80.10	0.0	0.0	13.30	0.331E-04	23.0	0
A	50	2.400	109.90	82.90	0.0	0.0	13.20	0.202E-03	22.8	0
A	51	2.510	335.80	72.90	0.0	0.0	22.90	0.267E-03	38.9	0
A	52	2.500	305.70	45.00	0.0	0.0	26.90	0.543E-03	45.2	0
A	53	2.600	127.20	74.10	0.0	0.0	8.90	0.117E-03	15.4	0
A	54	2.600	41.80	84.60	0.0	0.0	4.50	0.397E-04	7.9	0
A	55	2.700	1.00	72.80	0.0	0.0	13.30	0.216E-04	23.0	0
A	56	2.700	353.40	50.40	0.0	0.0	14.60	0.243E-03	25.2	0
A	57	2.800	327.40	70.40	0.0	0.0	23.10	0.149E-03	39.2	0
A	58	2.800	336.90	61.70	0.0	0.0	13.60	0.133E-03	23.4	0
A	59	2.900	41.30	74.60	0.0	0.0	9.80	0.400E-04	17.0	0
A	60	2.900	0.90	49.90	0.0	0.0	19.50	0.885E-04	33.4	0
A	61	2.990	302.20	43.50	0.0	0.0	30.90	0.288E-03	51.4	0
A	62	3.000	20.80	62.90	0.0	0.0	7.00	0.219E-04	12.2	0
A	63	3.160	281.40	49.10	0.0	0.0	19.90	0.177E-03	34.1	0
A	64	3.160	351.40	75.00	0.0	0.0	13.00	0.681E-04	22.5	0
A	65	3.230	28.60	61.40	0.0	0.0	16.90	0.683E-04	29.1	0
A	66	3.230	354.10	80.10	0.0	0.0	16.80	0.250E-03	29.0	0
A	67	3.300	308.10	78.60	0.0	0.0	6.10	0.517E-03	10.7	0
A	68	3.300	54.70	60.70	0.0	0.0	14.50	0.428E-03	25.0	0
A	69	3.390	100.00	74.90	0.0	0.0	9.40	0.283E-03	16.3	0
A	70	3.390	48.10	77.40	0.0	0.0	15.80	0.491E-03	27.2	0
A	71	3.500	14.00	75.80	0.0	0.0	26.70	0.139E-03	44.9	0
A	72	3.500	38.70	69.10	0.0	0.0	13.80	0.217E-03	23.8	0
A	73	3.600	57.20	67.00	0.0	0.0	11.90	0.348E-03	20.6	0
A	74	3.600	63.10	74.20	0.0	0.0	9.30	0.278E-03	16.1	0
A	75	3.700	89.40	49.30	0.0	0.0	33.60	0.104E-03	55.3	0
A	76	3.700	20.50	71.80	0.0	0.0	8.50	0.853E-04	14.8	0
A	77	3.800	329.90	77.60	0.0	0.0	7.50	0.240E-04	13.1	0
A	78	3.800	321.20	50.80	0.0	0.0	14.60	0.829E-04	25.2	0
A	79	3.900	359.60	75.70	0.0	0.0	7.80	0.778E-04	13.6	0
A	80	3.900	9.50	56.00	0.0	0.0	12.90	0.572E-03	22.4	0
A	81	4.000	12.60	68.20	0.0	0.0	5.50	0.955E-04	9.6	0
A	82	4.000	58.40	48.60	0.0	0.0	14.70	0.214E-03	25.3	0
A	83	4.100	351.10	64.50	0.0	0.0	7.50	0.414E-04	13.1	0
A	83	4.100	346.40	60.00	0.0	0.0	8.90	0.286E-04	15.4	10
A	84	4.100	345.90	73.20	0.0	0.0	4.30	0.948E-04	7.4	0
A	84	4.100	333.60	70.60	0.0	0.0	3.80	0.468E-04	6.6	10
A	85	4.200	319.50	77.60	0.0	0.0	4.00	0.135E-03	6.9	0
A	85	4.200	309.90	73.90	0.0	0.0	3.90	0.915E-04	6.9	10
A	86	4.200	18.10	79.90	0.0	0.0	9.60	0.104E-03	16.6	0
A	86	4.200	1.80	78.00	0.0	0.0	9.80	0.631E-04	17.1	10
A	87	4.300	342.80	71.70	0.0	0.0	14.30	0.168E-04	24.7	0
A	88	4.300	303.70	73.70	0.0	0.0	12.70	0.938E-04	21.9	0
A	89	4.400	324.30	78.20	0.0	0.0	11.30	0.145E-04	18.6	0
A	90	4.400	1.70	70.40	0.0	0.0	9.90	0.120E-04	17.2	0
A	91	4.500	355.40	64.70	0.0	0.0	11.70	0.129E-04	20.3	0
A	92	4.500	334.60	75.90	0.0	0.0	12.90	0.101E-04	22.3	0
A	93	4.650	245.90	79.90	0.0	0.0	20.40	0.534E-05	34.8	0
A	94	4.650	80.40	79.30	0.0	0.0	25.30	0.428E-05	42.7	0
A	95	4.760	65.30	77.70	0.0	0.0	7.70	0.137E-04	13.4	0
A	96	4.750	56.80	75.80	0.0	0.0	15.20	0.109E-04	26.3	0
A	97	4.810	358.10	73.50	0.0	0.0	20.10	0.101E-04	34.3	0
A	98	4.810	1.60	70.30	0.0	0.0	5.50	0.171E-04	9.5	0
A	99	4.900	42.80	81.70	0.0	0.0	9.50	0.125E-04	16.6	0
A	99	4.900	20.90	76.40	0.0	0.0	9.50	0.762E-05	16.5	10
A	100	4.900	30.80	78.10	0.0	0.0	4.30	0.128E-04	7.5	0
A	100	4.900	17.10	71.20	0.0	0.0	3.50	0.972E-05	6.1	10
A	101	5.000	319.60	79.70	0.0	0.0	9.60	0.120E-04	16.6	0
A	101	5.000	294.70	79.20	0.0	0.0	9.40	0.806E-05	16.4	10
A	102	5.000	26.50	66.00	0.0	0.0	5.70	0.124E-04	9.9	0
A	102	5.000	22.30	66.20	0.0	0.0	7.30	0.851E-05	12.8	10
A	103	5.130	33.70	79.10	0.0	0.0	5.70	0.170E-04	10.0	0
A	103	5.130	12.40	75.80	0.0	0.0	4.40	0.112E-04	7.7	10
A	104	5.130	5.80	77.80	0.0	0.0	7.00	0.170E-04	12.3	0
A	104	5.130	342.10	73.70	0.0	0.0	5.20	0.106E-04	9.0	10
A	105	5.220	9.90	75.70	0.0	0.0	6.10	0.165E-04	10.5	0
A	105	5.220	355.20	73.00	0.0	0.0	8.60	0.117E-04	14.9	10
A	106	5.220	18.60	73.90	0.0	0.0	6.10	0.164E-04	10.7	0
A	106	5.220	6.10	69.30	0.0	0.0	4.80	0.113E-04	8.5	10
A	107	5.350	20.30	73.30	0.0	0.0	7.60	0.198E-04	13.2	0
A	108	5.350	9.50	70.50	0.0	0.0	8.40	0.208E-04	14.6	0
A	109	5.650	56.50	76.10	0.0	0.0	6.50	0.157E-04	11.2	0
A	109	5.650	53.50	73.70	0.0	0.0	7.80	0.106E-04	13.7	10
A	110	5.650	10.80	76.40	0.0	0.0	5.60	0.180E-04	9.7	0

A110	5 650	4 90	70.20	0.0	0 0	8 10	0.123E-04	14 0	10
A111	5.750	52 80	79.60	0.0	0.0	8.20	0.157E-04	14.3	0
A112	5 750	23 30	79 10	0.0	0.0	18.00	0.116E-04	31.0	0
A113	5 850	50.30	79 70	0 0	0 0	7.20	0.103E-04	12.4	0
A114	5 840	65 30	84.60	0.0	0 0	10.20	0.124E-04	17.7	0
A115	5 950	52 50	76 90	0 0	0.0	8.30	0.1088-04	16.2	0
A116	5 940	62 70	75.60	0 0	0 0	11 40	0.131E-04	19.8	0
A117	6 060	41.60	77 20	0.0	0.0	15.20	0.114E-04	26 2	0
A118	6.050	56.20	77.70	0.0	0 0	7.80	0.133E-04	13 5	0
A119	6 150	306.70	64 90	0.0	0.0	11.80	0.306E-04	20.6	0
A120	6 150	20.20	69 90	0 0	0.0	10.00	0.195E-04	17.4	0
A121	6.240	308.30	82.60	0 0	0.0	6.60	0.326E-04	11 5	0
A122	6.240	350.20	82.30	0 0	0.0	22.60	0.283E-04	39.5	0
A123	6.310	325.30	72.30	0.0	0.0	6.00	0.583E-04	10.4	0
A123	6 310	320.70	70.10	0 0	0.0	2.90	0.429E-04	5.0	10
A124	6 310	342.00	54.20	0.0	0 0	5.30	0.609E-04	9.3	0
A124	6.310	339.90	51.90	0.0	0.0	3.80	0.447E-04	6.6	10
A125	6.400	358 10	71.10	0.0	0.0	7.60	0.355E-04	13.2	0
A125	6.400	349.20	71 80	0.0	0.0	6.00	0.275E-04	10.4	10
A126	6 400	10.00	69 10	0 0	0.0	4.60	0.413E-04	8 0	0
A126	6 400	9.00	67 50	0 0	0 0	4.20	0 304E-04	7.3	10
A127	6.500	322.80	75.70	0.0	0 0	7.70	0.182E-04	13.5	0
A127	6 500	356.80	79.50	0.0	0.0	7.60	0.124E-04	13.2	10
A128	6 500	302.50	69.30	0.0	0.0	5.70	0.421E-04	9.9	0
A128	6 500	293 50	69 50	0.0	0.0	8.40	0.308E-04	14.6	10
A129	6 600	329.90	74 80	0 0	0.0	5 60	0.490E-04	9.8	0
A129	6 600	343 70	76 00	0 0	0 0	4.80	0.355E-04	8 4	10
A130	6 600	322.80	79.60	0.0	0.0	2.80	0.416E-04	4.8	0
A130	6 600	312 80	79 00	0 0	0 0	3.30	0.288E-04	5.7	10
A131	6 700	321 60	57 70	0 0	0 0	8.20	0.315E-04	14.2	0
A131	6 700	320.60	54 30	0 0	0.0	6.90	0 237E-04	12.0	10
A132	6 700	306.60	58.20	0 0	0 0	8.30	0.614E-04	14.5	0
A132	6.700	302.30	59.00	0 0	0.0	4.80	0.461E-04	8.3	10
A133	6 800	343 90	79 40	0 0	0 0	5 [illegible]	0.400E-04	9.8	0
A133	6 800	325 30	82.00	0 0	0.0	4.30	0.295E-04	7.4	10
A134	6.800	249.20	82.90	0.0	0 0	6.20	0.429E-04	10.9	0
A134	6 800	217.30	83.50	0.0	0.0	6.50	0.313E-04	11.3	10
A135	6.900	321 70	59.80	0 0	0 0	3.70	0.343E-04	6.4	0
A135	6 900	315 90	57 20	0 0	0 0	5.80	0.243E-04	10.2	10
A136	6.900	346.30	72.00	0.0	0 0	4.60	0.309E-04	8.1	0
A136	6.900	336.60	70.50	0.0	0 0	6.50	0.207E-04	11 2	10
A137	7 110	310 80	65.00	0.0	0 0	19.80	0.377E-05	33.8	0
A138	7 110	317 80	74.70	0 0	0.0	20 30	0.466E-05	34 7	0
A139	7.250	342 10	82 20	0.0	0.0	8.00	0.121E-04	13.9	0
A139	7.250	311 90	79.10	0 0	0.0	10.60	0.827E-05	18 5	10
A140	7.250	333.80	79.90	0 0	0.0	10.30	0.216E-04	17.9	0
A140	7.250	330.80	71 20	0.0	0 0	7.30	0.145E-04	12.8	10
A141	7 340	33 00	79.50	0 0	0 0	6 10	0.776E-05	10 6	0
A142	7 330	109.80	84.10	0 0	0 0	8.60	0.632E-05	15 0	0
A143	7 520	358 50	74 00	0 0	0 0	4 70	0.352E-04	8.2	0
A143	7 520	348.90	72 50	0 0	0 0	5 40	0.271E-04	9.3	10
A144	7 520	345 80	70 00	0.0	0.0	5.40	0.291E-04	9 5	0
A144	7.520	342.30	66.90	0 0	0 0	5.40	0.228E-04	9.4	10
A145	7 760	358.80	62.30	0.0	0.0	4.60	0.240E-04	8.0	0
A145	7 760	356.00	59.70	0.0	0.0	4.20	0.192E-04	7.4	10
A146	7 760	342.10	71 20	0.0	0.0	7.90	0.162E-04	13.7	0
A146	7 760	334.00	67 00	0.0	0 0	6.30	0.111E-04	10.9	10
A147	7 840	359.40	70.30	0.0	0 0	6.50	0.239E-04	11 3	0
A147	7 840	353.60	65.40	0.0	0.0	7.30	0.167E-04	12.7	10
A148	7 840	335.60	61.70	0.0	0.0	10.00	0.227E-04	17.4	0
A148	7 840	326.50	57 10	0.0	0 0	6.40	0.176E-04	11.1	10
A149	7 940	28 50	75.90	0.0	0.0	7 00	0 682E-05	12 1	0
A149	7 940	23 50	78.80	0.0	0.0	10.30	0 403E-05	17 8	10
A150	7 940	10 30	73.40	0.0	0.0	10.30	0.607E-05	17.9	0
A150	7 940	357 40	67.40	0.0	0.0	11 50	0.430E-05	19.9	10
A151	8 200	233 50	59.20	0.0	0 0	47.70	0.611E-05	74.0	0
A152	8 200	342 50	83.60	0.0	0.0	7.80	0.514E-05	13.5	0
A153	8 310	336.80	66 70	0.0	0.0	9.20	0.937E-05	15 9	0
A153	8 310	331.60	58.80	0.0	0.0	10.60	0.672E-05	18.5	10

A154	8 310	353 40	71 00	0 0	0.0	[illegible] 20	0.988E-05	12 5	0
A154	8 310	338 20	66 10	0 0	0.0	[illegible] 20	0 672E-05	11.0	10
A155	8 400	347 50	66 00	0 0	0 0	[illegible] 20	0 174E-04	7.6	0
A155	8 400	334 60	63.20	0 0	0.0	[illegible] 60	0.110E-04	11.4	10
A156	8 400	342 90	62 00	0 0	0 0	4.00	0.190E-04	6.9	0
A156	8 400	336 10	60 20	0 0	0 0	8.60	0.116E-04	15.0	10
A157	8 500	31 70	73 50	0 0	0.0	10 60	0.946E-05	18.3	0
A157	8 500	6 00	77 60	0 0	0 0	8.50	0.536E-05	14.7	10
A158	8 500	14 90	81 00	0 0	0.0	4.40	0.825E-05	7.7	0
A158	8 500	340 80	77 70	0 0	0 0	4 70	0 550E-05	8.2	10
A159	8 610	27 40	75 60	0 0	0 0	6 20	0 862E-05	10 8	0
A159	8 610	1 70	68 10	0 0	0 0	5.10	0.539E-05	10.6	10
A160	8 610	37 10	80 50	0 0	0 0	6 40	0.788E-05	11.1	0
A160	8 610	4 50	74 20	0.0	0 0	7.80	0.520E-05	13.6	10
A161	8 710	339 00	66 50	0 0	0 0	5.30	0.981E-05	9.2	0
A161	8 710	337 00	69 90	0 0	0.0	8.00	0.578E-05	13.8	10
A162	8 710	358.30	73 20	0 0	0.0	8.50	0.830E-05	14.8	0
A162	8 710	356.70	73 00	0 0	0.0	10.40	0.539E-05	18.1	10
A163	8 820	352 60	64 80	0 0	0 0	8 40	0.180E-04	14.6	0
A163	8 820	339 10	66 70	0 0	0 0	7.40	0.112E-04	12.9	10
A164	8 820	356 60	69.90	0 0	0.0	5.30	0.144E-04	9.2	0
A164	8 820	348 00	64 00	0 0	0 0	7.40	0.916E-05	12.9	10
A165	8.930	2 50	64.30	0 0	0 0	6.20	0.375E-04	10.8	0
A165	8 930	358 20	61 50	0 0	0.0	6.80	0.292E-04	11.9	10
A166	8.920	6 60	70.20	0 0	0 0	4.90	0.336E-04	8.6	0
A166	8.920	4 20	68.30	0 0	0 0	4 10	0.237E-04	7.2	10
A167	9 020	24 80	72 70	0 0	0.0	6 60	0.152E-04	11.5	0
A167	9 020	12 50	70 00	0 0	0 0	6.70	0.897E-05	11.7	10
A168	9 020	9 30	72 50	0 0	0 0	7.00	0.118E-04	12.2	0
A168	9 020	354 10	66 00	0 0	0.0	9 80	0.727E-05	17.2	10
A169	9 120	5 10	62 70	0 0	0 0	15 70	0.112E-04	27.4	0
A169	9.120	353.80	55.80	0 0	0.0	7.80	0.641E-05	13.6	10
A170	9 120	8.20	64.10	0 0	0.0	10.00	0.108E-04	17.4	0
A170	9 120	358.90	56.20	0 0	0.0	10.80	0.671E-05	18.7	10
A171	9 240	10.90	71.00	0 0	0.0	5.60	0.182E-04	9.8	0
A171	9 240	6 60	67.60	0 0	0.0	7.50	0.134E-04	13.0	10
A172	9 240	354 00	69 50	0 0	0.0	8.30	0.230E-04	14.4	0
A172	9 240	354 70	65.90	0 0	0 0	6.90	0.167E-04	13.0	10
A173	9 360	348 70	65 30	0 0	0 0	13 50	0.880E-05	23 3	0
A173	9 360	357.40	65.60	0 0	0 0	10.50	0.646E-05	18.3	10
A174	9 360	1 70	66 20	0 0	0 0	10.20	0.190E-04	17.7	0
A174	9 360	353 60	58 60	0 0	0 0	10.80	0.765E-05	18.8	10
A175	9 450	3 20	64 80	0 0	0 0	8.20	0.198E-04	14.3	0
A175	9 450	351 10	62 90	0 0	0 0	6.60	0.958E-05	11.4	10
A176	9 450	350 80	43 60	0 0	0 0	11.70	0.182E-04	20.3	0
A176	9 450	350 10	40 00	0 0	0 0	10 80	0 146E-04	18.7	10
A177	9 550	347 40	26 90	0 0	0 0	5.90	0.116E-04	10.2	0
A177	9 550	347 50	16.20	0 0	0.0	5.80	0 898E-05	10.1	10
A178	9 550	347 50	47 60	0 0	0.0	9.00	0.118E-04	15.6	0
A178	9 550	346 00	40 10	0 0	0.0	4.10	0.773E-05	7.2	10
A179	9 600	350 30	42 70	0 0	0 0	16.90	0 237E-04	29.1	0
A179	9 600	347 30	49.00	0 0	0 0	2.90	0 165E-04	5.1	10
A180	9 600	345 70	52 70	0 0	0 0	18 40	0.200E-04	31.6	0
A180	9 600	342 10	41 00	0 0	0 0	10 10	0 149E-04	11.5	10
A181	9 700	323.70	47 20	0 0	0.0	7.10	0.360E-04	12.3	0
A181	9 700	323 00	41 40	0 0	0 0	6.30	0.282E-04	11.0	10
A182	9 700	357.80	35 70	0 0	0.0	5.30	0.213E-04	9.3	0
A182	9.700	354 00	30 60	0 0	0 0	4.40	0.154E-04	7.7	10
A183	9 800	353 00	52 50	0 0	0 0	7.20	0.175E-04	12.5	0
A183	9 800	333 90	48 [illegible]	0 0	0.0	2.00	0.122E-04	3.5	10
A184	9 800	348 80	57 40	0 0	0.0	3.60	0.188E-04	6.3	0
A184	9 800	336 80	49 90	0 0	0.0	3.70	0.125E-04	6.5	10
A185	9 900	358.30	55 [illegible]	0 0	0.0	6.60	0.205E-04	11.5	0
A185	9 900	357.30	50 [illegible]	0 0	0.0	6.30	0.139E-04	11.0	10
A186	9 900	344.10	5 [illegible]	0 0	0.0	4.80	0.201E-04	8.4	0
A186	9 900	341.60	4 [illegible]	0 0	0.0	4.00	0.142E-04	7.0	10
A187	10 000	358.00	[illegible]	0 0	0.0	10.70	0.761E-05	18.5	0
A187	10 000	325 30	[illegible]	0 0	0.0	16.20	0.333E-05	27.9	10
A188	10 000	353 70	[illegible]	0 0	0.0	7 00	0.790E-05	12.1	0

A188	10 000	336 80	59 00	0 0	0 0	11 30	0 449E-05	19 5	10
A189	10 130	335.30	53.50	0 0	0 0	28 50	0.146E-04	47 7	0
A189	10 130	331.50	44 40	0 0	0 0	36.80	0.936E-05	60.0	10
A190	10.130	323.70	53.60	0.0	0 0	17.50	0.246E-04	30 1	0
A190	10 130	318.00	49 40	0.0	0 0	20 30	0.174E-04	34.6	10
A191	10 210	5 30	72 30	0 0	0 0	18 00	0 588E-05	30 9	0
A191	10 210	356 00	66.30	0 0	0 0	23 90	0 339E-05	40 5	10
A192	10 210	36.10	76 30	0 0	0 0	11.80	0.637E-05	20 5	0
A192	10 210	97 20	78 90	0 0	0 0	26 70	0 359E-05	45 0	10
A193	10 300	319 20	72 50	0.0	0 0	17.70	0.622E-05	30.4	0
A193	10 300	308 20	75 80	0.0	0 0	43.30	0 315E-05	68 5	10
A194	10.300	258 90	68 50	0 0	0 0	9 50	0 649E-05	16 6	0
A194	10 300	285.30	58 30	0.0	0.0	25.00	0.285E-05	42 2	10
A195	10.400	37 80	77.00	0 0	0 0	13 10	0.629E-05	22 6	0
A195	10.400	39.70	74 50	0 0	0 0	33.20	0.229E-05	54 7	10
A196	10 400	92.30	79.80	0 0	0 0	9.60	0.824E-05	16.6	0
A197	10 500	59.50	73 90	0 0	0 0	11 90	0.907E-05	20 6	0
A198	10.500	99 50	84.50	0.0	0 0	5.70	0.108E-04	9 9	0
A199	10.580	356.80	64 10	0 0	0 0	10 30	0.245E-04	17 8	0
A199	10.580	340 30	56 90	0 0	0 0	6.80	0.146E-04	11 9	10
A200	10.580	343 40	56 90	0 0	0 0	7 50	0 284E-04	13 0	0
A200	10 580	335 10	45.50	0 0	0 0	8 30	0.155E-04	14 5	10
A201	10 700	355 80	51.40	0 0	0 0	9 80	0.199E-04	17 1	0
A201	10 700	340 30	38 50	0 0	0 0	10.00	0.153E-04	17 3	10
A202	10 700	344.50	45.70	0.0	0.0	7.00	0.236E-04	12.1	0
A202	10 700	334 30	32.00	0 0	0 0	10 90	0.182E-04	18 9	10
A203	10 800	352.20	60 40	0 0	0 0	8.40	0 303E-04	14 7	0
A203	10 800	352 20	59 30	0 0	0 0	5.00	0.238E-04	8 7	10
A204	10 800	333 30	57 10	0 0	0 0	5 60	0.414E-04	9.8	0
A204	10 800	328.10	53.00	0.0	0 0	9.00	0.289E-04	15 6	10
A205	10.900	8.80	65 70	0 0	0 0	2.70	0.298E-04	4 6	0
A205	"	347.70	61 40	0 0	0 0	4 50	0.243E-04	7.8	2
A205	"	351.30	59.90	0 0	0 0	4.20	0.233E-04	7.3	5
A205	10 900	348 30	59 00	0 0	0 0	3 70	0 189E-04	6.5	10
A205	"	350.80	59.70	0 0	0 0	5.20	0.156E-04	9 1	15
A205	"	344.50	58 20	0 0	0 0	4 00	0 136E-04	7.0	20
A205	"	338 30	59.10	0 0	0 0	6 70	0.104E-04	11 6	30
A205	"	358.70	54 40	0 0	0 0	9 60	0.826E-05	16 7	40
A205	"	356.50	46 80	0 0	0 0	9.10	0.723E-05	15 8	50
A206	10 900	24 20	69 70	0 0	0 0	4.00	0.246E-04	7.0	0
A206	"	350 30	69 90	0 0	0 0	3.90	0 188E-04	6 7	2
A206	"	349.50	68.60	0 0	0 0	4 10	0.177E-04	7.2	5
A206	10 900	343.80	64 20	0 0	0 0	5.40	0 149E-04	9.5	10
A206	"	335 40	66 00	0 0	0 0	6 20	0 105E-04	10.9	15
A206	"	341 80	67 70	0 0	0 0	9 80	0.935E-05	17 0	20
A206	"	359 90	67 90	0 0	0 0	11 30	0 659E-05	19.5	30
A206	"	353 30	64 20	0 0	0 0	10 90	0 660E-05	19.0	40
A206	"	20.90	66 50	0 0	0 0	14.00	0.406E-05	24.2	50
A207	11 000	349 30	71 50	0 0	0 0	6 00	0.200E-04	10.4	0
A207	11.000	331 70	70 80	0 0	0 0	7.70	0 135E-04	13 4	10
A208	11.000	13.20	72 30	0.0	0 0	7.30	0 170E-04	12.7	0
A208	11 000	355 20	73 90	0 0	0 0	6 40	0 108E-04	11 1	10
A209	11 100	358.70	68 50	0 0	0 0	6 30	0.185E-04	10 9	0
A209	11 100	1 20	65.00	0 0	0 0	5.80	0.132E-04	10.1	10
A210	11.100	348.80	80.40	0 0	0 0	4 80	0.186E-04	7.8	0
A210	11 100	340.30	73 80	0 0	0 0	5.50	0.125E-04	9 6	10
A211	11 250	352.70	76.30	0 0	0 0	4.40	0.187E-04	7 6	0
A211	11 250	337 40	66 00	0 0	0 0	14.00	0.879E-05	24.1	10
A212	11 250	24.30	77 40	0 0	0 0	14.10	0.178E-04	24.4	0
A212	11 250	30.00	81.00	0 0	0 0	15 40	0 103E-04	26.6	10
A213	11 320	357 70	57.60	0 0	0 0	4.40	0.262E-04	7.8	0
A213	11.320	353.00	52 70	0 0	0 0	7.10	0.168E-04	12 4	0
A214	11 320	2.00	85 70	0 0	0 0	6 10	0.291E-04	10.6	0
A214	11 320	351.10	50 50	0 0	0 0	6 80	0.195E-04	11 9	0
A215	11 400	36.60	76 40	0 0	0 0	7 90	0 193E-04	13 7	0
A216	11 400	49.90	84.60	0 0	0 0	8 00	0.189E-04	14 0	0
A217	11 520	335.20	59.40	0 0	0 0	9.00	0.329E-04	15 6	0
A217	11 520	329.20	51 50	0 0	0 0	10.60	0.219E-04	18 3	10
A218	11 520	335.70	61.20	0 0	0 0	9 40	0 348E-04	16 3	0

A218	11 520	329 60	51 90	0 0	0 0	10 90	0 222E-04	18.0	10
A219	11 620	0 90	56 70	0 0	0 0	6.20	0 251E-04	10.8	0
A219	11 620	342 50	44 40	0 0	0 0	6.00	0 201E-04	10.4	10
A220	11 620	346 70	57 00	0 0	0 0	7 40	0 314E-04	12.8	0
A220	11 620	338 90	53 50	0 0	0 0	8 50	0 242E-04	14 9	10
A221	11 710	335 10	65 90	0 0	0 0	6 10	0.372E-04	10.6	0
A221	11 710	336 50	53 70	0 0	0 0	3 80	0 266E-04	6.6	10
A222	11 710	336 20	65.10	0 0	0 0	6.60	0 381E-04	11.6	0
A222	11 710	334 30	57 70	0 0	0 0	8.00	0.268E-04	13.9	10
A223	11 820	349 90	70 30	0 0	0 0	6.30	0.261E-04	11.0	0
A223	11 820	341 70	65 50	0 0	0 0	9.80	0.179E-04	17.1	10
A224	11 820	359 60	74 90	0 0	0 0	11 20	0.264E-04	18.4	0
A224	11 820	353 10	64 40	0 0	0 0	8 10	0.185E-04	14.0	10
A225	11 900	329 30	66 40	0 0	0 0	8 80	0.400E-04	15.3	0
A225	11 900	320 60	58 80	0 0	0 0	5 80	0.281E-04	10.2	10
A226	11 900	330 10	64 90	0 0	0 0	8.00	0 424E-04	13.8	0
A226	11 900	327 70	55 60	0 0	0 0	8.30	0.315E-04	14.4	10
A227	12 000	359.70	70 10	0 0	0 0	6.00	0.511E-04	10.4	0
A227	12 000	348.40	63.40	0 0	0 0	3.60	0.354E-04	6.2	10
A228	12 000	337 00	63 90	0 0	0 0	5 70	0.492E-04	9.9	0
A228	12 000	329.50	60.30	0 0	0 0	4 60	0.373E-04	8.0	10
A229	12 150	35 60	70 90	0 0	0 0	2 40	0.551E-04	4.2	0
A229	12 150	24 90	66 60	0 0	0 0	5 10	0 394E-04	8.9	10
A230	12 150	20 60	67 80	0 0	0 0	8 20	0.480E-04	14.2	0
A230	12 150	14 70	63 70	0 0	0 0	8 10	0 329E-04	14.1	10
A231	12 920	26 00	73 20	0 0	0 0	6.60	0.810E-04	11.4	0
A231	12 920	22 20	70 40	0 0	0 0	6 50	0.446E-04	11.3	10
A232	12 920	67 30	76 60	0 0	0 0	3.30	0.851E-04	5.8	0
A232	12 920	50 40	74 20	0 0	0 0	5.00	0.468E-04	8.8	10
A233	13 060	76 70	73.40	0 0	0 0	4.90	0.719E-04	8.5	0
A233	13 060	55 00	71 70	0 0	0 0	4 60	0.495E-04	8.0	10
A234	13 080	47 70	77 70	0 0	0 0	5.90	0.678E-04	10.2	0
A234	13 080	45 40	71 60	0 0	0 0	5 40	0.473E-04	9.3	10
A235	13 260	225 40	86 10	0 0	0 0	4.50	0.603E-04	7.8	0
A235	13 260	258 20	81 60	0 0	0 0	4.00	0.382E-04	6.9	10
A236	13 270	339 60	76 90	0 0	0 0	6.60	0.598E-04	11.5	0
A236	13 270	340 80	74 60	0 0	0 0	2 80	0.408E-04	5.1	10
A237	13 350	358 90	82.40	0 0	0 0	3.40	0.826E-04	6.0	0
A237	13 350	341 80	81 70	0 0	0 0	4.20	0.673E-04	7.3	10
A238	13 350	349 30	84 50	0 0	0 0	4 60	0.738E-04	8.0	0
A238	13 350	324 00	83 80	0 0	0 0	4 90	0.526E-04	8.5	10
A239	13.470	358 10	80 20	0 0	0 0	6.50	0.630E-04	11.3	0
A239	13 470	353 40	80 80	0 0	0 0	4 80	0.389E-04	8.4	10
A240	13 470	354 00	81 30	0 0	0 0	2 70	0.634E-04	4.6	0
A240	13 470	311 20	77.10	0 0	0 0	4.90	0.410E-04	8.6	10
A241	13 570	44 20	87 80	0 0	0 0	6 90	0 657E-04	12.1	0
A241	13 570	349 80	81 80	0 0	0 0	5 20	0.471E-04	9.0	10
A242	13 570	346 60	84 20	0 0	0 0	5 00	0.574E-04	8.8	0
A242	13 570	321 80	83 00	0 0	0 0	5.30	0.395E-04	9.3	10
A243	13 710	356 20	82.60	0 0	0 0	5 10	0.734E-04	8.9	0
A243	13 710	338.60	78 90	0 0	0 0	4 80	0.478E-04	8.3	10
A244	13 700	352 40	79 60	0 0	0 0	7 60	0.756E-04	13.2	0
A244	13.700	340 00	78 20	0 0	0 0	4 40	0.520E-04	7.8	10
A245	13 830	42 60	82 00	0 0	0 0	5.40	0.668E-04	9.4	0
A245	13 830	32 10	83 00	0 0	0 0	4 00	0.451E-04	6.9	10
A246	13 830	31 70	82 70	0 0	0 0	6.20	0.821E-04	10.8	0
A246	13 830	8 80	81 00	0 0	0 0	4.30	0.634E-04	7.6	10
A247	13 960	29 90	76.30	0 0	0 0	7.10	0.883E-04	12.4	0
A247	13 960	46.20	76 50	0 0	0 0	5.60	0.475E-04	9.8	10
A248	13 960	39 10	88 80	0 0	0 0	11 60	0.800E-04	20.1	0
A248	13 960	323 00	86 90	0 0	0 0	4.90	0.564E-04	8.5	10
A249	14 080	20 70	78 20	0 0	0 0	9 90	0.946E-04	17.3	0
A249	14 080	25.30	76 40	0 0	0 0	4 60	0.737E-04	8.1	10
A250	14 080	7 60	79 80	0 0	0 0	5.00	0.103E-03	8.7	0
A250	14 080	355 10	78 20	0 0	0 0	3 90	0.750E-04	6.8	10
A251	14 190	8 90	78.50	0 0	0 0	3 60	0.753E-04	6.3	0
A251	14 190	350 10	79 80	0 0	0 0	5 50	0.514E-04	10.5	10
A252	14 190	352.40	81 70	0 0	0 0	5 40	0.763E-04	9.4	0
A252	14 190	336 00	80 70	0 0	0 0	2 90	0.563E-04	5.1	10

A253	14 200	54 70	78 30	0.0	0.0	3.10	0.112E-03	5.5	0
A253	14 200	31 90	77 90	0.0	0.0	2.80	0.790E-04	4.8	10
A254	14 200	50 20	78 00	0.0	0.0	3.50	0.101E-03	6.1	0
A254	14 200	23 40	78 60	0.0	0.0	4.50	0.683E-04	7.8	10
A255	14 280	18 90	76 80	0.0	0.0	4.00	0.107E-03	6.9	0
A255	14 280	3 60	76 90	0.0	0.0	3.00	0.775E-04	5.2	10
A256	14 280	38 70	80 30	0.0	0.0	4.90	0.116E-03	8.5	0
A256	14 280	17 80	78 50	0.0	0.0	3.50	0.808E-04	6.2	10
A257	14 370	18 10	75 00	0.0	0.0	4.40	0.850E-04	7.6	0
A257	14 370	16 60	75 40	0.0	0.0	4.60	0.565E-04	8.1	10
A258	14 370	51 50	76 90	0.0	0.0	3.70	0.899E-04	6.5	0
A258	14 370	30 30	77 20	0.0	0.0	4.10	0.587E-04	7.1	10
A259	14 460	29 40	71 50	0.0	0.0	4.70	0.932E-04	8.2	0
A259	14 460	24 60	72 30	0.0	0.0	3.10	0.618E-04	5.4	10
A260	14 460	33 30	70 40	0.0	0.0	4.40	0.950E-04	7.7	0
A260	14 460	34 70	70 40	0.0	0.0	5.20	0.634E-04	9.1	10
A261	14 560	34 60	68 50	0.0	0.0	5.10	0.993E-04	8.8	0
A261	14 560	30 30	68 40	0.0	0.0	4.90	0.699E-04	8.6	10
A262	14 560	33 90	71 20	0.0	0.0	6.10	0.104E-03	10.7	0
A262	14 560	25 90	70 50	0.0	0.0	6.00	0.748E-04	10.4	10
A263	14 710	24 40	73 40	0.0	0.0	6.50	0.136E-03	11.3	0
A263	14 710	25 30	75 30	0.0	0.0	6.40	0.972E-04	11.2	10
A264	14 710	28 60	77 00	0.0	0.0	7.10	0.120E-03	12.3	0
A264	14 710	14 90	77 80	0.0	0.0	5.00	0.885E-04	8.7	10
A265	14 820	7 60	74 40	0.0	0.0	4.30	0.105E-03	7.5	0
A265	14 820	0 10	73 30	0.0	0.0	4.30	0.771E-04	7.5	10
A266	14 820	1 00	77 60	0.0	0.0	3.00	0.110E-03	5.3	0
A266	14 820	341 20	77 20	0.0	0.0	3.30	0.830E-04	5.7	10
A267	15 880	343 20	75 70	0.0	0.0	5.80	0.927E-04	10.1	0
A267	15 880	333 00	76 10	0.0	0.0	5.10	0.647E-04	8.9	10
A268	15 880	311 60	84 40	0.0	0.0	3.70	0.909E-04	6.5	0
A268	15 880	305 90	80 50	0.0	0.0	3.90	0.633E-04	6.8	10
A269	16 000	4 00	84 50	0.0	0.0	3.80	0.610E-04	6.7	0
A269	16 000	352 70	86 90	0.0	0.0	3.70	0.469E-04	6.5	10
A270	16 000	303 60	86 10	0.0	0.0	3.50	0.938E-04	6.2	0
A270	16 000	291 90	85 50	0.0	0.0	3.00	0.685E-04	5.2	10
A271	16 270	212 60	84 20	0.0	0.0	5.50	0.922E-04	9.6	0
A271	16 270	224 50	82 30	0.0	0.0	5.90	0.686E-04	10.3	10
A272	16 270	86 70	86 20	0.0	0.0	5.40	0.891E-04	9.3	0
A272	16 270	328 20	83 60	0.0	0.0	6.20	0.652E-04	10.9	10
A273	16 710	18 10	68 20	0.0	0.0	4.70	0.964E-04	8.2	0
A273	16 710	15 40	67 50	0.0	0.0	4.00	0.595E-04	6.9	10
A274	16 710	13 50	64 80	0.0	0.0	6.10	0.888E-04	10.6	0
A274	16 710	10 60	62 90	0.0	0.0	5.20	0.617E-04	9.1	10
A275	16 820	11 40	71 60	0.0	0.0	5.50	0.899E-04	9.6	0
A275	16 820	9 50	70 60	0.0	0.0	3.10	0.566E-04	5.5	10
A276	16 820	356 90	67 00	0.0	0.0	4.50	0.148E-03	7.8	0
A276	16 820	355 00	66 50	0.0	0.0	3.80	0.105E-03	6.7	10
A277	16 920	7 30	76 30	0.0	0.0	3.30	0.108E-03	5.7	0
A277	-	4 50	77 90	0.0	0.0	6.00	0.861E-04	10.5	2
A277	-	8 10	76 50	0.0	0.0	5.60	0.841E-04	9.7	5
A277	16 920	4 50	75 80	0.0	0.0	6.70	0.711E-04	11.6	10
A277	-	4 70	78 00	0.0	0.0	5.90	0.634E-04	10.3	15
A277	-	359 70	75 30	0.0	0.0	6.20	0.526E-04	10.7	20
A277	-	5 80	75 50	0.0	0.0	6.00	0.378E-04	10.5	30
A277	-	5 30	71 40	0.0	0.0	7.40	0.256E-04	12.9	40
A277	-	305 60	79 50	0.0	0.0	8.80	0.207E-04	15.3	50
A278	16 920	10 30	73 00	0.0	0.0	1.90	0.863E-04	3.3	0
A278	-	12 40	75 80	0.0	0.0	2.90	0.741E-04	5.1	2
A278	-	7 70	75 50	0.0	0.0	1.90	0.711E-04	3.2	5
A278	16 920	15 00	77 00	0.0	0.0	3.80	0.653E-04	6.7	10
A278	-	8 90	75 80	0.0	0.0	2.90	0.523E-04	5.1	15
A278	-	6 70	76 20	0.0	0.0	3.80	0.458E-04	6.6	20
A278	-	5 90	76 00	0.0	0.0	4.40	0.351E-04	7.6	30
A278	-	16 60	76 50	0.0	0.0	7.20	0.215E-04	12.6	40
A278	-	42 90	42 90	0.0	0.0	10.90	0.131E-04	18.9	50
A279	16 980	35 80	78 00	0.0	0.0	5.40	0.131E-03	9.4	0

A279	16 980	22 40	78 30	0.0	0.0	6.40	0.710E-04	11.1	10
A280	16 980	36 60	80 00	0.0	0.0	6.20	0.116E-03	10.8	0
A280	16 980	18 90	75 50	0.0	0.0	3.70	0.721E-04	6.5	10
A281	17 100	36 10	79 60	0.0	0.0	3.40	0.778E-04	6.0	0
A281	17 100	13 80	77 70	0.0	0.0	3.40	0.532E-04	6.0	10
A282	17 100	3 10	75 10	0.0	0.0	7.70	0.894E-04	13.2	0
A282	17 100	355 10	72 50	0.0	0.0	7.20	0.641E-04	12.5	10
A283	17 200	357 70	75 40	0.0	0.0	4.80	0.108E-03	8.3	0
A283	17 200	350 90	73 80	0.0	0.0	5.60	0.115E-03	9.7	10
A284	17 200	26 10	73 90	0.0	0.0	1.70	0.143E-03	3.0	0
A284	17 200	16 80	73 50	0.0	0.0	2.50	0.970E-04	4.3	10
A285	17 300	334 70	63 40	0.0	0.0	3.00	0.994E-03	5.3	0
A285	17 300	332 00	59 90	0.0	0.0	2.70	0.141E-03	4.7	10
A286	17 300	359 40	68 20	0.0	0.0	2.30	0.180E-03	4.0	0
A286	17 300	355 70	62 30	0.0	0.0	5.40	0.122E-03	9.4	10
A287	17 400	22 20	79 20	0.0	0.0	1.20	0.235E-03	2.1	0
A287	17 400	359 00	78 80	0.0	0.0	2.10	0.144E-03	3.7	10
A288	17 400	48 30	82 50	0.0	0.0	2.10	0.128E-03	3.6	0
A288	17 400	25 00	85 00	0.0	0.0	2.30	0.860E-04	4.1	10
A289	17 500	27 30	82 10	0.0	0.0	2.40	0.239E-03	4.3	0
A289	17 500	357 70	81 40	0.0	0.0	2.20	0.156E-03	3.9	10
A290	17 500	74 50	83 20	0.0	0.0	2.10	0.206E-03	3.7	0
A290	17 500	76 90	86 00	0.0	0.0	1.90	0.188E-03	3.2	10
A291	17 610	28 30	81 10	0.0	0.0	2.20	0.258E-03	3.8	0
A291	17 610	358 30	80 90	0.0	0.0	2.60	0.235E-03	4.6	10
A292	17 610	7 20	82 50	0.0	0.0	1.70	0.298E-03	3.1	0
A292	17 610	345 00	82 60	0.0	0.0	3.10	0.229E-03	5.3	10
A293	17 700	28 20	83 40	0.0	0.0	1.90	0.288E-03	3.4	0
A293	-	8 40	83 40	0.0	0.0	1.80	0.309E-03	3.3	10
A293	-	8 00	83 50	0.0	0.0	2.00	0.340E-03	3.5	0
A293	17 700	4 60	83 50	0.0	0.0	1.70	0.222E-03	2.8	10
A293	-	8 70	83 10	0.0	0.0	1.90	0.177E-03	3.4	0
A293	-	7 30	83 50	0.0	0.0	2.30	0.190E-03	4.0	10
A293	-	5 50	84 20	0.0	0.0	4.30	0.864E-04	7.4	0
A293	-	11 30	86 60	0.0	0.0	4.10	0.657E-04	7.1	10
A293	-	333 60	86 40	0.0	0.0	12.00	0.461E-04	20.7	0
A294	17 700	16 30	79 90	0.0	0.0	2.80	0.206E-03	4.9	10
A294	-	9 00	79 30	0.0	0.0	2.70	0.221E-03	4.7	0
A294	-	7 70	78 70	0.0	0.0	2.80	0.212E-03	5.1	10
A294	17 700	6 90	79 00	0.0	0.0	3.00	0.195E-03	5.2	0
A294	-	8 00	79 10	0.0	0.0	2.60	0.158E-03	4.5	10
A294	-	6 90	79 20	0.0	0.0	2.70	0.128E-03	4.4	0
A294	-	4 70	77 00	0.0	0.0	3.50	0.800E-04	6.2	10
A294	-	8 20	77 20	0.0	0.0	3.50	0.542E-04	6.2	0
A294	-	24 30	78 10	0.0	0.0	3.40	0.381E-04	6.0	10
A295	17 800	121 10	82 20	0.0	0.0	2.40	0.243E-03	4.2	0
A295	17 800	147 60	84 50	0.0	0.0	2.50	0.172E-03	4.3	10
A296	17 800	60 10	82 20	0.0	0.0	2.70	0.260E-03	4.7	0
A296	17 800	334 80	86 80	0.0	0.0	2.70	0.174E-03	4.6	10
A297	17 900	136 10	77 00	0.0	0.0	1.70	0.266E-03	2.8	0
A297	-	152 30	75 40	0.0	0.0	2.00	0.224E-03	3.6	10
A297	-	153 00	75 40	0.0	0.0	1.70	0.219E-03	2.8	0
A297	17 900	153 80	74 60	0.0	0.0	2.10	0.195E-03	3.7	10
A297	-	155 00	75 30	0.0	0.0	1.80	0.163E-03	3.4	0
A297	-	151 40	73 30	0.0	0.0	2.80	0.130E-03	4.9	10
A297	-	154 80	73 60	0.0	0.0	6.40	0.878E-04	11.1	0
A297	-	157 40	73 60	0.0	0.0	5.00	0.572E-04	8.8	10
A297	-	161 00	72 40	0.0	0.0	3.80	0.351E-04	6.6	0
A298	17 900	122 50	78 20	0.0	0.0	1.90	0.242E-03	3.3	10
A298	-	141 30	76 10	0.0	0.0	3.30	0.208E-03	5.7	0
A298	-	131 70	75 80	0.0	0.0	3.90	0.198E-03	6.7	10
A298	17 900	144 30	75 90	0.0	0.0	3.10	0.179E-03	5.4	0
A298	-	144 20	74 80	0.0	0.0	4.30	0.149E-03	7.5	10
A298	-	142 50	74 00	0.0	0.0	6.00	0.122E-03	10.5	0
A298	-	147 20	76 10	0.0	0.0	5.40	0.810E-04	9.6	10
A298	-	148 70	73 70	0.0	0.0	3.80	0.484E-04	6.7	0
A298	-	148 80	72 00	0.0	0.0	4.90	0.467E-04	8.5	10

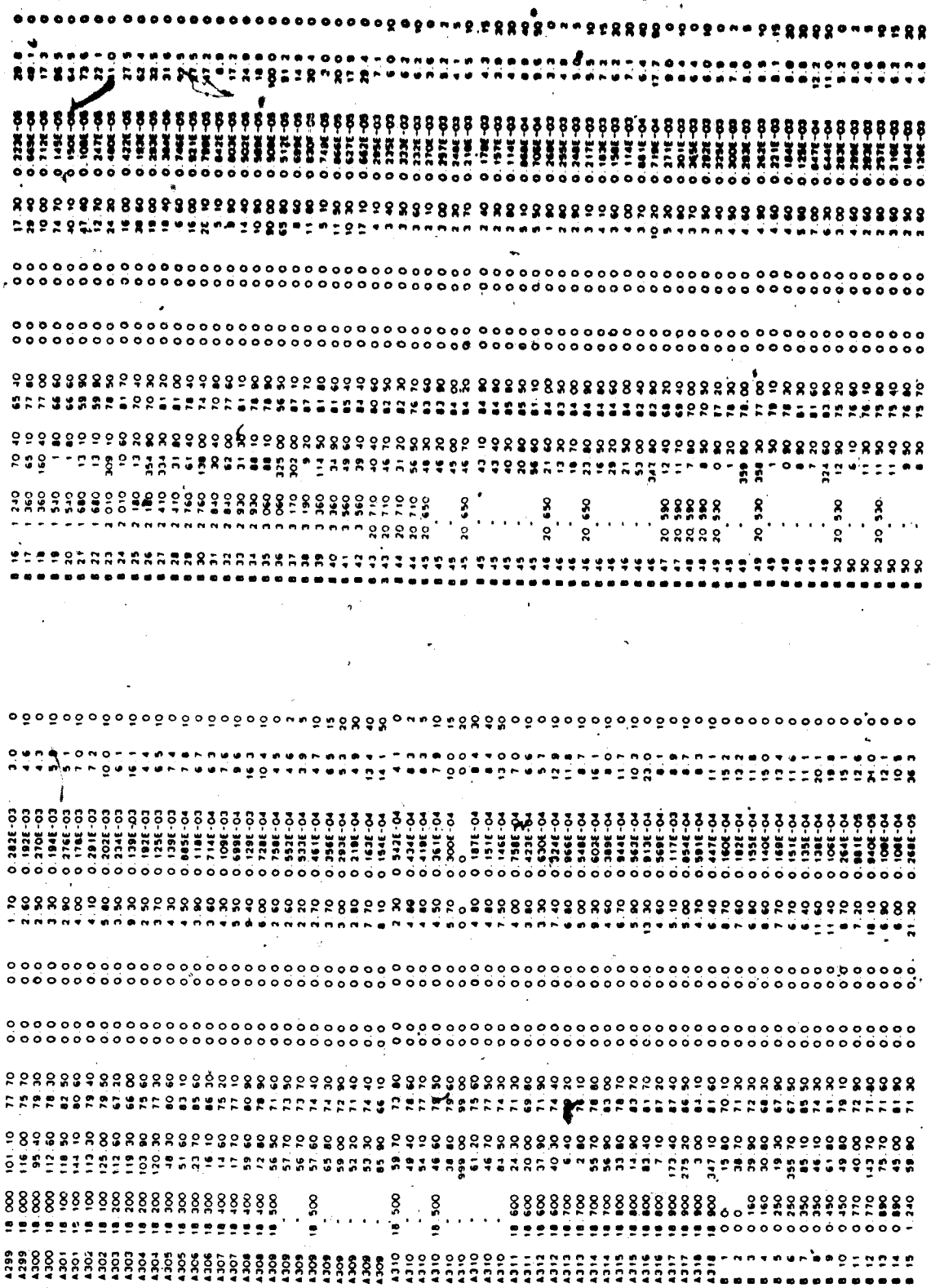

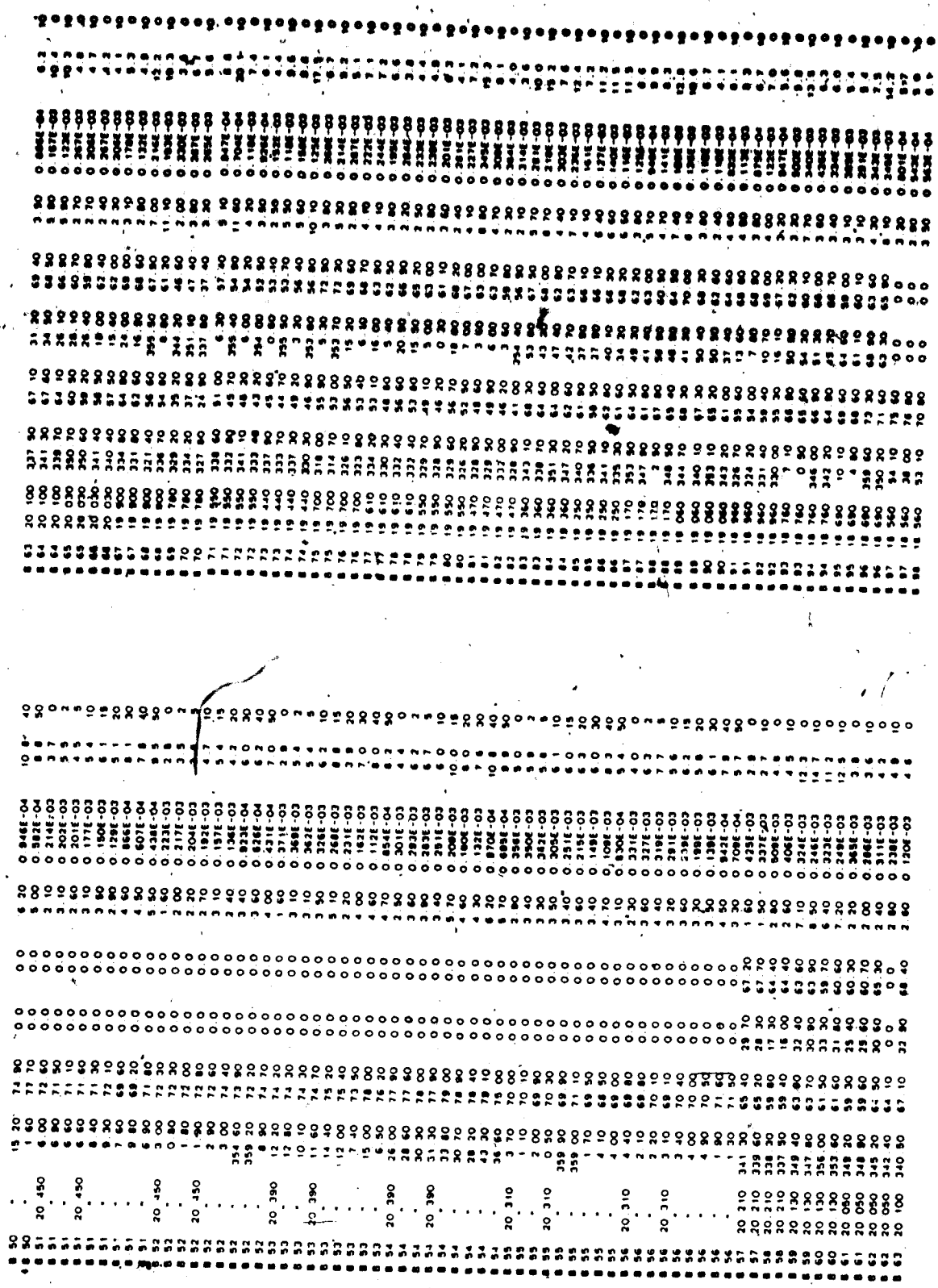

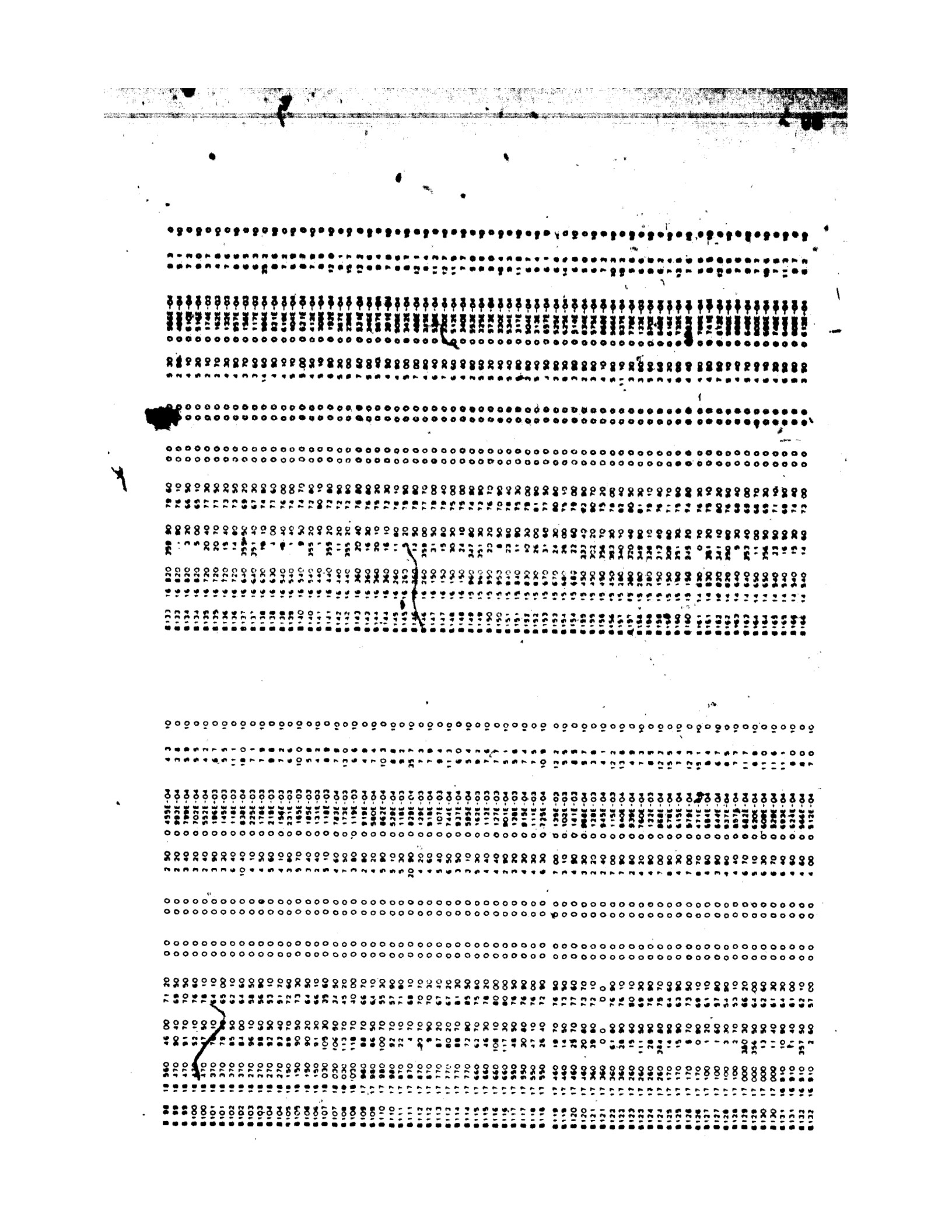

8167	14.450	32.60	75.80	0.0	0.0	6.00	0.781E-04	10.5	0
8167	14.450	8.80	76.20	0.0	0.0	5.50	0.580E-04	9.6	10
8168	14.450	20.10	76.70	0.0	0.0	1.70	0.785E-04	3.0	0
8168	14.450	8.30	75.70	0.0	0.0	3.50	0.657E-04	6.2	10
8169	14.330	32.70	72.00	0.0	0.0	4.50	0.622E-04	7.9	0
8169	14.330	13.40	77.50	0.0	0.0	5.00	0.551E-04	8.7	10
8170	14.330	48.80	67.70	0.0	0.0	4.90	0.722E-04	8.6	0
8170	14.330	36.70	73.70	0.0	0.0	5.10	0.641E-04	8.8	10
8171	14.230	19.10	71.60	0.0	0.0	9.70	0.102E-03	16.8	0
8171	14.230	358.00	73.80	0.0	0.0	7.70	0.609E-04	13.4	10
8172	14.230	40.60	68.10	0.0	0.0	5.40	0.537E-04	9.5	0
8172	14.230	19.00	75.20	0.0	0.0	4.90	0.339E-04	8.6	10
8173	14.110	36.20	75.70	0.0	0.0	3.50	0.512E-04	6.1	0
8173	14.110	358.60	82.40	0.0	0.0	3.70	0.347E-04	6.5	10
8174	14.110	29.30	72.50	0.0	0.0	5.10	0.547E-04	9.0	0
8174	14.110	13.80	77.50	0.0	0.0	5.30	0.378E-04	9.2	10
8175	14.010	27.00	68.60	0.0	0.0	4.80	0.550E-04	8.4	0
8175	14.010	7.90	71.70	0.0	0.0	4.80	0.371E-04	8.4	10
8176	14.010	38.40	73.30	0.0	0.0	4.30	0.586E-04	7.5	0
8176	14.010	9.80	79.10	0.0	0.0	5.00	0.386E-04	8.7	10
8177	13.900	22.50	74.20	0.0	0.0	3.40	0.484E-04	5.9	0
8177	13.900	16.00	78.10	0.0	0.0	4.90	0.309E-04	8.6	10
8178	13.900	9.60	78.50	0.0	0.0	3.10	0.494E-04	5.5	0
8178	13.900	0.20	79.90	0.0	0.0	5.40	0.343E-04	9.4	10
8179	13.900	19.40	83.60	0.0	0.0	7.10	0.493E-04	12.3	0
8179	13.900	342.20	82.80	0.0	0.0	5.40	0.317E-04	9.4	10
8180	13.900	3.30	80.80	0.0	0.0	6.50	0.451E-04	11.4	0
8180	13.900	342.70	80.30	0.0	0.0	7.30	0.302E-04	12.7	10
8181	13.840	13.30	82.50	0.0	0.0	10.00	0.139E-03	17.4	0
8181	13.840	24.70	80.30	0.0	0.0	7.70	0.378E-04	13.4	10
8182	13.840	14.80	83.30	0.0	0.0	8.50	0.225E-03	14.8	0
8182	13.840	350.50	80.70	0.0	0.0	7.40	0.482E-04	12.9	10
8183	13.740	30.30	84.30	0.0	0.0	4.50	0.641E-04	7.9	0
8183	13.740	10.80	86.30	0.0	0.0	6.10	0.441E-04	10.6	10
8184	13.740	340.10	80.40	0.0	0.0	9.50	0.657E-04	16.5	0
8184	13.740	333.20	82.70	0.0	0.0	9.10	0.303E-04	15.7	10
8185	13.610	40.30	83.00	0.0	0.0	10.00	0.134E-03	17.4	0
8185	13.610	8.30	81.10	0.0	0.0	7.00	0.905E-04	12.2	10
8186	13.610	32.10	80.30	0.0	0.0	3.80	0.107E-03	6.7	0
8186	13.610	27.00	81.30	0.0	0.0	3.80	0.743E-04	6.5	10
8187	13.500	11.40	80.70	0.0	0.0	4.00	0.929E-04	7.0	0
8187	13.500	5.20	80.70	0.0	0.0	3.00	0.664E-04	5.2	10
8188	13.500	4.70	78.30	0.0	0.0	4.50	0.106E-03	7.8	0
8188	13.500	344.60	78.40	0.0	0.0	5.50	0.834E-04	9.7	10
8189	13.400	10.80	79.40	0.0	0.0	2.60	0.105E-03	4.6	0
8189	13.400	344.40	78.90	0.0	0.0	4.60	0.505E-04	8.0	10
8190	13.400	24.60	76.90	0.0	0.0	3.30	0.989E-04	5.8	0
8190	13.400	8.50	76.60	0.0	0.0	4.90	0.548E-04	8.6	10
8191	12.950	10.20	72.10	0.0	0.0	5.50	0.298E-04	9.5	0
8191	12.950	4.80	69.70	0.0	0.0	4.00	0.183E-04	7.0	10
8192	12.950	0.30	64.50	0.0	0.0	7.00	0.262E-04	12.2	0
8192	12.950	5.60	61.90	0.0	0.0	3.70	0.174E-04	6.5	10
8193	12.840	19.00	64.90	0.0	0.0	7.10	0.310E-04	12.3	0
8193	12.840	17.60	60.60	0.0	0.0	6.20	0.220E-04	10.8	10
8194	12.840	14.80	68.60	0.0	0.0	6.00	0.302E-04	10.5	0
8194	12.840	7.40	62.50	0.0	0.0	7.60	0.209E-04	13.2	10
8195	12.750	21.70	72.30	0.0	0.0	8.00	0.314E-04	13.8	0
8195	12.750	21.60	70.70	0.0	0.0	6.10	0.227E-04	10.7	10
8196	12.750	25.30	72.20	0.0	0.0	8.70	0.288E-04	15.1	0
8196	12.750	22.70	74.00	0.0	0.0	5.20	0.220E-04	9.0	10
8197	12.650	11.30	64.10	0.0	0.0	8.80	0.335E-04	15.3	0
8197	12.650	3.90	61.70	0.0	0.0	5.10	0.242E-04	8.9	10
8198	12.650	11.70	64.00	0.0	0.0	8.40	0.295E-04	14.6	0
8198	12.650	8.00	57.50	0.0	0.0	5.00	0.195E-04	8.7	10
8199	12.550	17.50	72.70	0.0	0.0	6.40	0.216E-04	11.2	0
8199	12.550	2.40	75.50	0.0	0.0	4.80	0.163E-04	8.3	10
8200	12.550	38.80	67.00	0.0	0.0	6.40	0.168E-04	11.2	0
8200	12.550	30.20	71.60	0.0	0.0	4.10	0.127E-04	7.2	10
8201	12.450	358.80	57.10	0.0	0.0	17.20	0.301E-04	29.5	0

8201	12.450	355.40	58.80	0.0	0.0	9.10	0.227E-04	15.8	10
8202	12.450	359.40	63.70	0.0	0.0	7.00	0.310E-04	12.2	0
8202	12.450	344.20	54.50	0.0	0.0	7.00	0.192E-04	12.2	10
8203	12.250	354.30	68.00	0.0	0.0	9.50	0.211E-04	16.5	0
8203	12.250	355.20	59.80	0.0	0.0	5.30	0.168E-04	9.2	10
8204	12.250	357.00	67.00	0.0	0.0	4.80	0.237E-04	8.3	0
8204	12.250	355.30	61.10	0.0	0.0	6.10	0.172E-04	10.7	10
8205	12.150	78.00	75.50	0.0	0.0	14.30	0.141E-04	24.7	0
8206	12.150	8.80	63.10	0.0	0.0	20.80	0.123E-04	35.6	0
8206	12.150	37.80	74.00	0.0	0.0	9.10	0.731E-05	15.8	10
8207	12.000	333.40	66.20	0.0	0.0	37.50	0.944E-05	60.8	0
8207	12.000	343.50	62.80	0.0	0.0	10.80	0.603E-05	18.8	10
8208	12.000	359.80	83.60	0.0	0.0	15.80	0.981E-05	27.2	0
8208	12.000	332.20	80.10	0.0	0.0	19.20	0.521E-05	32.8	10
8209	11.880	53.50	76.40	0.0	0.0	7.60	0.144E-04	13.2	0
8209	11.880	44.80	73.20	0.0	0.0	6.20	0.783E-05	10.7	10
8210	11.880	66.70	78.10	0.0	0.0	6.30	0.124E-04	11.0	0
8210	11.880	111.00	76.90	0.0	0.0	9.00	0.650E-05	15.7	10
8211	11.700	78.30	72.20	0.0	0.0	4.80	0.850E-05	8.4	0
8211	11.700	99.00	68.60	0.0	0.0	9.00	0.446E-05	15.7	10
8212	11.700	105.20	76.00	0.0	0.0	6.50	0.897E-05	11.3	0
8212	11.700	82.00	80.40	0.0	0.0	7.60	0.521E-05	13.2	10
8213	11.570	69.10	74.50	0.0	0.0	6.80	0.911E-05	11.8	0
8213	11.570	39.80	79.90	0.0	0.0	6.20	0.499E-05	10.8	10
8214	11.570	80.60	77.30	0.0	0.0	8.20	0.108E-04	14.3	0
8214	11.570	83.20	86.70	0.0	0.0	9.60	0.503E-05	16.7	10
8215	11.460	40.40	74.80	0.0	0.0	10.40	0.892E-05	18.1	0
8215	11.460	27.80	80.30	0.0	0.0	8.90	0.610E-05	15.5	10
8216	11.460	51.40	79.40	0.0	0.0	6.80	0.106E-04	11.8	0
8216	11.460	357.90	85.40	0.0	0.0	7.40	0.617E-05	12.8	10
8217	11.350	70.40	81.00	0.0	0.0	12.20	0.885E-05	21.1	0
8217	11.350	53.80	81.50	0.0	0.0	6.40	0.669E-05	11.1	10
8218	11.350	326.10	75.20	0.0	0.0	9.30	0.709E-05	16.2	0
8218	11.350	345.50	84.10	0.0	0.0	9.50	0.598E-05	16.5	10
8219	11.250	25.10	72.90	0.0	0.0	9.70	0.925E-05	16.9	0
8219	11.250	24.00	74.40	0.0	0.0	8.50	0.823E-05	14.8	10
8220	11.250	39.80	72.70	0.0	0.0	4.50	0.120E-04	7.8	0
8220	11.250	28.40	72.10	0.0	0.0	8.00	0.107E-04	14.0	10
8221	11.150	35.90	74.80	0.0	0.0	12.80	0.906E-05	22.2	0
8221	11.150	21.60	79.40	0.0	0.0	6.40	0.801E-05	11.2	10
8222	11.150	347.60	72.80	0.0	0.0	11.60	0.747E-05	20.2	0
8222	11.150	351.80	64.80	0.0	0.0	10.20	0.514E-05	17.8	10
8223	11.050	39.70	68.20	0.0	0.0	18.10	0.122E-04	31.1	0
8223	11.050	20.40	64.80	0.0	0.0	17.30	0.736E-05	29.7	10
8224	11.050	0.0	69.60	0.0	0.0	11.30	0.114E-04	19.5	0
8225	10.940	29.70	75.20	0.0	0.0	11.20	0.826E-05	19.4	0
8225	10.940	343.00	85.30	0.0	0.0	8.60	0.485E-05	15.0	10
8226	10.940	37.70	65.30	0.0	0.0	8.00	0.876E-05	13.9	0
8226	10.940	13.20	74.60	0.0	0.0	13.60	0.401E-05	23.5	10
8227	10.820	34.30	79.70	0.0	0.0	5.60	0.988E-04	9.8	0
8227	10.820	8.20	78.80	0.0	0.0	5.80	0.125E-04	10.1	10
8228	10.820	340.50	71.30	0.0	0.0	9.60	0.105E-04	16.6	0
8229	10.710	17.70	64.40	0.0	0.0	12.10	0.112E-04	21.0	0
8229	10.710	9.80	71.60	0.0	0.0	6.70	0.668E-05	11.6	10
8230	10.710	12.70	69.20	0.0	0.0	12.70	0.105E-04	22.1	0
8230	10.710	13.30	66.50	0.0	0.0	9.40	0.731E-05	16.4	10
8231	10.600	43.40	66.50	0.0	0.0	6.80	0.718E-05	11.8	0
8231	10.600	28.70	72.30	0.0	0.0	7.60	0.493E-05	13.2	10
8232	10.600	33.60	67.50	0.0	0.0	8.90	0.779E-05	15.4	0
8232	10.600	16.80	65.50	0.0	0.0	15.40	0.481E-05	26.5	10
8233	10.500	8.10	71.70	0.0	0.0	10.80	0.136E-04	18.7	0
8233	10.500	350.10	66.80	0.0	0.0	8.70	0.812E-05	16.9	10
8234	10.500	4.90	70.20	0.0	0.0	5.60	0.170E-04	9.8	0
8234	10.500	355.80	69.40	0.0	0.0	6.90	0.117E-04	12.0	10
8235	10.350	8.80	65.90	0.0	0.0	3.80	0.852E-05	6.7	0
8235	10.350	2.10	62.00	0.0	0.0	5.50	0.575E-05	9.5	10
8236	10.350	355.10	67.50	0.0	0.0	5.40	0.833E-05	9.3	0
8236	10.350	344.50	65.10	0.0	0.0	6.30	0.580E-05	10.9	10
8237	10.250	8.00	61.20	0.0	0.0	12.30	0.522E-05	21.3	0

8237	10.250	350.80	69.40	0.0	0.0	10.60	0.348E-05	18.4	10
8238	10.250	11.20	63.50	0.0	0.0	12.40	0.638E-05	21.5	0
8238	10.250	0.40	52.40	0.0	0.0	16.70	0.376E-05	28.8	10
8239	10.140	317.10	78.30	0.0	0.0	11.80	0.484E-05	20.4	0
8239	10.140	300.80	80.20	0.0	0.0	12.00	0.310E-05	20.8	10
8240	10.140	358.30	64.00	0.0	0.0	11.10	0.121E-04	19.3	0
8241	10.020	42.40	61.80	0.0	0.0	10.50	0.501E-05	18.1	0
8241	10.020	40.70	61.60	0.0	0.0	11.50	0.360E-05	19.9	10
8242	10.020	24.70	52.10	0.0	0.0	10.80	0.496E-05	18.8	0
8243	9.880	25.30	66.40	0.0	0.0	9.60	0.118E-04	16.7	0
8244	9.880	25.60	62.10	0.0	0.0	9.90	0.199E-04	17.2	0
8245	9.040	353.20	64.60	0.0	0.0	11.80	0.469E-05	20.4	0
8246	9.040	30.90	53.80	0.0	0.0	10.90	0.434E-05	18.9	0
8247	8.940	36.60	78.50	0.0	0.0	20.30	0.359E-05	34.7	0
8248	8.940	36.60	73.90	0.0	0.0	90.00	0.279E-05	100.0	0
8249	8.860	53.60	73.40	0.0	0.0	8.60	0.521E-05	14.9	0
8250	8.860	62.80	79.60	0.0	0.0	8.50	0.101E-04	14.8	0
8251	8.700	14.30	64.50	0.0	0.0	22.70	0.500E-05	38.6	0
8252	8.700	30.00	73.80	0.0	0.0	21.50	0.545E-05	36.7	0
8253	8.580	335.90	76.90	0.0	0.0	10.50	0.672E-05	18.2	0
8254	8.580	28.20	65.90	0.0	0.0	5.60	0.777E-05	9.7	0
8255	8.340	28.20	69.00	0.0	0.0	52.40	0.376E-05	79.2	0
8256	8.340	76.30	63.30	0.0	0.0	14.10	0.426E-05	24.3	0
8257	8.210	353.80	71.20	0.0	0.0	8.80	0.944E-05	15.2	0
8258	8.210	340.70	66.00	0.0	0.0	10.30	0.947E-05	17.9	0
8259	8.120	25.90	74.00	0.0	0.0	14.60	0.479E-05	25.2	0
8260	8.120	24.50	70.20	0.0	0.0	23.20	0.440E-05	39.3	0
8261	8.030	356.80	65.00	0.0	0.0	5.90	0.254E-04	10.3	0
8261	8.030	359.90	65.70	0.0	0.0	9.00	0.180E-04	15.6	10
8262	8.030	346.60	64.90	0.0	0.0	5.40	0.254E-04	9.4	0
8262	8.030	337.30	68.00	0.0	0.0	9.10	0.180E-04	15.8	10
8263	7.920	325.00	72.20	0.0	0.0	6.80	0.123E-04	11.9	0
8264	7.920	350.70	63.70	0.0	0.0	14.20	0.148E-04	24.5	0
8265	7.820	357.60	67.40	0.0	0.0	6.50	0.118E-04	11.4	0
8265	7.820	356.10	67.00	0.0	0.0	6.20	0.851E-05	10.8	10
8266	7.820	347.40	55.30	0.0	0.0	4.50	0.157E-04	7.8	0
8266	7.820	338.50	51.60	0.0	0.0	5.00	0.127E-04	8.8	10
8267	7.720	352.30	64.10	0.0	0.0	4.10	0.223E-04	7.1	0
8267	7.720	347.20	59.40	0.0	0.0	5.30	0.186E-04	9.2	10
8268	7.720	349.10	63.00	0.0	0.0	8.40	0.228E-04	14.6	0
8268	7.720	350.70	60.60	0.0	0.0	7.50	0.183E-04	13.1	10
8269	7.620	343.70	54.00	0.0	0.0	4.90	0.290E-04	8.5	0
8269	7.620	339.60	53.00	0.0	0.0	6.80	0.239E-04	11.8	10
8270	7.620	338.00	63.60	0.0	0.0	4.60	0.193E-04	7.9	0
8270	7.620	336.00	61.90	0.0	0.0	6.90	0.137E-04	12.1	10
8271	7.520	354.70	68.80	0.0	0.0	8.90	0.839E-05	15.5	0
8272	7.510	0.40	71.10	0.0	0.0	4.90	0.867E-05	8.5	0
8273	7.420	34.50	61.20	0.0	0.0	8.50	0.570E-05	14.8	0
8274	7.410	359.00	70.80	0.0	0.0	8.20	0.609E-05	14.2	0
8275	7.240	345.40	64.80	0.0	0.0	5.80	0.266E-04	10.1	0
8275	7.240	337.60	61.20	0.0	0.0	4.20	0.196E-04	7.3	10
8276	7.230	339.10	66.60	0.0	0.0	8.30	0.228E-04	14.4	0
8276	7.230	339.50	62.40	0.0	0.0	12.70	0.157E-04	21.9	10
8277	7.130	19.30	73.60	0.0	0.0	12.40	0.416E-05	21.5	0
8278	7.130	29.00	77.80	0.0	0.0	20.20	0.452E-05	34.6	0
8279	7.030	60.00	54.10	0.0	0.0	17.40	0.341E-05	30.0	0
8280	7.030	347.20	70.30	0.0	0.0	12.00	0.451E-05	20.8	0
8281	6.740	6.70	73.90	0.0	0.0	5.70	0.352E-04	9.8	0
8281	6.740	2.10	71.00	0.0	0.0	5.60	0.257E-04	9.7	10
8282	6.730	345.50	58.70	0.0	0.0	4.50	0.324E-04	7.9	0
8282	6.730	343.10	58.40	0.0	0.0	4.30	0.249E-04	7.4	10
8283	6.410	356.80	63.50	0.0	0.0	5.60	0.260E-04	9.7	0
8283	6.410	345.30	63.90	0.0	0.0	9.00	0.192E-04	15.7	10
8284	6.400	357.80	66.70	0.0	0.0	3.80	0.275E-04	6.6	0
8284	6.400	349.60	64.80	0.0	0.0	8.40	0.196E-04	14.7	10
8285	6.060	49.60	79.30	0.0	0.0	9.90	0.546E-05	17.2	0
8286	6.060	53.40	62.40	0.0	0.0	11.90	0.426E-05	20.7	0
8287	5.930	8.20	78.00	0.0	0.0	6.50	0.645E-05	11.2	0
8288	5.930	291.30	59.70	0.0	0.0	34.90	0.693E-05	57.3	0
8289	5.720	7.30	68.70	0.0	0.0	12.10	0.544E-05	21.0	0
8290	5.720	29.80	65.40	0.0	0.0	44.80	0.124E-04	70.5	0
8291	5.570	335.80	53.60	0.0	0.0	5.60	0.234E-04	9.7	0
8291	5.570	332.70	53.40	0.0	0.0	7.30	0.176E-04	12.7	10
8292	5.570	319.10	57.10	0.0	0.0	5.40	0.459E-04	9.5	0
8292	5.570	317.30	58.50	0.0	0.0	4.30	-0.320E-04	7.5	10
8293	5.430	8.30	40.60	0.0	0.0	38.60	0.454E-05	62.4	0
8294	5.430	55.20	72.20	0.0	0.0	43.20	0.191E-05	68.5	0
8295	5.280	148.70	80.90	0.0	0.0	41.70	0.263E-05	66.5	0
8296	5.280	17.20	63.60	0.0	0.0	32.40	0.330E-05	53.6	0
8297	5.190	9.80	82.30	0.0	0.0	27.20	0.439E-05	45.8	0
8298	5.190	153.20	83.90	0.0	0.0	14.80	0.306E-05	25.5	0
8299	5.080	48.70	88.60	0.0	0.0	28.40	0.245E-05	47.5	0
8300	5.080	27.60	79.90	0.0	0.0	14.50	0.284E-05	25.1	0
8301	4.900	42.40	73.40	0.0	0.0	11.40	0.415E-05	19.7	0
8302	4.900	68.20	73.70	0.0	0.0	7.60	0.390E-05	13.2	0
8303	4.730	61.00	88.10	0.0	0.0	7.40	0.557E-05	12.9	0
8304	4.730	222.00	-37.20	0.0	0.0	90.00	0.545E-05	100.0	0
8305	4.520	329.00	79.80	0.0	0.0	7.90	0.701E-05	13.7	0
8306	4.520	357.80	72.40	0.0	0.0	11.20	0.817E-05	19.5	0
8307	4.240	5.00	67.90	0.0	0.0	10.80	0.763E-05	18.8	0
8308	4.240	317.10	70.20	0.0	0.0	6.30	0.101E-04	11.0	0